UNIVERSITY OF YAOUNDE I
FACULTY OF SCIENCE
Department of Physics

VRIJE UNIVERSITEIT BRUSSEL
FACULTY OF SCIENCE
Applied Physics Research Group

Study of coupled self-sustained oscillators : circadian oscillations in cyanobacteria and powering of biological loads

Submitted and defended for the award of Doctorat/PhD in Physics

By:

YOUMBI FOUEGO DOROTA

Masters of Science in Physics
10W0903

Joint PhD Thesis

University of Yaounde I, Cameroon
Vrije Universiteit Brussel, Belgium

Public defense:

Private defense:

Promoters:

WOAFO Paul, Professor,
University of Yaounde I, Cameroon

Sophie de BUYL, Associate Professor
Vrije Universiteit Brussel, Belgium

UNIVERSITÉ DE YAOUNDÉ
THE UNIVERSITY OF YAOUNDE I

FACULTÉ DES SCIENCES
FACULTY OF SCIENCES

DÉPARTEMENT DE PHYSIQUE
DEPARTMENT OF PHYSICS

ATTESTATION DE CORRECTION DE LA THÈSE DE DOCTORAT/Ph.D

Nous, Professeur **NANA NBENDJO Blaise Romeo** et Professeur **ESSIMBI ZOBO Bernard**, respectivement Examinateur et Président du jury de la Thèse de Doctorat/PhD de Madame **YOUMBI FOUEGO Dorota**, Matricule **10W0903**, préparée sous la direction des Professeurs **WOAFO Paul** (Université de Yaoundé 1) et **Sophie DE BUYL**(Vrije Universiteit Brussel), intitulée : « **Study of coupled self-sustained oscillators : circadian oscillations in cynobacteria and powering of biological loads**», soutenue le Lundi, **20 Février 2023**, en vue de l'obtention du grade de Docteur/PhD en Physique, Spécialité **Mécanique, Matériaux et Structures,** option **Mécanique Fondamentale et Systèmes Complexes** attestons que toutes les corrections demandées par le jury de soutenance ont été effectuées.

En foi de quoi, la présente attestation lui est délivrée pour servir et valoir ce que de droit.

Fait à Yaoundé, le 06 MARS 2023

Examinateur	Le Président du jury	Le Chef de Département de Physique
Pr NANA NBENDJO B. R	Pr ESSIMBI ZOBO Bernard	Pr NDJAKA Jean-Marie

Contents

List of Figures

List of Tables

Dedication

I dedicate this thesis:

- To **God Almighty** for all the strength and mercy, you give me everyday.
- To my mother **Taguimdjeu Foueteu Sidonie** for the unconditional support she has given me everyday. Her love and guidance enabled me to complete this job.
- To my late father **Youmbi Adolphe** whose goal was to let me be a scientist. May he find in this document the fulfillment of his dreams and a reason for his satisfaction.
- To my brothers and sisters**Youmbi Freddy**,**Youmbi Sandra** ,**Youmbi Phanuelle** and **Youmbi Jason** for their assistance and encouragement.
- To my **maternal and paternal families** for the support provided during these years.

Acknowledgements

This thesis is the fruit of the efforts of those who participated to its accomplishment. Therefore I would like to pay a tribute and thank:

- To **Professor WOAFO Paul** my supervisor at the UYI in Yaounde, who despite his multiple occupations, gave me adequate supervision. Thank you, professor, for believing in me.
- To **Professor Sophie de BUYL** my supervisor at the VUB in Brussels, Thank you Professor for having passed on to me your passion and patience in the work to be done.
- To **the Research and Doctoral Training Unit for Physics and Applications** for the opportunity it gave me to benefit to this doctoral training.
- To **the Applied Physics Research Group** of the Vrije Universiteit Brussel (VUB) in Belgium.
- To **the jury** in advance for accepting to examine this thesis.
- To **Professor NDJAKA Jean Marie**, Head of the Department of Physics, Faculty of Science, UYI and the teaching staff of this department for their valuable teachings.
- To **Professor KOFANE Timoleon Crepin** for his teachings and the fruitfull advice.
- To **Professor NANA NBENDJO Blaise Romeo** for the support and advice he has given me along this journey.
- To **Dr. DONGMO Eric Donald** for his fruitfull scientific advices. May he find my sincere gratitude here.
- To **Drs. SIFEU TAKOUGANG kingni, TALLA Mbe, SIMO Herve, TALLA Francis, NWAGOUM Peguy, NDJOMATCHOUA Frank, NDEMANOU Peguy, METSOBO Jules, TOKOUE Ngatcha, TCHAKUI Murielle, TSAPLA Rolande, ANAGUE Lionnel, MAKOUO Lucienne, SIMO Ulrich , THEPI Raoul, MBA Steve, FANKEM Raissa** for the scientific advice that I had with each of them during the development of this thesis.

- To the PhD students of LAMSEBP for the welcome and support they had for me. Special thanks to: **ESSAMBA Ursule, MBOU Bertrand, NGATCHA Nelly, MONKAM Joel, FONKOU Rodrigue, MBOYO Rene, KOUAM Fidele, KOUAMI Nadine, DEUMI Juliete, YOUTHA Octave, NGOUNOU Martial, MOKOLA Lazare, KOUEMOU Cedric, TEMGOUA Pavel, KOUNCHIE Prosper** .

- To **His Majesty TAGUIMDJEU 2 Aristide, Madame NDJILLE Clarisse, TAGUIMDJEU Narcisse, Madame DJEUKAM Hermine, NDJINGA Prisques, MBAKO Leonard** for the moral and financial support they gave me during my training.

- To my friends in particular to: **KOUAMEGNI Victoire, KENFACK Richid, NGAGOM Hillary, FEULEFACK Edwige, MANETSA Roseline, NDJANG Dolyne, DIMO Sonia, TAGUENA Rodrigue, NGANGUE Medda, KEMAYOU adrien, NGOMSI Steff, DJUIDJEU Gael, GEORGES Pascal, SITOUOK Christian, KOUWE Eric, TALLA Patrick Hermann, BITJOKA Albert, NDJINGA Vanessa** for having always been by my side in order to support me during my studies.

- To my elder brothers: **NGOUNOU Romuald, KOUEFOUET Adolphe and KINGUE Arnauld** for their support during these last fourth years. In them I had the comfort of real big brothers.

- To all my family of **ACMP** for the love they brought me and their prayer for me.

- To the Association des Ressortissants Nzalla de Yaoundé **(ARNY)** , the Association des Jeunes Fontsa Touala de Yaoundé **(AJFTY)** for all the moral support provided.

- To all my brothers and sisters in **Nzalla, Ntsalla, Foreke and Leunlah** villages for the love they brought me.

- All those whose names have not been mentioned here, but who have contributed in one or other way to the success of this work should hereby receive my sincere gratitude.

List of abbreviations

ATP: adenosine-triphosphate

AV: Atrio Ventricuar

ECG: Electro Cardiogramm

HH: Hodgkin-Huxley

HR: Hindmarsh-Rose

PER: Protein Efficiency Ratio

PTR: Post Translational Regulation

TTR: Transcriptional-Translational Regulation

RNA: ribonucleic acid

SA: Sino Atrial

SR: Sarcoplasmic Reticulum

VdP: Van der Pol

WTR: Wild Type regulation

Abstract

This thesis deals firstly with the analysis of the dynamics of coupled systems considered here as a set of self-sustained oscillators (Van der Pol, Grudzinski-Zebrowski, Hindmarsch-Rose) powering an electrical load (RLC, RL, RC or R). Secondly, to simulate the circadian clock in cyanobacteria made up of three proteins under its simplified structure (monomer) and its basic structure (hexamer). The harmonic balance method, the Kirchoff's laws, RK4 method and the criteria of synchronization have been used to obtain the following results:

- In the case of an array of Van der Pol oscillators coupled to a load, it is found that after a threshold number of oscillators under which the power is equal to zero, increase versus number of oscillator. A high order nonlinearity in the damping of the Van der Pol oscillator increases the power in the load.

- In the case of an array of oscillator Grudzinski-Zebrowski oscillators coupled to a load, we design an equivalent electrical circuit whose equation is similar to the self-sustained oscillator model presented by Grudzinski-Zebrowski. It is then demonstrated that the power in electrical loads (RLC, RL, RC and R) coupled to an array of such oscillator's increases with the number of oscillators till a constant values depending on the types of loads and values of the load parameters. The synchronization domain is seen to depend on the values of the direct coupling, the values of the indirect coupling and on the number of oscillators in the array.

- In the case of an array of Hindmarsch-Rose oscillators coupled to a load, it is shown that varying the coupling coefficient leads to the appearance of chaotic dynamics in the system. It is also found that the voltage amplitudes decrease when the size of the array of the HR oscillators increases.

- For the hexameric model of the cyanobacterial circadian clock, we propose an *in vivo* model of cyanobacterial circadian clock based on the *in vitro* model and it is shown that there is a large range of values where there are oscillations.

Keys words: Grudzinski and Zebrowski oscillator, cyanobacteria, circadian rhythm

Samenvatting

Dit proefschrift behandelt ten eerste de analyse van de dynamica van gekoppelde systemen, hier beschouwd als set van self-sustained oscillatoren (Van der Pol, Grudzinski-Zebrowski, Hindmarsch-Rose) die een elektrische belasting (RLC, RL, RC of R) aandrijven. Ten tweede modelleren we de circadiane klok van cyanobacteriën en bestuderen we de koppeling tussen de transcriptionele regulatie en de post-translationele regulatie. De harmonische balansmethode, de wetten van Kirchoff, de Runge-Kutta RK4-methode en de synchronisatiecriteria zijn gebruikt in onze verschillende projecten:

- Wij hebben een array van Van der Pol-oscillatoren gekoppeld aan een belasting beschouwd en vastgesteld dat na een drempelaantal oscillatoren waaronder het vermogen gelijk is aan nul, het vermogen toeneemt met het aantal oscillatoren. Een niet-lineariteit van hoge orde in de demping van de Van der Pol-oscillator verhoogt het vermogen in de belasting.

- In het geval van een reeks Grudzinski-Zebrowski-oscillatoren gekoppeld aan een belasting, ontwerpen wij een equivalent elektrisch circuit waarvan de vergelijking vergelijkbaar is met het self-sustained oscillator model voorgesteld door Grudzinski en Zebrowski. Vervolgens wordt aangetoond dat het vermogen in elektrische belastingen (RLC, RL, RC en R) gekoppeld aan een reeks van dergelijke oscillatoren toeneemt met het aantal oscillatoren tot een constante waarde die afhangt van de soorten belastingen en de waarden van de belastingsparameters. Het synchronisatiegebied blijkt af te hangen van de waarden van de directe koppeling, de waarden van de indirecte koppeling en van het aantal oscillatoren in de array.

- In het geval van een array van Hindmarsch-Rose-oscillatoren gekoppeld aan een belasting, wordt aangetoond dat het variëren van de koppelingscoëfficiënt leidt tot het ontstaan van een chaotische dynamiek in het systeem. Ook blijkt dat de spanningsamplitudes afnemen wanneer de grootte van de array van de HR-oscillatoren toeneemt.

- Wij stellen een in vivo model voor van de circadiane klok van cyanobacteriën, gebaseerd op het hexamere in vitro model, en er wordt aangetoond dat er een groot bereik is van waarden die leiden tot een oscillatoir gedrag, zowel voor de wildtype cyanobacteriën als voor de mutanten die de transcriptionele regulatie missen. Dit

resultaat suggereert dat, hoewel de transcriptionele feedback de robuustheid van de klok enigszins verbetert, het effect niet zo sterk is als eerder werd beweerd. Onze conclusie is in overeenstemming met de experimenten.

trefwoorden: Grudzinski en Zebrowski-oscillator, cyanobacteriën, circadian ritme

Résumé

Cette thèse traite tout d'abord de l'analyse de la dynamique des systèmes couplés considérés ici comme un ensemble d'oscillateurs auto-entretenus (Van der Pol, Grudzinski-Zebrowski, Hindmarsch - Rose) alimentant une charge électrique (RLC, RL, RC ou R). Deuxièmement, simuler l'horloge circadienne des cyanobactéries composées de trois protéines sous sa structure simplifiée (monomère) et sa structure de base (hexamère). La méthode de la balance des harmoniques, les lois des Kirchoff, la méthode de RK4 et le critère de synchronisation ont été utilisés pour obtenir les résultats suivants:

- Dans le cas d'un réseau d'oscillateurs de Van der Pol couplés à une charge, on constate qu'après un nombre seuil d'oscillateurs sous lequel la puissance est égale à zéro, la puissance augmente en fonction du nombre d'oscillateurs. Une non-linéarité d'ordre élevé dans l'amortissement de l'oscillateur de Van der Pol augmente la puissance de la charge.

- Dans le cas d'un réseau d'oscillateurs de Grudzinski-Zebrowski couplés à une charge, nous concevons un circuit électrique équivalent. Nous démontrons alors que la puissance dans les charges électriques (RLC, RL, RC et R) couplées à un réseau de tels oscillateurs augmente avec le nombre d'oscillateurs jusqu'à des valeurs constantes dépendant des types de charges et des valeurs des paramètres de charge. Le domaine de synchronisation dépend des valeurs du couplage direct, des valeurs du couplage indirect et du nombre d'oscillateurs dans le réseau.

- Dans le cas d'un réseau d'oscillateurs de Hindmarsch-Rose couplés à une charge, on montre que la variation du coefficient de couplage conduit à l'apparition d'une dynamique chaotique dans le système. On constate également que les amplitudes de la tension électrique diminuent lorsque la taille du réseau des oscillateurs HR augmente.

- Pour le modèle hexamèrique de l'horloge circadienne des cyanobactéries, on propose le modèle *in vivo* de l'horloge circadienne des cyanobactéries basé sur le modèle *in vitro* et on montre qu'il y'a une grande gamme de valeurs où il y'a des oscillations.
  Mots clés : Oscillateur de Grudzinski Zebrowski, cyanobactérie, rythme circadien

General introduction

The study of the dynamical behavior of single or coupled mechanical and electrical systems powered by self-sustained and bio inspired oscillators is a subject that has attracted the attention to various scientists [1–3]. Coupling the self-sustained oscillators of the electrical nature to a load can be interesting as this can be used as a representative model to analyze the effects of biological signals on biological organs (e.g an ensemble of cells constituting the pacemaker acting on the heart or the image of an ensemble of neurons acting on a muscle).

The modeling, followed by mathematical and numerical studies of the electrical conduction system models of the heart, has attracted the attention of several researchers [4–9]. Several models to mimic the rhythm of heartbeat were developed, from the Hodgkin-Huxley model [10] to the Van der Pol (VdP) model [11]. The VdP model was the pioneer in providing relaxation oscillations. It was also used to qualitatively model heartbeat [12]. The research deepened and later Kaiser showed in Ref. [13] that the modified Van der Pol oscillator seems to be more appropriate to describe oscillatory biological processes better than the classic Van der Pol oscillator. In 2004, the Grudzinski and Zebrowski oscillator whose dynamics is close to the physiological behavior of the electric signal of the heart, was presented [5]. Derived from the classical Van der Pol oscillator, it suitably presents signals having the shapes of physiological signals such as the resting potential, refraction time and diastolic period depending on its parameters. Depending on its initial conditions and the values of its parameters and certain values of external inputs [14, 15], the Grudzinski and Zebrowski oscillator may have periodic or chaotic behaviors. To be able to use such an oscillator in a system, one possibility is to use its electric model, but it did not yet exist in the literature. Using discrete electronic components we designed an equivalent electric model of the Grudzinski and Zebrowski oscillator

The coupling of these self- sustained oscillators (Van der Pol, Grudzinski and Zebrowski) to an electrical charge made up of one or more conventional electrical components such as the resistance R, the inductance L and the capacitance C, could be interesting as it would have a behavior close to that of the pacemaker maintain the rest of the heart or the rest of the body [16].

The Hindmarsh-Rose oscillator is a self-sustained biological oscillator whose dynamics is based on the overall behavior of neurons [17, 18]. The Hindmarsh-Rose model

is commonly used to study the behavior of interacting neurons [19]. Its coupling with an electrical load made up of resistance R, inductance L and capacitor C will be studied to analyze how neurons behave when powering electrical loads.

The dynamics of synchronized oscillators is revelant in several fields such as engineering, medicine, astronomy, etc. [20]. The phenomenon of synchronization is extremely widespread in nature as well as in the realm of technology. In the study of several nonlinear dynamical systems, the study of synchronization was made. It was observed its important role in problems in various fields such as in biology and physics. Synchronization in systems of coupled oscillators provides a unifying framework for different phenomena observed in nature [21, 22]. Enjieu et al. [23] coupled a set of VdP oscillators and demonstrated that full synchronization is observed after critical values of the coupling coefficient and number of oscillators are reached. Nana and Woafo [24] investigated different states of synchronization in a ring of four mutually coupled Van der Pol oscillators, both in their regular and chaotic states. They were able to obtain the boundaries of the synchronization process when the external force is present. In the case of Grudzinski-Zebrowski oscillators, a synchronization study considering both the direct coupling and the indirect coupling is of interest and will be considered in this work.

Rhythms are found at all levels of the biological organization with periods ranging from fractions of a second to ten years [25]. The circadian rhythms observed in all eukaryotes and in some prokaryotes allow organisms to adapt and anticipate the alternation of day and night [26]. They are endogenous due to the fact that they result from internal mechanisms. The first work on the genetics of circadian rhythms focused on the locomotor activity cycle in Drosophila, which showed that this behavior is accompanied by circadian oscillations in the concentration of the protein efficiency ratio (PER) , and its messenger ribonucleic acid (RNA) [27, 28]. It was thought before the 1980s that only eukaryotic cells benefit from an endogenous circadian rhythm. But cyanobacteria (photosynthetic bacteria of the phylum Eubacteria) have also been shown to have an endogenous biological rhythm. Huang and al. [29, 30] were the pioneers in demonstrating the existence of circadian rhythms in cyanobacteria. From 1986, published articles showed that the three main characteristics (an endogenous free-running cycle, entrainability and temperature compensation) of circadian rhythms can be described in the same organism. The first to

demonstrate the temperature compensation of a daily rhythm in marine cyanobacteria were Sweeney and Borgese [31]. Cyanobacteria is one of the simplest organism with the circadian clock that produces stable rhythms close to 24 hours. $KaiC$ is always hexameric but the first model did not consider this. Its modeling was done in order to investigate on the properties of the circadian clock and the extension in the *in vivo* state will be the subject of this part study on must remember that this existence of the circadian clock is based on the phosphorylation of the central component. The objective is to show that the *in vivo* PTR (Post translational regulation) of the hexameric model has a wide range of values where there is oscillation. The cyanobacterial clock is constituted of an ensemble of monomeric units. Each monomeric unit or form is an oscillator as we presented in the first part of study on the cyanobacterial circadian clock. This clock can be considered as an ensemble of oscillators, which act in a synchronized manner to produce the signal. More importantly, we are also studying a coupling of two oscillators; the coupling of the transcriptional regulation oscillator (TTR) and the in vitro oscillator (PTR). The TTR regulation is the typical mechanism leading to oscillations in circadian clocks and consists of a negative feedback of the core protein of the clock on its own production. The PTR oscillator is the ensemble of monomeric units mentioned above and which can be reconstituted in vitro.

So this thesis will treat the following questions related to self- sustained oscillators of biological origin:

- Analyze the response of several heart cells modeled by the Van der Pol oscillator when they are coupled to a biological organ (load).
- Find an equivalent electrical circuit for the Grudzinski and Zebrowski oscillator and analyze the response of several heart cells modeled by the Grudzinski and Zebrowski oscillator when they are coupled to a biological organ (load).
- Analyze the response of several nerve cells modeled by the Hindmarsh-Rose oscillator when they are coupled to a biological organ (load).
- Propose an *in vivo* model of the cyanobacterial circadian clock based on the *in vitro* model and analyze the existence of ranges of values where there is oscillation.

The thesis is structured as follows:

- The first chapter presents the literature review and details the problem to solve.
- In chapter 2, we focus on the mathematical formalism, numerical and analytical methods used to characterize the dynamics of the systems studied.
- Chapter 3 is devoted to the presentation of the results obtained.
- We end this thesis with a conclusion containing the main results and perspectives for future investigations.

Chapter I

Litterature review

1.1 Introduction

The purpose of this chapter is to present some known results on the electrical models modeling the heart cells, the neurons and the circadian cycle and then present the questions adressed in this thesis. Section 1.2 deals the electrical models of the pacemakers. Electrical models of nerve cells are presented in section 1.3. Section 1.4 presents the models of circadian cycle. The problems to be solved are detailed in section 1.5. Section 1.6 concludes the chapter.

1.2 Electrical models of the pacemakers

There are several models describing cardiac electrical activity, classified into two categories: physiological models and reduced membrane models. Physiological models, which are models closely related to the techniques of recording experimental data, attempt to integrate as much information as possible in order to account for the most important and complicated electro-physiological phenomena. As for the reduced membrane models, they are subdivided into two sub-groups: ionic and non-ionic models. In non-ionic models, there are two categories: models from physics and phenomenological models. We will consider for the rest of the work the models from physics which are characterized by an analogy with the models of relaxation oscillators. These are electrical circuits capable of moving alternately between two operating states of different energies without external sources such as the RLC circuit with nonlinear Van der Pol damping coefficient [32] and the RLC circuit with Nagumo diode [33].

1.2.1 Basic models

The heart cells are surrounded by a membrane crossed by channels, which, when opened, allow ions to pass through and generate a certain current. At rest, these cells are polarized: $\ominus$ inside and $\oplus$ outside, due to the differences in ion concentrations on either side of the membrane: -Sodium Na and Calcium Ca on the outside, - Potassium K on the interior. Excited by a stimulus, these cells respond, with a variation of the membrane potential with respect to time. A model of the heart cell takes into account the structure of the cell, the internal and external ionic environment, and the dynamic properties of the membrane.

So each heart cell is modeled separately depending on where it is located.

Basic electrical models of the heart cells have been improved over the years by various researchers. Hodgkin and Huxley published in 1952 their ionic theory of the genesis of membrane-level action potential for the giant squid axon [10]. It models the action potential from three ionic currents, mainly due to sodium (incoming current responsible for depolarization) and potassium (outgoing current responsible for repolarization) and a low leakage current due to chlorine. Their work established the foundations of current electrophysiology. Thus, the human atrial cell model is based on a classic Hodgkin and Huxley formulation coupled with a compartment model to describe changes in concentrations in the cytoplasm and RS (Sarcoplasmic Reticulum) [34]. FitzHugh and Nagumo in 1961 modified the Bonhoeffer-Van der Pol model which has only two state variables representative of the excitability and inexcitability of the cell. While taking into account the geometric analysis in the phase plane, this led to a good understanding of the dynamics. We can cite among others Noble who proposed the model of cardiac cells in 1962 [35] where he studied the Purkinje network cells which seem to be easier to study due to their large size. This model encounters the drawback of not being able to explain the return of sodium and potassium concentrations to their initial level. Other models have emerged in order to seek to remedy these shortcomings. In 1985, Di Francesco and Noble modeled pumps and exchangers [36], by a model describing depolarization by the rapid sodium channel and repolarization by three potassium channels and two calcium channels. Two transporters were modeled: the Na^+/K^+ pump and Na^+/Ca^{2+} exchanger whose action allows the sodium, potassium and calcium concentrations to return to their initial states. Luo and Rudy in 1994 proposed a model of a ventricular cell which took into account the intracellular mechanisms of calcium regulation [37, 38]. These models were derived from experiments on the ventricles of animals, but Ten Tusscher proposed a model that was more suited to human ventricles [39].

1.2.2 Van der Pol oscillator

The Van der Pol is considered as a relaxation oscillator. In order to reproduce heartbeat rhythms, multiple models were proposed over the last hundred years. Most of these models can be classified into two categories: HH (Hodgkin and Huxley)-type models and

relaxation oscillator models. One of the pioneering models based on relaxation oscillations was proposed by Van der Pol and Van der Mark [11]. In 1928, they published an article in which they presented an electrical model of the heart [40]. The original electrical model was based on a triode as presented in figure 1.1. It delivered self-sustained oscillations.

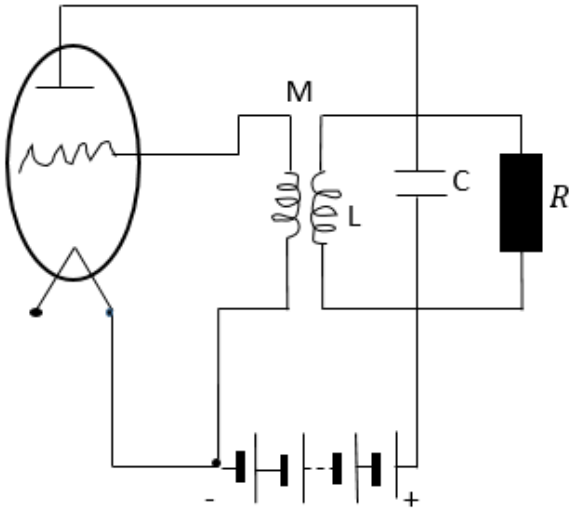

Figure 1.1: Original Van der Pol oscillator.

With the advent of modern electronics, the original model can be replaced by the new model given in figure 1.2 where NLR is the nonlinear part of the resistance with the following $i-v$ characteristics is $i_{vj} = -a\left(\frac{v_j}{V_0}\right) + b\left(\frac{v_j}{V_0}\right)^3$ where a, b and V_0 are the positive parameters.

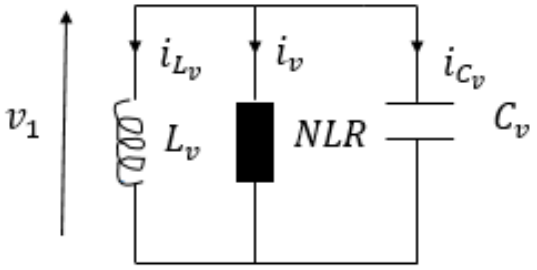

Figure 1.2: Electrical circuit for the Van der Pol oscillator.

By applying the Kirchhoff laws on this circuit, on finds that the electric potential v_1 is described in dimensionless form by equation (1.1).

$$\ddot{x} - d\left[1 - x^2\right]\dot{x} + x = 0 \tag{1.1}$$

The Van der Pol oscillator has been studied extensively for several years and is considered to be the classic prototype of a self-sustaining oscillator [11]. It is used to model oscillations in several areas such as biological rhythms, heartbeats, electrical circuits and circadian rhythms [24].

Gois and Savi [41] proposed a mathematical model based on the Van der Pol equations to emulate the cardiac conduction system composed of a Sino-Atrial node (SA), Atrio-Ventricular node (AV) and His-Purkinje system (HS). These equations were added to calculate the response of an oscillator system in the form of electrocardiogram (ECG). This allowed them to evaluate heart functioning qualitatively and gave an opportunity to compare the obtained results with the experimental (clinical) data. Bernardo et al. [42] suggested a model of two coupled Van der Pol oscillators to generate the action potential by the SA and AV nodes. Santos et al. [43] used a model composed of two coupled Van der Pol oscillators with unidirectional or bidirectional coupling and subjected to external driving. The sinus node (AS) and the atrioventricular node (AV) are modeled by a coupling of Van der Pol oscillators with the aim of being able to explain beat phenomena such as the Wenckebach periodicity, extra systoles, and pseudo-blocks [44]. Other papers have used Van der Pol's model to also model heartbeats [45, 46]. Makouo and al. [47] were able to highlight the pulsed behavior of the Van der Pol oscillator numerically and experimentally subjected to two types of excitations and showed that the period of the bursting oscillations diminishes when the excitation frequencies increase. Nana et al. [16] studied theoretically and experimentally the dynamics of a set of Van der Pol oscillators coupled to an RLC load and were able to show that the power delivered to the load by the array of active oscillator increases with the number of oscillators till a limiting value increasing with the quality factor of the load. In this thesis, we consider the same model and add a high degree of nonlinearity.

1.2.3 Grudzinski and Zebrowski oscillator

Since the Van der Pol oscillator does not capture all the signals observed biologically, the researchers thought about modifying it so that it could reproduce physiologically important properties, such as the refraction period, phase-sensitivity properties, and modes of change of the action potential frequency. It is with this in mind that two researchers Grudzinski and Zebrowski thus added more terms in the Van der Pol equation to obtain equation (1.2) with the coefficients given in (1.3).

$$\ddot{x} + \beta\left(x^2 - (\theta_1 + \theta_2)x + \theta_1\theta_2\right)\dot{x} + x + \frac{(\gamma+\eta)}{\gamma\eta}x^2 + \frac{x^3}{\gamma\eta} = 0 \tag{1.2}$$

$$\beta = 3; \theta_1 + \theta_2 = 0; \theta_1\theta_2 = -0.6889; \frac{1}{\gamma\eta} = 0.05; \frac{(\gamma+\eta)}{\gamma\eta} = 0.5 \tag{1.3}$$

The time series of x for different values of the coefficient lead to shape very close to the physiological voltage delivered by the pacemaker by providing pulsatile shape with resting period. They discussed the possibility of modeling the properties of the conduction system of the heart using equation (1.2). Zebrowski et al. [6] also relied on the mathematical model of Grudzinski and Zebrowski and were able to reproduce the decrease of heart rate variability with an increase in sympathetic activity, several phenomena well known in cardiology, such as certain properties of the sinus rhythm and heart block. Behnia et al. [14] used this and showed the chaotic effects on the external stimuli on the heartbeat dynamics. In addition, they showed that one can be able to discern either normal or abnormal behavior of the cardiac pacemaker. Ryzhii et al. [48] presented a novel model of cardiac conduction system including the main pacemakers and heart muscles. The modified Van der Pol oscillator used to model the sinoatrial node, atrioventricular node and Purkinje fiber. Their complete model allows to reproduce several well-known electro-cardiological phenomena, such as tachycardia, complete heart block, atrial flutter, and ventricular fibrillation. Cardarilli et al. [49] improved the work of Ryzhii and Ryzhii, by coupling four oscillators and obtained the same results, but also reproduced the communication interruption in the heart electrical conduction system when one of the bundle branches does not work. Fabi´an et al. [50] proposed an approach for modeling cardiac pulses from electrocardiographic signals (ECG). Therefore they took as a mathematical model that of Grudzinski and Zebrowski and showed that the model used can resemble the ideal cardiac rate pulse under optimal parameters.

Considering the fact that the equivalent electrical circuit of the Grudzinski and Zebrowski oscillator does not exist, we design one in this thesis. Moreover, we analyze the response of several heart cells modelled by the Grudzinski and Zebrowski oscillator when they are coupled to a biological organ (load) to control or excite it. To the best of our knowledge, this question has not yet be considered.

1.3 Electrical models of nerve cells

Nerve cells, inlike other cells in the body, have a more complex structure. A neuron is a cell with all the characteristics of a classic octopus-like cell, with arms (which can be either a dendrite or an axon) that go all over the place. It contains the same organelles and cytoplasmic elements as other cells in the body.

The most common type of neuron in the brain has several dendrites, but only one axon (figure 1.3). Its role is to process a nervous message by receiving, treating and transmitting. The transmission of information within a nerve fiber corresponds to the propagation along the fiber of potential differences called action potentials. The nerve fiber, or axon, is a linear outgrowth of the nerve cell that transmits electrical impulses through the nervous system.

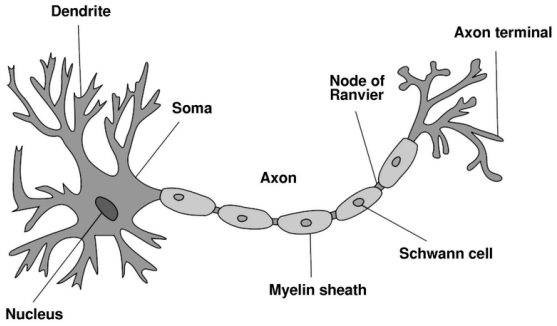

Figure 1.3: Schematic of a neuron.

There are different types of electrical modeling of nerve cells: multi-compartment models, the Hodgkin-Huxley model, the phenomenological model (integrates - and - pulls) and discharge rate models.

1.3.1 Hodgkin-Huxley model

Nerve impulse was first modeled by Hodgkin and Huxley in 1952, with the aim to correctly predict the main characteristics of excitability, like the shape of the action potential, the speed of conduction. This model is cited as a reference to describe the electrical activity of the membrane potential of nerve cells. The Hodgkin-Huxley's work associated with those of John Carew Eccles on synaptic mechanisms allowed them to share the Nobel Prize of Medicine in 1963. The equivalent electrical circuit of this model is presented in figure 1.4.

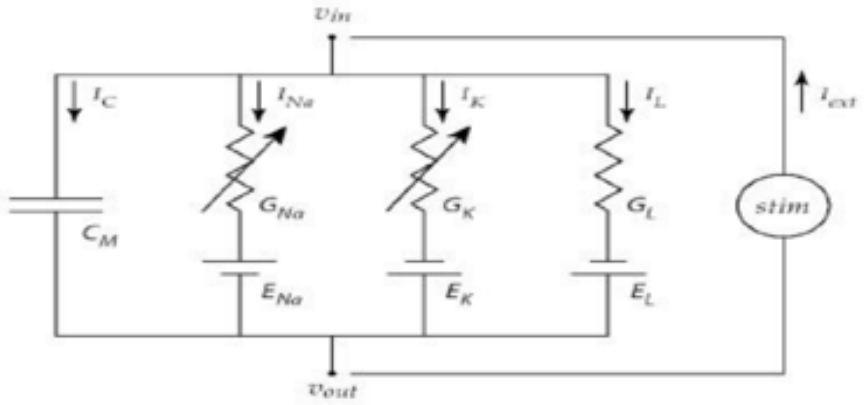

Figure 1.4: Equivalent electrical circuit of the cell membrane

The different branches that make up this electrical circuit are the C_{MEM} membrane capacitance which separates the extra and intracellular media, the sodium (Na) and potassium (K) current generators which have voltage dependent conductances and finally a constant conductance leakage channel.

Mathematically, the current flowing through the membrane is written as (1.4)

$$I_C = C_{MEM} \frac{dV_{MEM}}{dt} \tag{1.4}$$

and the current through a given ion channel is the product (1.5)

$$I_i = g_i \left(V_{MEM} - V_i\right) \tag{1.5}$$

where V_i is the reversal potential of the $i-th$ ion channel. Thus, for a cell with sodium and potassium channels, the total current through the membrane is given by:

$$I = C_{MEM} \frac{dV_{MEM}}{dt} + g_{Na} \left(V_{MEM} - V_{Na}\right) + g_K \left(V_{MEM} - V_k\right) + g_{leak} \left(V_{MEM} - V_{leak}\right) \tag{1.6}$$

where I is the total membrane current per unit area, C_{MEM} is the membrane capacitance per unit area, g_K and g_{Na} are the potassium and sodium conductance per unit area, respectively, V_K and V_{Na} are the potassium and sodium reversal potentials, respectively, and g_{leak} and V_{leak} are the leak conductance per unit area and leak reversal potential, respectively. The time dependent elements of this equation are V_{MEM}, g_{Na}, and g_K, where the last two conductance depend explicitly on voltage as well.

Using a series of voltage clamp experiments and by varying extracellular sodium and potassium concentrations, Hodgkin and Huxley developed a model in which the properties of an excitable cell are described by a set of four ordinary differential equations [10]. The Hodgkin-Huxley model, or conductance-based model, is a mathematical model that describes how action potentials in neurons are initiated and propagated. It is a set of nonlinear differential equations that approximates the electrical characteristics of excitable cells such as neurons and cardiac myocytes. It is a continuous-time dynamical system. Together with the equation for the total current mentioned above, the set of equations is given in (1.7).

$$\begin{cases} I = C_{MEM}\frac{dV_{MEM}}{dt} + \overline{g}_K n^4 \left(V_{MEM} - V_k\right) + \overline{g}_{Na} m^3 h \left(V_{MEM} - V_{Na}\right) + \overline{g}_{leak} \left(V_{MEM} - V_{leak}\right) \\ \frac{dn}{dt} = \alpha_n \left(V_m\right)(1-n) - \beta_n \left(V_m\right) n \\ \frac{dm}{dt} = \alpha_m \left(V_m\right)(1-m) - \beta_m \left(V_m\right) m \\ \frac{dh}{dt} = \alpha_h \left(V_m\right)(1-h) - \beta_h \left(V_m\right) h \end{cases} \tag{1.7}$$

where α_i and β_i are rate constants for the $i-th$ ion channel, which depend on voltage but not time. $\overline{g}_n$ is the maximal value of the conductance. n , m , and h are dimensionless quantities between 0 and 1 that are associated with potassium channel activation, sodium channel activation, and sodium channel inactivation, respectively.

The Hodgkin and Huxley model later formed the basis for many other electrical models of nerve cells [51–53]. Thus, in 1961 Fitzhugh [54] derived a simplified model of the nerve cell equation. Subsequently the very first model of Hindmarsh and Rose [55] was presented in 1982 and improved in 1984. All the modifications that the Fitzhugh-Nagumo model underwent made it possible to reproduce most of the behaviors observed in neurons, such as the slow-rapid phenomena of oscillations in bursts or even regular or irregular emissions of action [56].

1.3.2 Hindmarsh-Rose model

In 1982, Hindmarsh and Rose (HR) simplified the Hodgkin-Huxley model to a system of two ordinary differential equations [17, 55]. This new oscillator model is capable of reproducing many of the generic bifurcation scenarios present in more realistic models. The Hindmarsh and Rose oscillator is adapted for a slow-fast system. It has the advantage of being simple than the H-H model. There are two models of Hindmarsh and Rose oscillators: one with two first order differential equations and the other with three first order differential equations.

The Hindmarsh and Rose two-equation model exhibits neuron signal going from a stable resting state to stable emissions of action potentials by applying a positive excitation of short time. This model is defined by the differential equations given in (1.8).

$$\begin{cases} \dot{x} = -x^3 + w + a_1 x^2 + I \\ \dot{w} = 1 - dx^2 - w \end{cases} \tag{1.8}$$

where a_1 and d are the positive constants.

The two equations model is not capable of reproducing bursting or trains of action potentials which are sometimes delivered by the neurons. Because of this limit, Hindmarsh and Rose proposed in 1984 the three equations model by adding a third equation which takes into account the slowly changing current. So the three equations model is described by the following set of equations given in (1.9) where a_0 is the coordinate of the stable equilibrium of the two-equation system (1.8) when $I = 0$.

$$\begin{cases} \dot{x} = -x^3 + w + a_1 x^2 + I - z \\ \dot{w} = 1 - dx^2 - w \\ \dot{z} = \gamma \left(s \left(x - a_0 \right) - z \right) \end{cases} \tag{1.9}$$

where x corresponds to the membrane potential, which measures the potential difference between the interior and exterior of the neuron, w describes the exchange of ions through the membrane by fast channels, while z describes the exchange of ions through the membrane by slow channels. a_1 indicates the qualitative behavior of the oscillator. a_0 is the resting potential of the system. I is the external current injected in the oscillator. d is a positive constant while S and γ are constants of small values. The parameter d is not a crucial parameter for the elaboration of the different characteristics of the oscillations

that are peculiar to the Hindmarsh-Rose oscillator whereas depending on the values of parameters (I, γ , S), we can have several kinds of dynamics which correspond to the different signals delivered by real neurons [57]:

- Quiescence: the input to the neuron is below a certain threshold and the output reaches a stationary regime.
- Spiking: the output is made up of a regular series of equally spaced spikes.
- Bursting: the output is made up of groups of two or more spikes called bursts separated by periods of inactivity. The successive impulses can have different amplitudes
- Irregular spiking: the output is made up of an aperiodic series of spikes.
- Irregular bursting: the output is made up of an aperiodic series of bursts.

Since the Hindmarsh-Rose works, several researchers have been working on the Hindmarsh-Rose model in order to be able to better explain nerve cells dynamics. Kazemi et al. [18] proposed a digital structure for HR model and performed simulations which showed that the outputs of proposed circuit can mimic the original model with a high match. Corson et al. [58] made a numerical study on the Hindmarsh-Rose model and a discussion on the chaotic dynamics of the HR model was done and they showed that the parameters such as the time scale difference between the slow dynamics and the rapid dynamics γ , and the current I applied to the neuron to stimulate, have been designated as bifurcation parameters for their biological interest. Moreover, Carson et al. [59] made a study on the analysis of the asymptotic dynamics of Hindmarsh-Rose model and showed that the slow-fast motions due to the small parameter γ makes the dynamics even more interesting. Ginoux and al. [60] presented a method that may be able to capture the slow variety of the Hindmarsh-Rose model. Storace and al. [61] analyzed the bifurcations using the HR model and were able to conclude that the bifurcation scenario, gives concrete information about the HR model and its organizing principles that are useful in more biophysically oriented studies.

All of the above works on HR aimed at better understanding of the nerve cells dynamics. But none of them considered the response of several nerve cells modeled by the

Hindmarsh-Rose oscillator when coupled to a biological organ (load) to control or excite it. This question will be considered in this thesis.

1.4 Models of the circadian cycle

Humans, animals and plants are all subject to natural rhythms which are a periodic or cyclical variation of a particular function of a living being. It can be of several types: either physiological (heartbeat, cerebral electrical activity, etc), biochemical (molecular synthesis, hormonal, etc) or behavioral (sleep). The notion of rhythm of living beings was described as far back as the 4th century BC by Androsthenes Thasius [62].

Most organisms possess a circadian clock allowing them to anticipate the day and night cycle. Most living organisms have their internal clock. The clock plays an important role in the functioning of the body. It controls the major biological functions such as sleep, body temperature and the immune system [63]. Thanks to the circadian clock, the secretion of melatonin begins at the end of the day, and sleep is deep during the night. This clock is nestled in the brain which imposes the circadian rhythm on the body like a conductor. In humans, this clock is found in the hypothalamus, which is made up of two suprachiasmatic nuclei, each containing about 10,000 neurons that exhibit electrical activity oscillating over about 24 hours. This electrical activity is controlled by the cyclic expression of about 15 clock genes. The internal clock is therefore continuously resynchronized over a 24 hour cycle by external agents. [64].

1.4.1 Studies on biological clocks

The first publication that can be linked to the existence of the biological clock dates from 1729 by the French astronomer d´Ortous de Mariam [65]. Thirty years later, other researchers made the same observation, showing that leaf movements were not due to the variations in ambient temperature. In 1832, de Candole noticed that the rhythm of leaf movements had a period a little shorter 24 hours [66]. In the years of 1920-1930, Karl Von Frish and his student Ingeborg Beling showed that bees only forage on flowers at very specific times and that the deletion of environmental data such as daily illumination did not modify the behavior of bees that obeyed internal programming [67]. Subsequently,

Kramer proved the existence of a biological clock in the 1950s. Pittendrigh demonstrated in 1952 that unlike most metabolic activities, the biochemical mechanisms of the clock were not influenced by the body temperature and that the clock period was independent of temperature (temperature compensation). Subsequently, he resumed the work of Klamus on the hatching rate of a species of fly *Drosoplila pseudoobscura* (which concludes that the period of the hatching rate increased from 24 h to 36 h) and showed that the second peak hatching was much less late than the first and that the rhythm then resumed with an almost unchanged period, close to 24 hours, which shows the temperature compensation. His results thus established the main universal characteristics of the circadian clock. The locomotive activity cycle in Drosophila made use of the early work on the genetics of circadian rhythms. This work showed that cyclic behavior is accompanied by circadian oscillations in the concentration of the PER (Protein Efficiency Ratio) and its RNA (Ribonucleic acid) messenger [68, 69]. The mechanism of the circadian rhythm is based on the negative feedback regulation exerted on the PER protein on the expression of its own gene [68] and involves the phosphorylation of the PER protein which leads to its degradation and entry into the nucleus. In the circadian clock mechanism in mammals [70], there is a similar set of interlocking positive and negative regulations. This study leads to several predictions that reveal the possibility of multiple sources of oscillations in the genetic regulatory network controlling the circadian rhythms.

1.4.2 Models for cyanobacteria

Cyanobacteria are the classes of bacteria (2-8 micrometers in length and 1 micrometer in width) commonly known as blue algae. They are prokaryotic photosynthetic cells due to the fact that they use sunlight as an energy source. Due to its photosynthetic activity, cyanobacteria are responsible for the enrichment of oxygen in the atmosphere. Spherical, filamentous and rod shaped, they reproduce by binary section. It is one of the simplest genetically tractable organism known to possess a circadian clock. It is experimentally tractable because cyanobacteria are easy to grow, fast to reproduce and the state of the clock is measurable *in vivo* via yellow fluorescent protein. This biological clock improves the survival of cyanobacteria by allowing them to easily adapt to daily variations in the environment. It also controls the division of its cells. The cyanobacteria is a living

organism, it is much more complicated than 3 proteins. The cyanobacterial circadian clock is composed of three proteins: $KaiA$, $KaiB$ and $KaiC$ which put together in the presence of ATP in a test tube, can generate self-sustained oscillations of 24 hours period [71]. These oscillations correspond to the phosphorylation of the $KaiC$ protein. In the absence of the $KaiA$, $KaiC$ completely de-phosphorylates. As for the $KaiB$ protein, it interferes with the activity of $KaiA$ on $KaiC$. The $KaiC$ protein happens to be the main component of the process. It can self-phosphorylate and self-de-phosphorylate at S (Serine 431) and T (Threonine 432) residus which are two of the four forms of phosphorylated $KaiC$. The other two forms are U (unphosphorylated), and ST (doubly phosphorylated at T and S).

So, the modeling of cyanobacterial circadian clock focuses on the structure of the $KaiC$ protein. The simplest stucture is that of modeling $KaiC$ as a monomer and the most complex is that of modeling $KaiC$ as a hexamer.

The modeling of cyanobacterial circadian clock has attracted the attention of several researchers.

A mathematical model of the *in vitro* clock relying on careful experiments measuring all kinetic rates and concentrations of proteins involved was proposed in [72]. This simple model beautifully reproduces oscillations with a period of about 24 hours, without any parameter space exploration as all parameters have been measured. Shu-Wen Teng et al. in 2013 [73] proposed an extension to the *in vivo* case. This model showed that PTR regulation is sufficient to generate oscillations, as observed in the experiments with mutant cyanobacteria lacking the TTR regulation. It also showed that the transcriptional regulation helps maintaining synchrony in a population of growing cyanobacteria. However, the model requires finely tuned parameters to lead to oscillatory behavior of the mutant cyanobacteria lacking the transcriptional regulation. The *in vitro* model it is based on did not explicitly described the hexameric structure of the $KaiC$ protein. More recently, a more realistic model of the *in vitro* clock has been proposed in [74]. It describes explicitly the hexameric nature of $KaiC$ and the binding of $KaiB$ to $KaiC$. Kitayama1 and al. [75] also studied cyanobacteria as being hexameric assuming that the $KaiC$ hexameric structure is critical for regulation of the circadian clock. However, the underlying molecular mechanism of such regulation remained unclear. They found that local interactions at subunit interfaces regulate the $KaiC$ activities by coupling the nucleotide-binding states.

Several researchers have studied cyanobacteria and looked for the phosphorylation of $KaiC$ which would amplify the existence of the biological clock. In this thesis, we propose here to build an *in vivo* model based on this more realistic *in vitro* model.

1.5 Problems to be solved

As indicated above, in this thesis, we will solve four problems. It is therefore a question here of recalling the problems which were mentioned in the preceding pages.

1.5.1 Problem 1

Analyze the response of several heart cells modeled by the Van der Pol oscillator when they are coupled to a biological organ (load). Here the order of the nonlinearity of the Van der Pol oscillator has been increased to see its influence on the variation of the electric power in the load.

1.5.2 Problem 2

Find an equivalent electric circuit for the Grudzinski and Zebrowski oscillator making use of the differential equations of the Grudzinski and Zebrowski oscillator. After finding this circuit, it will be a question of analyzing the response of several heart cells modeled by the Grudzinski and Zebrowski oscillator when they are coupled to a biological organ (charge) to control or excite it and determine the variation of the electrical power in the load.

1.5.3 Problem 3

Analyze the response of several nerve cells modeled by the Hindmarsh-Rose oscillator when they are coupled to a biological organ (load) and determine the variation of the electrical power in the load.

1.5.4 Problem 4

Investigate the stability of the circadian clock in cyanobacteria taken as a monomer and to extend in the vivo state of the cyanobacteria taken in a hexamer form. Compare the robustness of the hexameric model *in vivo* and *in vivo* with the monomeric model.

1.6 Conclusion

In this chapter, we provided some background about the electrical models of pacemakers (Van der Pol oscillator and Grudzinski and Zebrowski oscillator), about the model of nerves cells (Hodgkin- Huxley model and Hindmarsh-Rose model) and about the models of the circadian cycle (models for cyanobacteria). The problems that we will have to solve in the thesis have also been presented. The following chapter will be devoted to the mathematical formalisms, numerical simulation method used to solve the problems of the thesis.

Chapter II

Modeling, mathematical, numerical methods and electronic implementation

2.1 Introduction

In the previous chapter, we presented some background about the electrical models pacemakers (Van der Pol oscillator and Grudzinski and Zebrowski oscillator), about the model of nerves cells (Hodgkin- Huxley model and Hindmarsh-Rose model) and about the models of the circadian cycle (models for cyanobacteria). The objective of this chapter is to present the methods used to understand the dynamic behavior of its different models. The analytical numerical methods used to carry out our study will be listed below.

2.2 Modeling the coupling of a load to arrays of electrical oscillators

2.2.1 Physical modeling of the coupling

a) Coupling one oscillator to a load

In the case of an oscillator coupled to a load, there can only be direct coupling between the two circuits. Figure 2.1 shows the coupling between the Van der Pol oscillator and the RLC load through the capacitor C_0.

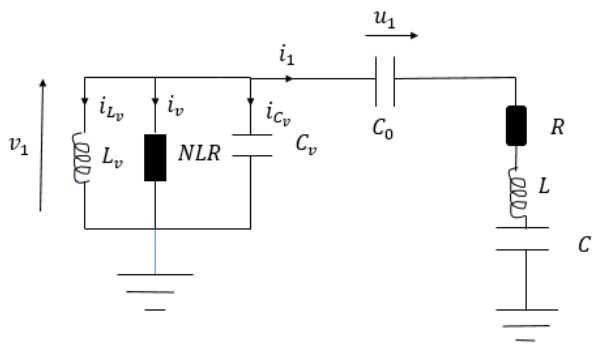

Figure 2.1: Van der Pol oscillator coupled directly with the RLC load.

b) Coupling many oscillators to a load

Figure 2.2 shows a set of Van der Pol oscillators coupled directly to each other using a capacitor C_2, this set of oscillators is then indirectly coupled to the RLC load C_0. Figure 2.3 shows a set of Van der Pol oscillators coupled indirectly to each other using a capacitor C_0, this set of oscillators is then indirectly coupled to the RLC load.

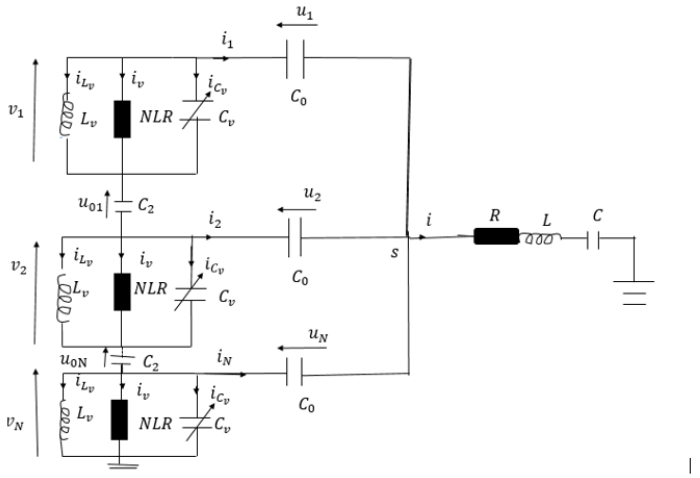

Figure 2.2: Array of mutually coupled Van der Pol oscillators indirectly coupled by a RLC load.

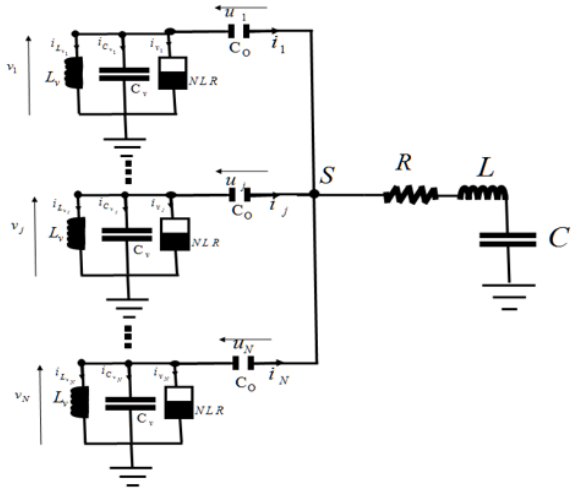

Figure 2.3: An array of Van der Pol oscillators coupled to a RLC oscillator.

2.2.2 Mathematical modeling

The first electrical model of the heart to be used is that of an array of Van der Pol oscillators indirectly coupled via capacitors to a resonant RLC load. The Van der Pol oscillator was the first oscillator to mimic the behavior of the heart, in order to obtain the differential equations corresponding to the system studied, we use Kirchhoff's laws to the system which express the conservation of energy and of the load in an electrical circuit. They bear the name of the German physicist who established them in 1845 by Gustav Kirchhoff. In a complex circuit, it is possible to calculate the potential differences at the terminals of each resistance and the intensity of the direct current in each branch of circuit by applying the two laws of Kirchhoff: the law of nodes and the law of meshes.

Considering figure 2.3 of the j-th oscillator and using Kirchhoff's laws, we have the following equations:

$$C_v\ddot{v}_j - \left[-a - 3b\left(\frac{v_j}{V_0}\right)^2\right]\frac{\dot{v}_j}{V_0} + C_0\ddot{u}_j + \frac{1}{L_v}v_j = 0 \tag{2.1}$$

$$\sum_{k=1}^{N}\left(L\ddot{u}_k + R\dot{u}_k + \frac{1}{C}u_k\right) = \frac{1}{C_0}\left(v_1 - u_1\right) \tag{2.2}$$

with $2 \leq j \leq N$

Subsequently, to have the characteristic Van der Pol equations coupled to the load, we will proceed by a change of variables, which induces a normalization of the voltage as $x_j = \frac{v_j}{V_0}$ and $y_j = \frac{u_j}{V_0}$ with time which is also normalized in the form $t_{ref} = \frac{1}{\omega_0}$. Where $\omega_0 = \frac{1}{\sqrt{L_v C_v}}$ is the natural frequency of the electric oscillator.
By replacing each term by its normalized value in equations (2.1), (2.2) we obtain the system of equations (2.3) describing the dynamics of the system

$$\begin{cases} \ddot{x}_j + \alpha\ddot{y}_j - d\left[1 - x_j^2 + bx_j^4\right]\dot{x}_j + x_j = 0; 1 \leq j \leq N \\ \sum\limits_{k=1}^{N}\left(\ddot{y}_k + \lambda\dot{y}_k + \mu y_k\right) = \beta\left(x_1 - y_1\right) \end{cases} \tag{2.3}$$

where $\lambda = \frac{R}{L\omega_0}, \mu = \frac{L_v C_v}{LC}, \beta = \frac{L_v C_v}{LC_0}, \alpha = \frac{C_0}{C_v}$ and $d = \frac{a}{C_v V_0 \omega_0}$

2.3 Modeling the protein KaiC kinetics in cyanobacteria

An image of cyanobacteria is presented in figure 2.4. The cyanobacterial clock can be described based on the monomer structure or based on the hexamer structure. They key element cyanobacterial clock is the phosphorylation level of its $KaiC$ protein, which is a hexameric protein. The simplest mathematical model of this clock did not take into account the hexameric character of the protein [73]. More recently, a model investigating the role of the hexameric structure has been proposed [74], they show that when $KaiC$ hexamers consist of a mixture of differentially phosphorylated subunits, the two phosphorylation sites have opposing effects on the ability of each hexamer to bind to the negative regulator $KaiB$. They likewise show that the ability of the positive regulator $KaiA$ to act on $KaiC$ depends on the phosphorylation state of the hexamer and that $KaiA$ and $KaiB$ recognize alternative alternative allosteric states of the $KaiC$ ring.

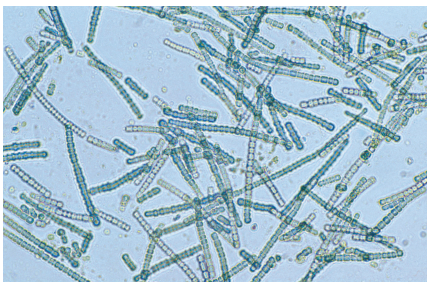

Figure 2.4: An image of cyanobacteria [76].

2.3.1 A simple model of the cyanobacterial circadian clock

The modeling of cyanobacterial clock focuses on phosphorylation state of the $KaiC$ protein which is its central component. The simplest model considers $KaiC$ as a monomeric protein. The $KaiC$ protein can be in one of its four phosphoforms: U (not phosphorylated); S (phosphorylated to serine); T (phosphorylated to threonine) and ST (doubly phosphorylated at serine and threonine). S, T, ST and U are also the concentrations of $S-KaiC$ ($KaiC$ phosphorylated only on serine), $T-KaiC$ ($KaiC$ phosphorylated only on threonine), $ST-KaiC$ ($KaiC$ phosphorylated on both serine and threonine) and $U-KaiC$ (unphosphorylated $KaiC$) respectively.

The transformations between different forms are given as in chemical kinetics as presented in figure 2.5. The concentration of the ST forms will be noted D.

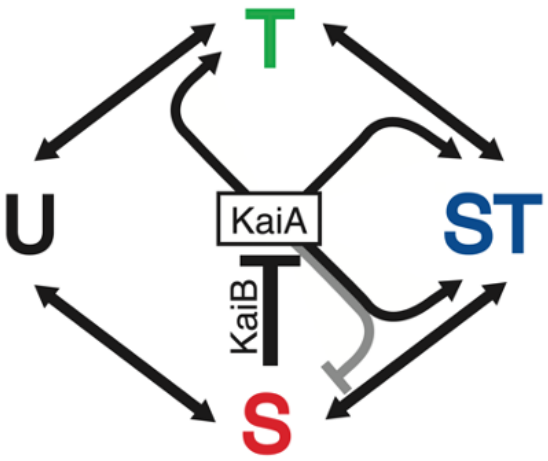

Figure 2.5: Transformations between different forms of the $KaiC$ protein [73].

The resulting equations of kinetics of the interconversions between phosphoforms are of first order but with the rates depending on S. They are given by the system of equations (2.4).

$$\begin{cases} \frac{dT}{dt} = k_{UT}(S) * U + k_{DT}(S) * D - k_{TU}(S) * T - k_{TD}(S) * T \\ \frac{dS}{dt} = k_{US}(S) * U + k_{DS}(S) * D - k_{SU}(S) * S - k_{SD}(S) * S \\ \frac{dD}{dt} = k_{TD}(S) * T + k_{SD}(S) * S - k_{DT}(S) * D - k_{DS}(S) * D \\ k_{XY}(S) = k^0_{XY} + \frac{k^A_{XY} * A(S)}{k_{1/2} + A(S)} \\ A(S) = \max\{0, [kaiA] - 2 * S\} \end{cases} \tag{2.4}$$

Equation (2.4.a) indicates that the rate of change of the concentration of the T form is composed of a growth term resulting from the phosphorylation of U at the residue T with a k_{UT} coefficient, from a growth term resulting from the dephosphorylation of D to T with a k_{DT} coefficient, an inhibitory effect proportional to T which arises from the dephosphorylation of T into U with a k_{TU} coefficient and the dephosphorylation of T to D with a coefficient k_{TD}.

The equations for the rate of change other phosphoforms of $KaiC$ are similar.

The phosphorylation and the dephosphorylation rates from the state x to state y are denoted k_{xy}, with k^0_{xy} being the rate in the absence of $KaiA$ and k^A_{xy} being the maximal influence of $KaiA$ on that rate. If $KaiA$ promotes the transition, then $K^A_{xy} \succ 0$; if $KaiA$

inhibits the transition, then $K_{xy}^{A} \prec 0$. The explicit effects of $KaiB$ binding to $S-KaiC$ are not included in the model, as we assume that $KaiB$ is in excess at all times and that its binding with $S-KaiC$ is instantaneous.

The effect of $KaiB$ is therefore indirectly taken into account in the dependence of k_{xy} in S. Indeed, the form of k_{xy} is given in eq.(2.4.d) depend hyperbolically on the concentration $A(S)$ of $KaiA$ active monomers and is the source of the nonlinearitity in the model.

For the *in vivo* model, it is based on the *in vitro* model given previously. But, one adds terms for production K_S, dilution V_d and degradation term V . All phosphorylated forms of $KaiC$ are assumed to have the same linear dilution rate and degradation rate (V, K) . The terms of degradation of the mRNA is given by (V_m, K_m). The unphosphorylated form of $KaiC$ now appears with the addition of the term production. So equation (2.5) describes the *in vivo* model

$$\begin{cases} \frac{dU}{dt} = k_{TU}(S) * T + k_{SU}(S) * S - k_{UT}(S) * U - k_{US}(S) * U - V * \frac{U}{K+U} - V_d * U + K_s * M \\ \frac{dT}{dt} = k_{UT}(S) * U + k_{DT}(S) * D - k_{TU}(S) * T - k_{TD}(S) * T - V * \frac{T}{K+T} - V_d * T \\ \frac{dD}{dt} = k_{TD}(S) * T + k_{SD}(S) * S - k_{DT}(S) * D - k_{DS}(S) * D - V * \frac{D}{K+D} - V_d * D \\ \frac{dS}{dt} = k_{US}(S) * U + k_{DS}(S) * D - k_{SU}(S) * S - k_{SD}(S) * S - V * \frac{S}{K+S} - V_d * S \\ \frac{dM}{dt} = V_s * \frac{K_i^n}{K_i^n + C_r^n} - V_m * \frac{M}{K_m + M} \end{cases} \tag{2.5}$$

where $C_r = C_U * U + C_T * T + C_S * S + C_D * D$ is a transcriptional regulation knowing that the coefficients C_U, C_T, C_S, C_D are these parameters determine how $KaiBC$ transcription is repressed by each of the four phosphorylated forms of $KaiC$.

2.3.2 Hexameric model of the cyanobacterial circadian clock

In this part, we present the equations of the hexameric form as reported in Ref [77]. The $KaiC$ hexamers in the $KaiB$ binding competent state undergo a slow process associated with the CI ATPase activity that will result in the $KaiB * KaiC$ complex. They assume 6 $KaiB$ molecules bind in a concerted or highly cooperative manner to one $KaiC$ hexamer. For each $KaiB$ molecule, they assume that one $KaiA$ dimer can be sequestered. Each $KaiC$ hexamer has 6 subunits, each containing two sites which can be phosphorylated or dephosphorylated, can progress to a total of 12 possible reactions which will increase

or decrease i, j, k by 1. The equation thus describing the dynamics of our system with as hexamer is given by the equations below in (2.6).

$$\begin{aligned}
&\tfrac{d\left[KaiC_{i,j,k}\right]}{dt} = k_{UT}^{i,j,k}\,(7-(i+j+k))\,[KaiC_{i-1,j,k}] + \\
&k_{US}^{i,j,k}\,(7-(i+j+k))\,[KaiC_{i,j-1,k}] + \\
&k_{TD}^{i,j,k}\,(i+1)\,[KaiC_{i+1,j,k-1}] + k_{TU}^{i,j,k}\,(i+1)\,[KaiC_{i+1,j,k}] + \\
&k_{DT}^{i,j,k}\,(k+1)\,[KaiC_{i-1,j,k+1}] + \\
&k_{DS}^{i,j,k}\,(k+1)\,[KaiC_{i,j-1,k+1}] + k_{SD}^{i,j,k}\,(j+1)\,[KaiC_{i,j+1,k-1}] + \\
&k_{SU}^{i,j,k}\,(j+1)\,[KaiC_{i,j+1,k}] - \\
&\left(\begin{array}{l}(6-i-j-k)*k_{UT}^{i+1,j,k} + (6-i-j-k)*k_{US}^{i,j+1,k} + i*k_{TD}^{i-1,j,k+1} + \\ i*k_{TU}^{i-1,j,k} + k*k_{DT}^{i+1,j,k-1} + k*k_{DS}^{i,j+1,k-1} \\ +j*k_{SD}^{i,j-1,k+1} + j*k_{SU}^{i,j-1,k} + k_{on,B}*F_B^{i,j,k}\end{array}\right)*[KaiC_{i,j,k}] \\
&+k_{off,B}*[KaiB*KaiC_{i,j,k}]
\end{aligned} \tag{2.6}$$

By assuming $KaiC$ in a complex $KaiB*KaiC$, the latter can be activated by free $KaiA$, therefore an equation similar to the equation (2.6) is given in (2.7).

$$\begin{aligned}
&\tfrac{d\left[KaiB*KaiC_{i,j,k}\right]}{dt} = k_{UT}^{i,j,k}\,(7-(i+j+k))\,[KaiB*KaiC_{i-1,j,k}] + \\
&k_{US}^{i,j,k}\,(7-(i+j+k))\,[KaiB*KaiC_{i,j-1,k}] + \\
&k_{TD}^{i,j,k}\,(i+1)\,[KaiB*KaiC_{i+1,j,k-1}] + k_{TU}^{i,j,k}\,(i+1)\,[KaiB*KaiC_{i+1,j,k}] + \\
&k_{DT}^{i,j,k}\,(k+1)\,[KaiB*KaiC_{i-1,j,k+1}] + \\
&k_{DS}^{i,j,k}\,(k+1)\,[KaiB*KaiC_{i,j-1,k+1}] + k_{SD}^{i,j,k}\,(j+1)\,[KaiB*KaiC_{i,j+1,k-1}] + \\
&k_{SU}^{i,j,k}\,(j+1)\,[KaiB*KaiC_{i,j+1,k}] - \\
&\left(\begin{array}{l}(6-i-j-k)*k_{UT}^{i+1,j,k} + (6-i-j-k)*k_{US}^{i,j+1,k} + i*k_{TD}^{i-1,j,k+1} + \\ i*k_{TU}^{i-1,j,k} + k*k_{DT}^{i+1,j,k-1} + k*k_{DS}^{i,j+1,k-1} \\ +j*k_{SD}^{i,j-1,k+1} + j*k_{SU}^{i,j-1,k} + k_{off,B}*F_B^{i,j,k}\end{array}\right)*[KaiB*KaiC_{i,j,k}] \\
&+k_{on,B}*[KaiC_{i,j,k}]
\end{aligned} \tag{2.7}$$

The concentration of the $KaiC_{i,j,k}$ ($KaiC$ hexamer) and $[KaiB*KaiC_{i,j,k}]$ (the complex of $KaiC$ hexamer with $KaiB$) are described by the following set of differential equations

(2.8).

$$
\begin{cases}
\frac{d\left[KaiC_{i,j,k}\right]}{dt} = k_{UT}^{i,j,k}\left(7-(i+j+k)\right)\left[KaiC_{i-1,j,k}\right] + \\
k_{US}^{i,j,k}\left(7-(i+j+k)\right)\left[KaiC_{i,j-1,k}\right] + \\
k_{TD}^{i,j,k}\left(i+1\right)\left[KaiC_{i+1,j,k-1}\right] + k_{TU}^{i,j,k}\left(i+1\right)\left[KaiC_{i+1,j,k}\right] + \\
k_{DT}^{i,j,k}\left(k+1\right)\left[KaiC_{i-1,j,k+1}\right] + \\
k_{DS}^{i,j,k}\left(k+1\right)\left[KaiC_{i,j-1,k+1}\right] + k_{SD}^{i,j,k}\left(j+1\right)\left[KaiC_{i,j+1,k-1}\right] + \\
k_{SU}^{i,j,k}\left(j+1\right)\left[KaiC_{i,j+1,k}\right] - \\
\left(\begin{array}{l}
(6-i-j-k)*k_{UT}^{i+1,j,k} + (6-i-j-k)*k_{US}^{i,j+1,k} + i*k_{TD}^{i-1,j,k+1} + \\
i*k_{TU}^{i-1,j,k} + k*k_{DT}^{i+1,j,k-1} + k*k_{DS}^{i,j+1,k-1} \\
+j*k_{SD}^{i,j-1,k+1} + j*k_{SU}^{i,j-1,k} + k_{on,B}*F_B^{i,j,k}
\end{array}\right)*\left[KaiC_{i,j,k}\right] \\
+k_{off,B}*\left[KaiB*KaiC_{i,j,k}\right] \\
\frac{d\left[KaiB*KaiC_{i,j,k}\right]}{dt} = k_{UT}^{i,j,k}\left(7-(i+j+k)\right)\left[KaiB*KaiC_{i-1,j,k}\right] + \\
k_{US}^{i,j,k}\left(7-(i+j+k)\right)\left[KaiB*KaiC_{i,j-1,k}\right] + \\
k_{TD}^{i,j,k}\left(i+1\right)\left[KaiB*KaiC_{i+1,j,k-1}\right] + k_{TU}^{i,j,k}\left(i+1\right)\left[KaiB*KaiC_{i+1,j,k}\right] + \\
k_{DT}^{i,j,k}\left(k+1\right)\left[KaiB*KaiC_{i-1,j,k+1}\right] + \\
k_{DS}^{i,j,k}\left(k+1\right)\left[KaiB*KaiC_{i,j-1,k+1}\right] + k_{SD}^{i,j,k}\left(j+1\right)\left[KaiB*KaiC_{i,j+1,k-1}\right] + \\
k_{SU}^{i,j,k}\left(j+1\right)\left[KaiB*KaiC_{i,j+1,k}\right] - \\
\left(\begin{array}{l}
(6-i-j-k)*k_{UT}^{i+1,j,k} + (6-i-j-k)*k_{US}^{i,j+1,k} + i*k_{TD}^{i-1,j,k+1} + \\
i*k_{TU}^{i-1,j,k} + k*k_{DT}^{i+1,j,k-1} + k*k_{DS}^{i,j+1,k-1} \\
+j*k_{SD}^{i,j-1,k+1} + j*k_{SU}^{i,j-1,k} + k_{off,B}*F_B^{i,j,k}
\end{array}\right)* \\
\left[KaiB*KaiC_{i,j,k}\right] \\
+k_{on,B}*\left[KaiC_{i,j,k}\right]
\end{cases}
\tag{2.8}
$$

with $0 \leq i,j,k \leq 6$

The details allowing to arrive at the system of equations (2.8) describing the dynamics of the hexamer are given in appendix 2.

2.4 Mathematical and numerical methods

Generally non-linear ordinary differential equations do not have exact analytical solutions. The harmonic balance method and other suitable methods allow approximate solutions to be found. Given the fact that we sometimes encounter difficulties in solving

these equations analytically with exactitude, numerical simulations appear as complementary adapted solutions. In this thesis, we will use as numerical scheme the Runge-Kutta method of order 4 (RK4) to solve numerically the different differential equations which model our models and the balance of harmonics to analytically solve the less complex differential equations. The programming language we used are FORTRAN 95, Python and Matlab.

2.4.1 Harmonic balance method

The principle of balances of harmonics is a method generally used to determine the exact or approximate periodic solutions of ordinary differential equations (linear or nonlinear) subjected to sinusoidal periodic excitations [78]. Let us consider the following differential equation [78, 79]

$$\ddot{y} + y = g(\dot{y}; y, t) \tag{2.9}$$

Where the function g satisfies the following condition $g(\dot{y}; y, t + T) = g(\dot{y}; y, t)$. The harmonic solution of equation is expressed as follows:

$$y = B \sin(\omega_1 t + \Phi) \tag{2.10}$$

Where B is the amplitude of oscillations, ω_1 the pulsation of the sinusoidal excitation and Φ the phase at the origin. In substituting Eq. (2.10) into Eq. (2.9) and equating separately the terms in cosine and sine which have the same harmonics, one obtains after neglecting harmonics order greater than the first harmonic, a system of algebraic equations which are the amplitude equations. This method is used in chapter 3 to determine the harmonic solutions.

2.4.2 RK4 method for ordinary differential equations

Developed for the first time in 1894 by Runge and subsequently improved in 1901 by Kutta hence its name the method of Runge Kutta. It has the advantage of being a numerically stable method [80]. Consider the ordinary first order differential equation:

$$\frac{dX(t)}{dt} = f(X(t), t) \,\text{with} X(t_0) = X_0 \tag{2.11}$$

Where $f = (f_1, f_2....f_n)$ is the vector function with the unknown vector variable $X(t) = (x_1(t), x_2(t), ...x_n(t))$. For such an equation, we use the RK4 method for the resolution given in [81, 82] in equation (2.12):

$$\begin{aligned} x_{i+1,j} &= x_{i,j} + (L_{1,j} + 2 * L_{2,j} + 2 * L_{3,j} + L_{4,j}) \\ t &= t + \Delta t \end{aligned} \tag{2.12}$$

Where $\begin{cases} L_{1,j} = \Delta t * f_j\left(x_{i,j}, t\right) \\ L_{2,j} = \Delta t * f_j\left(x_{i,j} + L_{1,j}, t + \frac{\Delta t}{2}\right) \\ L_{3,j} = \Delta t * f_j\left(x_{i,j} + L_{2,j}, t + \frac{\Delta t}{2}\right) \\ L_{4,j} = \Delta t * f_j\left(x_{i,j} + L_{3,j}, t + \Delta t\right) \end{cases}$

Where i is counted for the increment of time and j labels the variables related to $x_{i,j}, L_{1,j}, L_{2,j}, L_{3,j}$ and $L_{4,j}$ are the intermediate coefficients and Δt is the time step.

2.4.3 Numerical criterion for synchronization

a) Criteria for synchronization

Consider two coupled systems having different initial conditions, we say that the synchronization is reached numerically when the deviation ε_1 obeys to the following synchronization condition given in equation (2.13).

$$|\varepsilon_1| = |u - x| \prec h, \forall t \geq t_{synch} \tag{2.13}$$

Where t_{synch} is the time instant at which the two trajectories are close enough to be considered as synchronized. h is the synchronization precision or tolerance. In the simulation, we considered $h = 10^{-2}$.

We suppose that complete synchronization is achieved in the network after a certain time t_{synch}, after which one of the following criteria is verified.

$$\left|x_i\left(t\right) - x_j\left(t\right)\right| \prec h, \forall\left(i, j\right), \forall t \succ t_{synch} \tag{2.14}$$

$$\begin{aligned} &\frac{\sum_{i=1}^{N} |x_i(t) - x_{i+1}(t)|}{N} \prec h, \forall t \succ t_{synch} \\ &\text{with}, x_{N+1} = x_1 \end{aligned} \tag{2.15}$$

Where $h = 10^{-2}$ is the synchronization precision. These two criteria lead to the same result.

b)Bifurcation diagram and Lyapunov exponent

The bifurcation diagram and the Lyapunov exponent are drawn in order to look for the different dynamical states of the system (such as periodic orbit, chaotic attractors, and fixed points). This diagram also allows us to identify the routes to chaos taken by dynamical systems such as: the period doubling route, the quasi-periodic route and intermittency route.

Consider the system of equations (2.16)

$$\begin{cases} \dot{x} = y \\ \dot{y} = x \end{cases} \tag{2.16}$$

The Lyapunov exponents is given by the equation (2.17):

$$Lya = \lim_{t\to\infty} \left(\frac{\ln\left(\sqrt{\left((dx)^2 + (dy)^2\right)}\right)}{t} \right) \tag{2.17}$$

where dx are dy the variations corresponding to x and y respectively.

2.4.4 Simulation softwares

To solve numerically the differential equations, we have used the Fortran and the Python languages. We used both the Python and FORTRAN language because we faced the difficulty of implementing the hexameric model of the cyanobacteria in FORTRAN. Therefore we had recourse to the Python language which was able to manage the complexity of the equations. The Matlab platform has been used to plot the curves which have been obtained from the numerical simulations.

2.5 Conclusion

This chapter has first provided the methods to model the electronic models and the cyanobacteria. Then the mathematical and numerical methods as well as the softwares used in this thesis have been presented. In the next chapter, the results obtained will presented.

Chapter III

Results and discussion

3.1 Introduction

This chapter is devoted to the presentation of the main results obtained in this thesis. Section 3.2 deals with the analysis of the dynamics of an array of Van der Pol oscillators coupled to an electrical load. The electrical power in the load is analyzed as some control parameters are varied. Some attention is paid on the effect of a high non-linear term in the damping of the Van der Pol oscillators. Section 3.3 is concerned with a question as in section 3.2 using the Grudzinski and Zebrowski oscillator. But an interesting point is the design of an equivalent electric circuit of the Grudzinski and Zebrowski oscillator. The power generated in a load by an array of Hindmarsh- Rose neuron oscillators is considered in section 3.4. The analysis of the stability of the cyanobacteria oscillations is conducted in section 3.5. Section 3.6 concludes the chapter.

3.2 Powering an electrical load by an array of Van der Pol oscillators

3.2.1 Reminder of the physical system

In chapter 2, we explain how to derive the equations of an array of Van der Pol oscillators coupled to a RLC load. Now considering a high order nonlinear term in the dissipation coefficient, one arrives at the following set equations.

$$\begin{cases} \ddot{x}_j + \alpha\ddot{y}_j - d\left[1 - x_j^2 + bx_j^4\right]\dot{x}_j + x_j = 0; 1 \leq j \leq N \\ \sum_{k=1}^{N} \left(\ddot{y}_k + \lambda\dot{y}_k + \mu y_k\right) = \beta\left(x_1 - y_1\right) \end{cases} \tag{3.1}$$

Where $x_j = \frac{v_j}{V_0}, y_j = \frac{u_j}{V_0}, \lambda = \frac{R}{L\omega_0}, \mu = \frac{L_v C_v}{LC}, \beta = \frac{L_v C_v}{LC_0}, \alpha = \frac{C_0}{C_v}$

In the case of a RL load, the term μy_k is removed from equation (3.1.b) while in the case of a RC load, the term $\ddot{y}_k$ is removed from equation (3.1.b). But in this case, the coefficients λ , β and μ are replaced respectively by $1, \lambda_1$ and λ_2 defined as:$\lambda = 1; \lambda_1 = \frac{1}{CR\omega_0}$ and $\lambda_2 = \frac{1}{C_0 R\omega_0}$.

In this case of a simple R load, the terms $\ddot{y}_k$ and μy_k are removed from equation (3.1.b). But in this last case, the coefficient β is replaced by β_1 defined as $\beta_1 = \frac{1}{C_0 R\omega_0}$.

3.2.2 Voltages variations across each oscillator and across the load

Let us assume that all the Van der Pol oscillators are synchronized, when the nonlinear coefficient d and the coupling coefficients α and β are small, the approximate analytical solution of equations (3.1) can be found using the harmonic balance method which considers that the solutions are in the form of (3.2).

$$\begin{cases} x = A\cos(t+\phi) \\ y = B\cos(t+\varphi) \end{cases} \tag{3.2}$$

where A and B are voltage amplitudes and, ϕ and φ are the phases of the voltages across the Van der Pol oscillators and the coupling capacitor respectively. Inserting these expressions in the equations (3.1), one obtains the voltage amplitudes A and B as:

$$A = \sqrt{\frac{\frac{1}{4} - \sqrt{\frac{1}{16} - \frac{b}{2}\left(1 - \frac{\beta\alpha}{d\sqrt{(\mu N - N + \beta)^2 + \lambda^2 N^2}}\right)}}{\frac{b}{4}}} \tag{3.3}$$

and

$$B = \frac{\beta A}{\sqrt{(\mu N - N + \beta)^2 + \lambda^2 N^2}} \tag{3.4}$$

The voltage amplitude A exists under the following conditions

$$\begin{cases} N \in]N_1, N_{11}[\cup]N_{22}, N_2[\,; \text{if}, b > 1/8 \\ N \in]0, N_1[\cup]N_2, +\infty[\,; \text{if}, 0 < b < 1/8 \end{cases} \tag{3.5}$$

where N_1, N_2, N_{11} and N_{22} are given below: $N_1 = \frac{(-2\mu\beta+2\beta)-\sqrt{Q}}{2(\mu^2+1-2\mu+\lambda^2)}$, $N_2 = \frac{(-2\mu\beta+2\beta)+\sqrt{Q}}{2(\mu^2+1-2\mu+\lambda^2)}$, $N_{11} = \frac{(-2\mu\beta+2\beta)-\sqrt{S}}{2(\mu^2+1-2\mu+\lambda^2)}$ and $N_{22} = \frac{(-2\mu\beta+2\beta)+\sqrt{S}}{2(\mu^2+1-2\mu+\lambda^2)}$ with $S = \frac{4\beta^2\alpha^2}{d^2}\left(\mu^2+1-2\mu+\lambda^2\right) - 4\lambda^2\beta^2$ and $Q = \frac{4\beta^2\alpha^2}{d^2\left(1-\frac{1}{8b}\right)^2}\left[\mu^2+1-2\mu+\lambda^2\right] - 4\lambda^2\beta^2$

If conditions (3.5) are not satisfied, then A does not exist and there is no oscillation in the system.

The curves obtained from the analytical calculations are compared to those obtained from the direct numerical simulation of the set of differential equations (3.1). For small values of the nonlinear coefficients, there is a good agreement between the curves obtained from equations (3.3) and (3.4) and those obtained from the direct numerical simulation. The numerical simulation is therefore used only to present curves related to the case where

the values of the nonlinear coefficients are not small enough to warrant the validity of the analytical results.

Figure 3.1 presents the variations of A and B versus the number of the oscillators. When the number of oscillators is less than 29, there is no generation of voltage in the system. The Van der Pol oscillators are death because of the indirect coupling. After this critical value of N, the voltage in the Van der Pol oscillator increases with N and saturates at a value equal to 2 for large value of N. In its side, B increases with N and attains a maximal value (at N=50) after which it decreases with N. This behavior of B versus N indicates that there is an optimal value of the size of the array leading to a higher voltage in the load.

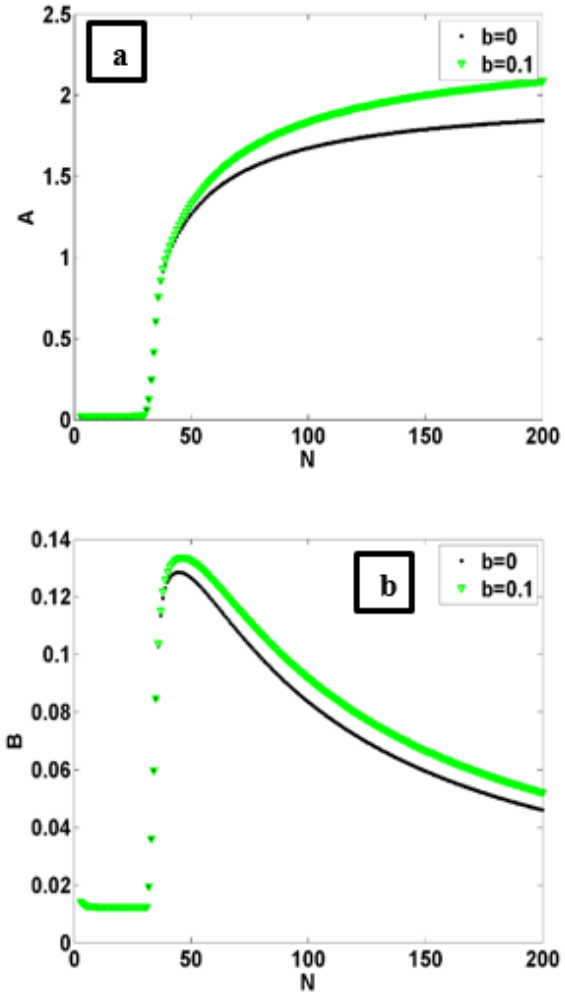

Figure 3.1: Variations of the voltages amplitudes versus N: a) Van der Pol oscillator; b) across the coupling capacitance C_0 for $\alpha = 0.6, \beta = 10, \mathrm{d} = 0.1, \lambda = 2$ and $\mu = 0.85$

3.2.3 Effect of the high order non linearity of the damping

As it also appears in Figure 3.1, the quartic nonlinear coefficient b affects the voltages by increasing their values. The analysis of the voltage amplitudes versus the d, for fixed value of N, has presented a voltage shape (for both the VdP oscillator and the RLC load) similar to what is observed in Figure 3.1.a. As d increases, the voltage amplitudes remain equal to zero until a threshold value of d after which they increase rapidly, then slowly with d and finally attain a plateau.

3.2.4 Power in the loads

The power in the load is consumed in the resistor and is given by the following expression:

$$P = R \prec i \succ^2 \tag{3.6}$$

where $\prec i \succ$ is the effective mean current through the load. The current in the load is given by:

$$i = \sum_{k=1}^{N} C_0 \frac{du_k}{dt} \tag{3.7}$$

The expression of the power in the resistor is thus:

$$P = \frac{RN^2 w_0^2 C_v^2 V_0^2 \alpha^2 \beta^2 A^2}{2\left(\lambda^2 N^2 + (\mu N - N + \beta)^2\right)} \tag{3.8}$$

Figure 3.2 presents the power variation versus the control parameters N, d and b. It is seen that the power increases with N after the critical value of N below which the power in the load is equal to zero (see Figure 3.2.b). The power begins to exist from $N = 30$ and increases until the value of $P = 16.53$ for $N = 200$ for $b = 0$. Like for the voltage amplitudes, the power increases with d (Figure 3.2.a) and with b (Figure 3.2.b).

In the case of RL load, the critical value of N below which there is no power in the load is 29 and that power increases until the value of $P = 13.84$ for $N = 200$ (Figure 3.3). While in the case of the RC load, that critical value of N is 3 and the power increases until the value of $P = 0.503$ for N=200 (Figure 3.4). In this case of the R load, that critical value of N is 6 and the power increases until the value of $P = 0.5983$ for $N = 200$ (Figure 3.5).

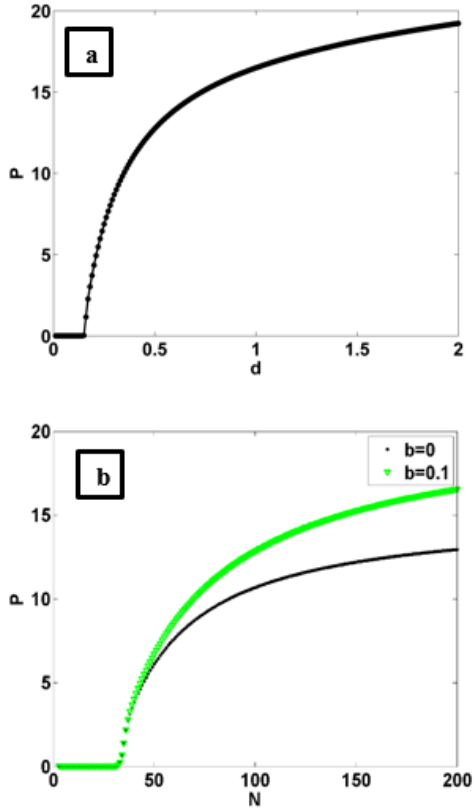

Figure 3.2: Power (Watt) in the RLC load versus d with $b = 0.1$ (figure 3.2.a) and versus N for two different value of b with $d = 0.1$ (figure 3.2.b) for $\alpha = 0.6, \beta = 10, \lambda = 2, \mu = 0.85$ and $R = 156\Omega$

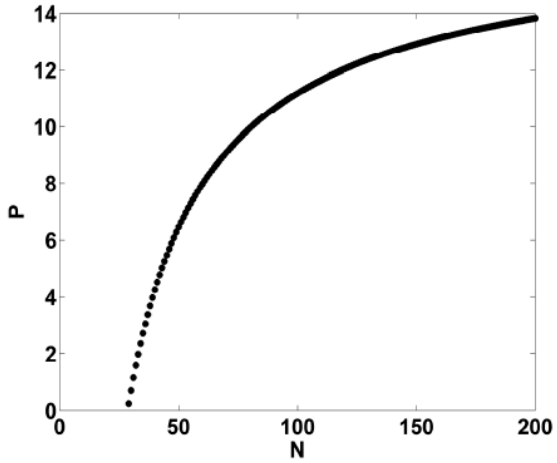

Figure 3.3: Power in the RL load versus the number of oscillators in the array for $\alpha = 0.6, \beta = 10, \mathrm{b} = 0.1, \lambda = 2$ and $R = 156\Omega$

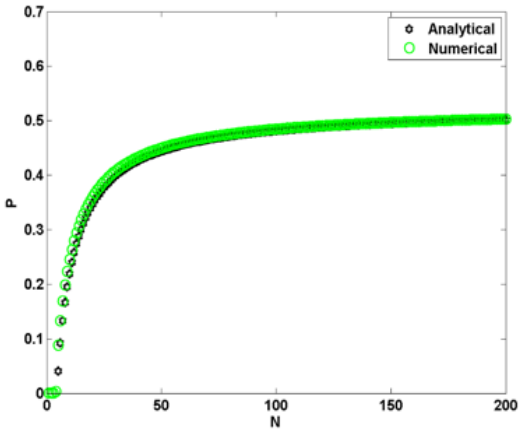

Figure 3.4: Power (Watt) in the RC load versus the number of oscillators in the array for: $\alpha = 0.6, \mathrm{b} = 0.1, \lambda_1 = 0.44, \lambda_2 = 0.86, \mathrm{d} = 0.1$ and $R = 156\Omega$

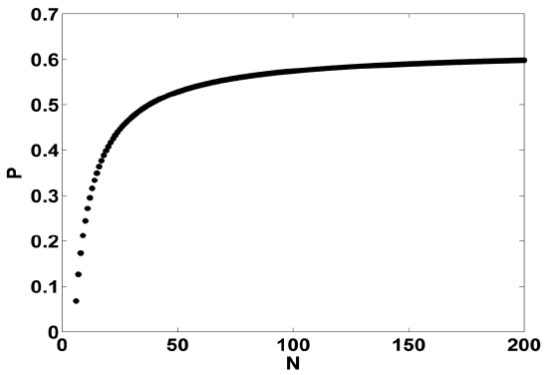

Figure 3.5: Power (Watt) in the R load versus the number of oscillators in the array for: $\alpha = 0.6, \mathrm{b} = 0.1, \beta_1 = 0.86, \mathrm{d} = 0.1$ and $R = 156\Omega$

According to figure 3.4, a good agreement is found between the analytical and numerical results.

Subsequently, we have fixed the value of N and we have plotted the power as a function of R which is given in figure 3.6. We observe a phenomenon of resonance of power. The curve increases to the maximum value 3.588, then decreases and remains almost constant around the zero with the evolution of resistance. The maximum value of the power P is reached at $R = 13\Omega$.

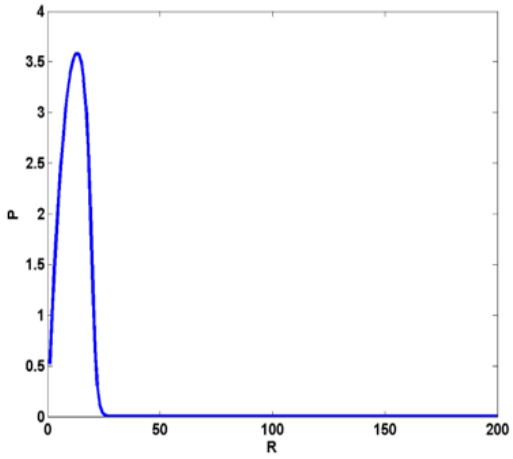

Figure 3.6: Power (Watt) in the RLC load versus R for: $L = 200 * 10^{-6}H, \alpha = 0.6, \beta = 10, \mu = 0.85, N = 10$

3.2.5 Implications for cardiac response

The fact that there are threshold values of the size of the array and of the nonlinear coefficient d can be related to the development of the heart pacemaker at its early stage. Indeed, it is known that, after its formation, the heart pacemaker remains silent and starts firing electrical signals after some days. A sort of quorum sensing phenomenon where the system starts its activity after a certain size, depending on the environment, is attained [83]. Inversely, after attaining its optimal functioning stage, if the number of pacemaker cells decreases, then the power delivered by the heart also decreases.

When the resistance increases, we observe an increase in power which reaches its maximum value, then decreases and remains almost constant around zero. With age, the heart tends to increase slightly in size and develop thicker walls and slightly larger chambers. The increase in its size is mainly due to an increase in the size of individual heart muscle cells. Age-related stiffness of the heart walls causes insufficient filling of the left ventricle and can sometimes lead to heart failure. With age the walls of the arteries and arterioles thicken and the space between the arteries increases slightly. All its changes make the vessels more rigid and less elastic. The loss of elasticity of arteries and arterioles due to aging prevents them from relaxing so quickly during the rhythmic contraction of the heart.

3.3 Power in an electrical load delivered an array of Grudzinski-Zebrowski oscillator

3.3.1 Equivalent electrical circuit for the Grudzinski-Zebrowski model

We remind that the mathematical equation of the Grudzinski-Zebrowski oscillator is given as in equation (3.9), where β is the damping constant.

$$\ddot{x} + \beta\left(x^2 - (\theta_1 + \theta_2)x + \theta_1\theta_2\right)\dot{x} + x + \frac{(\gamma+\eta)}{\gamma\eta}x^2 + \frac{x^3}{\gamma\eta} = 0 \tag{3.9}$$

From the literature review, we found that all the studies done on the Grudzinski-Zebrowski oscillator were essentially based on the mathematical model using numerical simulation. To the best of our knowledge, there is no equivalent electric circuit composed of discrete electronic components (diodes, resistance, transistors or analog components), as it is in the case of the Van der Pol oscillator. There is therefore, a need of an electrical model for the Grudzinski-Zebrowski oscillator since it will give way for more studies such as the one conducted in this thesis where loads are coupled to the electric equivalent circuits. It is also expected that experimental study can be undertaken using the electrical equivalent. After a series of tries and fails, we came out with the electrical model presented in Figure 3.7. It consists of 4 branches. The first branch comprises an inductor L_1 and a resistance R_1 ; the second contains a capacitor C_1 ; the third is a nonlinear resistance; and the last one has a diode.

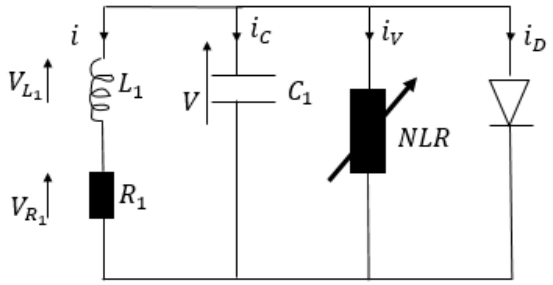

Figure 3.7: Equivalent electrical circuit of the Grudzinski-Zebrowski oscillator.

We assume that the current-voltage $(I - V)$ characteristics of the diode is given by (3.10).

$$i = i_0(e^{V/V_0} - 1) \tag{3.10}$$

whose after expansion gives

$$i = i_0(\frac{V}{V_0} + \frac{V^2}{2V_0^2}) \tag{3.11}$$

where i_0 and V_0 are constant coefficients related to the diode. $V$is the voltage across C_1 , or across the nonlinear resistance (NLR), or across the diode.

We also assume that the current-voltage characteristics of the nonlinear resistance NLR is given as follows:

$$i = -\frac{aV}{V_0} + \frac{bV^3}{V_0^3} \tag{3.12}$$

Using the first mesh of the circuit, one gets

$$L_1\frac{di}{dt} + R_1 i - V = 0 \tag{3.13}$$

Where i is the current flowing through L_1. where $V = \frac{q}{C_1}$, which is the voltage across the capacitor.

Considering the nodes law, one gets

$$i = -\frac{dq}{dt} + \frac{aV}{V_0} - \frac{bV^3}{V_0^3} - \frac{i_0 V}{V_0} - \frac{i_0 V^2}{2V_0^2} \tag{3.14}$$

where q is the electric charge in the capacitor.

By replacing (3.14) in (3.13), it comes that the voltage V satisfies the following equation:

$$\begin{array}{l} \frac{d^2V}{dt^2} + \frac{3b}{V_0^3 C_1}\left(V^2 + \frac{i_0 V_0 V}{3b} - \frac{V_0^2 a}{3b} + \frac{i_0 V_0^2}{3b} + \frac{R_1 V_0^3 C_1}{3bL_1}\right)\frac{dV}{dt} + \\ \frac{R_1 bV^3}{V_0^3 L_1 C_1} + \frac{R_1 i_0 V^2}{2V_0^2 L_1 C_1} - \frac{R_1 aV}{L_1 C_1 V_0} + \frac{V}{L_1 C_1} + \frac{R_1 i_0 V}{V_0 L_\partial C_1} = 0 \end{array} \tag{3.15}$$

Setting $x = \frac{V}{V_0}$ and normalizing the time t is normalized with respect $t_{ref} = \frac{1}{\omega_0}$ with $\omega_0 = \sqrt{\frac{-a+2i_0}{L_1 i_0 C_1}}$, one obtains the following equation:

$$\frac{d^2x}{dt^2} + \frac{3b}{V_0\omega_0 C_1}\left(x^2 + \frac{i_0 x}{3b} - \frac{a}{3b} + \frac{i_0}{3b} + \frac{R_1 V_0 C_1}{3bL_1}\right)\frac{dx}{dt} + x + \frac{R_1 i_0 x^2}{2L_1\omega_0^2 C_1 V_0} + \frac{R_1 bx^3}{L_1\omega_0^2 C_1 V_0} = 0 \tag{3.16}$$

The following values have been given to the electrical components and parameters: $L_1 = 200\times10^{-6}H; i_0 = 10^{-4}A; V_0 = 26\times10^{-3}V; \frac{1}{C_1} = 70921985,8156F^{-1}; a = 0.0001; b = 0.237.$

Equation (3.16) can thus take the form of equation (3.9) with the following dimensionless coefficients:

$$\beta = 3; \theta_1 + \theta_2 = 0; \theta_1\theta_2 = -0.6889; \frac{1}{\gamma\eta} = 0.05; \frac{(\gamma+\eta)}{\gamma\eta} = 0.5 \tag{3.17}$$

Figure 3.8 presents the phase portrait and the time trace of the signal delivered by equation (3.16) with the above parameters and the following initial conditions: $x(0) = -0.1$ and $\dot{x}(0) = 0.025$

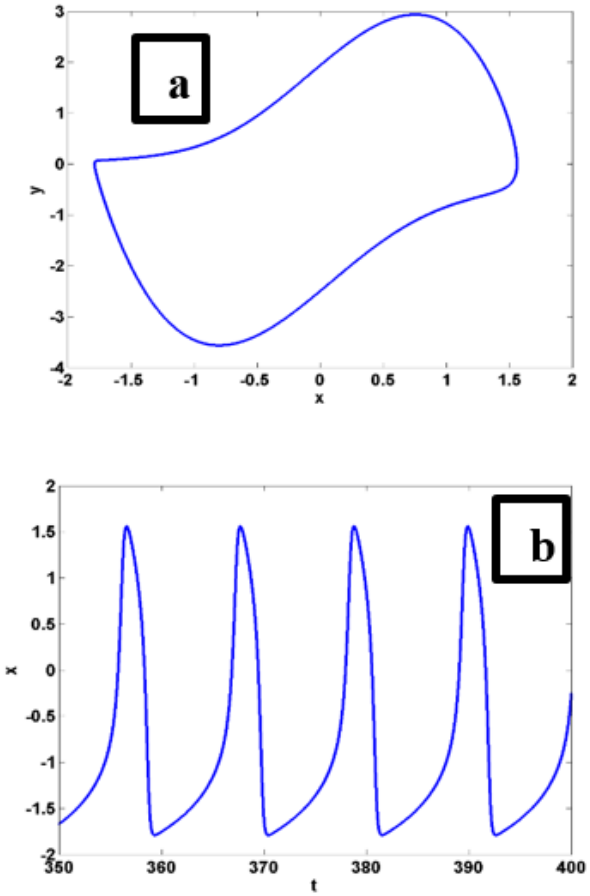

Figure 3.8: Signal delivered by the Grudzinski-Zebrowski oscillator: a) phase space, b) time history.

3.3.2 Voltage variation across oscillator and across the load

The Grudzinski-Zebrowski oscillator is a representative of electrical models of heart pacemaker cells. The cells can be coupled indirectly through the electrical load representing the rest of the heart or the rest of the cardiovascular system seen by the pacemaker or both directly and indirectly. In the case of the indirect coupling, each cell is coupled to the external load as in references [16, 84, 85]. When the direct and indirect coupling take place, each cell is coupled to the external load, but all the cells are coupled together in a diffusive manner with short or long range coupling [24]. We will consider both cases here

and come out with the behavior of the oscillatory states and the power received by the load. The system is presented in Figure 3.9, where we see a set of N Grudzinski-Zebrowski oscillators coupled to a RLC load. The coupling is through the capacitance C_0 as for the case of Van der pol oscillators analyzed in section 3.2.

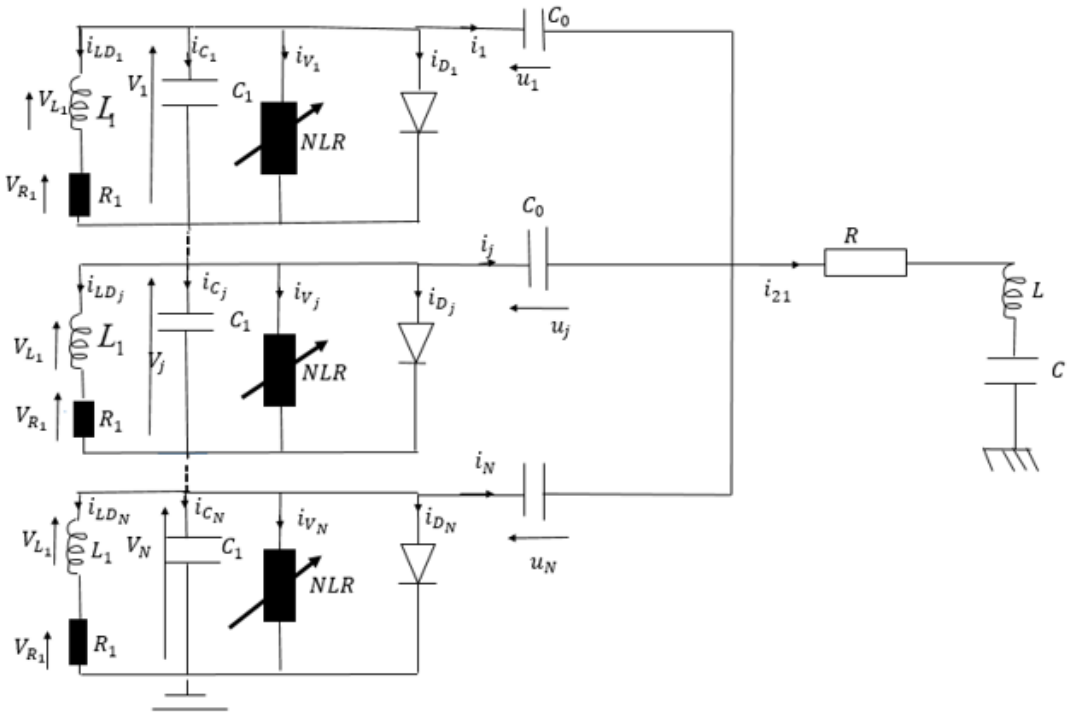

Figure 3.9: Array of Grudzinski and Zebrowski oscillators loaded by an RLC circuit.

Using Kirchhoff's laws, appropriate dimensionless variables and the same normalization as above and also setting $y_j = \frac{u_j}{V_0}$, one obtains the set of equations (3.18) which describes the variation of voltage x_j across each oscillator and the voltage y_j across the coupling capacitance.

$$\begin{cases} \ddot{x}_j + \mu\left({x_j}^2 - 0.6889\right)\dot{x}_j + x_j + 0.5x_j^2 + 0.05{x_j}^3 + A_1\ddot{y}_j + A_2\dot{y}_j = 0; 2 \leq \mathrm{j} \leq \mathrm{N} \\ \sum_{k=1}^{N}\left(\ddot{y}_k + B_1\dot{y}_k + B_2 y_k\right) = B_3\left(x_1 - y_1\right) \end{cases} \tag{3.18}$$

With $A_1 = \frac{C_0}{C_1}$ and $A_2 = \frac{R_1 C_0}{L_1 \omega_0 C_1}$.

The dimensionless parameters B_1, B_2 and B_3 are defined in Table 1 for different types of loads.

Table 3.1: Expressions of the coefficients B_i for each type of electrical load

Load	B_1	B_2	B_3
RLC load	$\frac{R}{L\omega_0}$	$\frac{1}{LC{\omega_0}^2}$	$\frac{1}{L{\omega_0}^2 C_0}$
R load	1	0	$\frac{1}{C_0 R\omega_0}$
RL load	$\frac{R}{L\omega_0}$	0	$\frac{1}{C_0 R\omega_0}$
RC load	1	$\frac{1}{R\omega_0 C}$	$\frac{1}{R\omega_0 C_0}$

We first analyze the variations of the voltage amplitude as the number of oscillators varies. The initial conditions used for the numerical simulation are $x\left(0\right) = -0.1$, $\dot{x}\left(0\right) = 0.025$, $y_i\left(0\right) = 0.025$ and $\frac{dy}{dt}_i\left(0\right) = 0.025$.

First considering the RLC load, we use the following values:$R = 156\Omega, L = 200 \times 10^{-6}H, C = 36.3 \times 10^{-9}F$ and $C_0 = 1.89 \times 10^{-8}F$. Figure 3.10 presents the amplitudes of the voltages x_j and y_j versus the number N of the oscillators. It is observed that the voltage amplitude increases in each Grudzinski-Zebrowski oscillator with the increase of N. One remarks that for lower values of N, the voltage is almost equal to zero as for the case of array of Van der Pol oscillators. But at the same time, the voltage amplitude across the capacitance C_0 decreases when N increases.

Considering the other types of loads (RL, RC, and R), we found similar variation as in the case of the RLC load. However quantitatively, it has been observed that the amplitudes is lower in the RC load compare to the other loads (see figure 3.11).

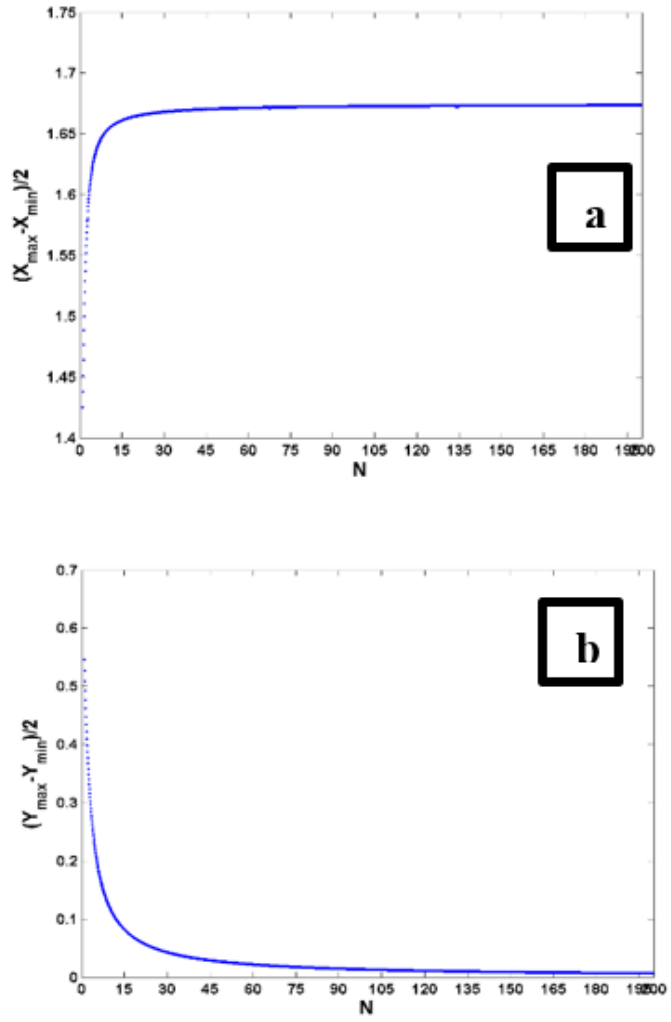

Figure 3.10: Voltage amplitudes responses versus the number N of the oscillator: a) in the Grudzinski-Zebrowski oscillator; b) across the coupling capacitance C_0, with $R = 156\Omega; L = 200 \times 10^{-6}H; C_1 = 36.3 \times 10^{-9}F; C_0 = 1.89 \times 10^{-8}F; R_1 = 156\Omega; V_0 = 26 \times 10^{-3}V; i_0 = 1 \times 10^{-4}A; L_1 = 200 \times 10^{-6}H; \mu$= 3 and $\omega_0 = 594228.361$.

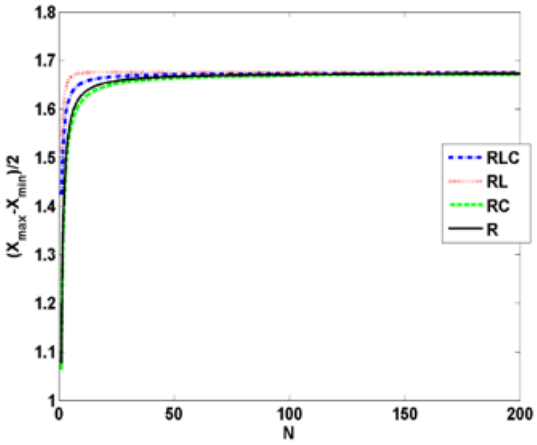

Figure 3.11: Voltage amplitudes responses in the Grudzinski-Zebrowski oscillator versus the number N of oscillators coupled to RLC, RL, RC and R loads across with $\omega_0 = 594228.361$ and parameters of figure 3.10.

Considering the effects of the coupling capacitance C_0 , figure 3.12 shows that the voltage amplitude across the Grudzinski-Zebrowski oscillator increases while the voltage amplitude across C_0 decreases with the increase of C_0 .

The effects of the nonlinear damping parameter μ has also been investigated. It is found that the voltage amplitude in each oscillator increases with μ up to the value $\mu = 8.5$. Then, a decrease takes place till $\mu = 84.8$, followed by a second smooth increase. For the voltage across C_0, its amplitude increases with the increase of μ (see figure 3.13).

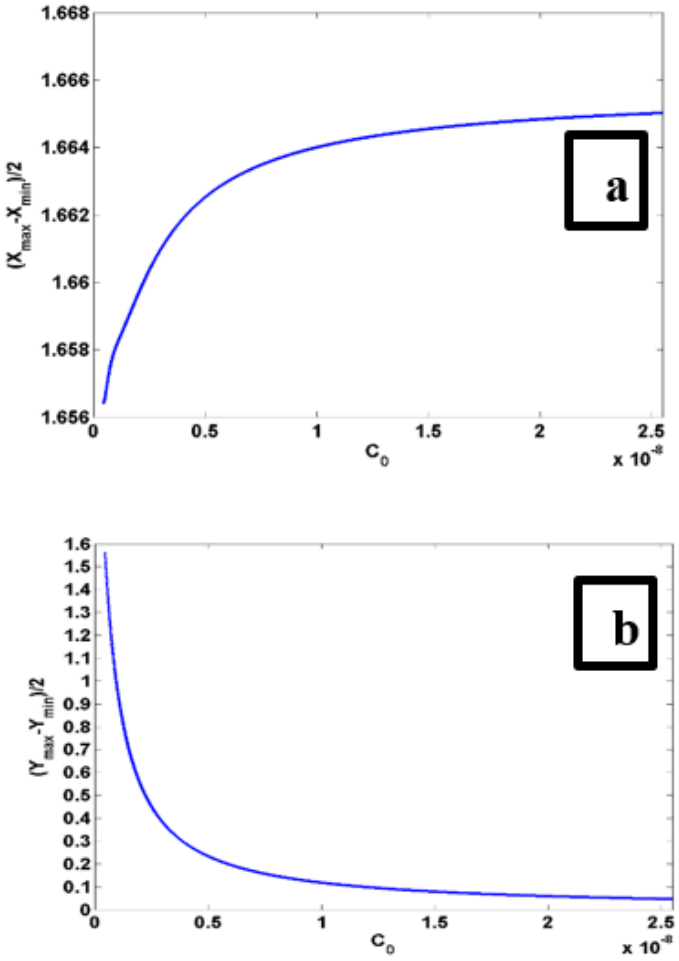

Figure 3.12: Voltage amplitudes responses versus the coupling capacitance C_0: a) across the Grudzinski and Zebrowski oscillator; b) across the coupling capacitance with $N = 20$, $\omega_0 = 594228.361$ and with the parameters of figure 3.10.

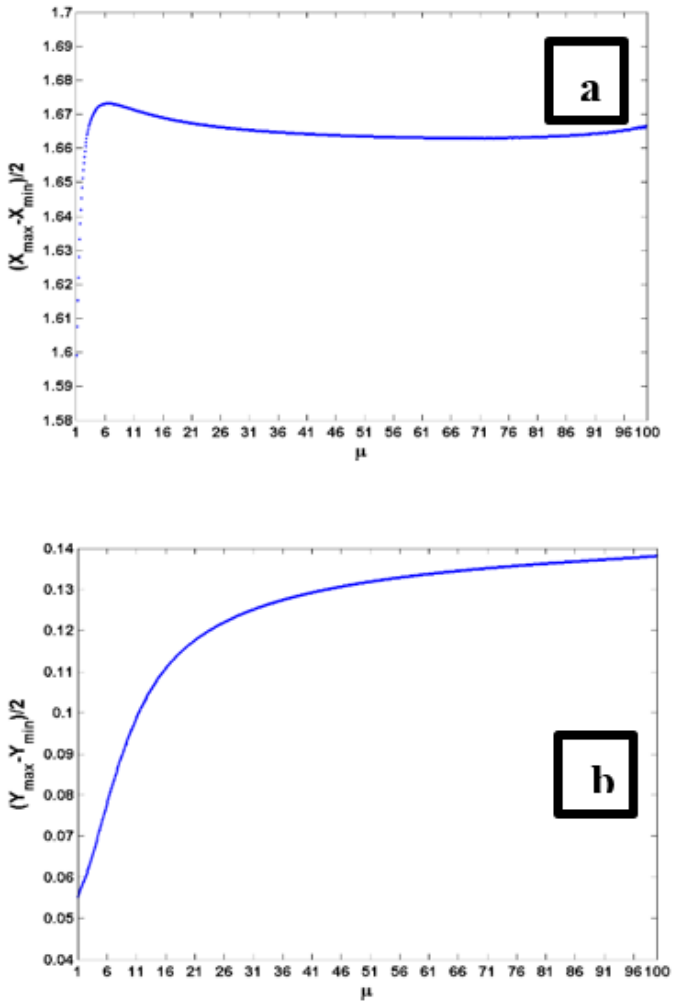

Figure 3.13: Voltage amplitudes responses versus the coupling coefficient μ : a) across the Grudzinski and Zebrowski oscillator; b) across the coupling capacitor C_0, $N = 20$, $\omega_0 = 594228.361$ and with the parameters of figure 3.10.

3.3.3 Power in different loads

The most interesting quantity in the load is the power delivered by the array of self-sustained oscillators. It is defined by the following equation.

$$P = R \times i_{21}^2 \tag{3.19}$$

Where R and i_{21} are respectively the load resistance and the current intensity.

Since $i_{21} = \sum_{k=1}^{N} C_0 \frac{du_k}{dt}$,and knowing that $u_k = y_k V_0$, one obtains $i_{21} = NC_0 \dot{y}_k V_0 \omega_0$.

By taking into account the above literal expression of i_{21} , the power in the load is:

$$P = R(NC_0 \dot{y}_k V_0 \omega_0)^2 \tag{3.20}$$

This expression remains the same for the different types of load, except that the value of the derivative of the component y will be determined according to the load that will be taken into account during the numerical simulations.

Figure 3.14 presents the power variation versus N in the R, RL, RLC and RC load. We remark that, the power increases with the increase of N for all types of loads. Quantitatively, one notes that the RL load consumes more power than the RLC load while the pure resistive load consumes the highest power. The power consumed by the RC load (which is more close to biological tissue) is at the intermediate level.

We have also considered the resistance Ras a control parameter and plot the power versus R. We found that, for all types of load, the power increases with R and attains a saturation level where it remains constant. Such a variation is presented in Figure 3.15 for the RLC, RC, RL, and R loads. Let us mention that the curve for the R load and that of the RLC load are almost the same.

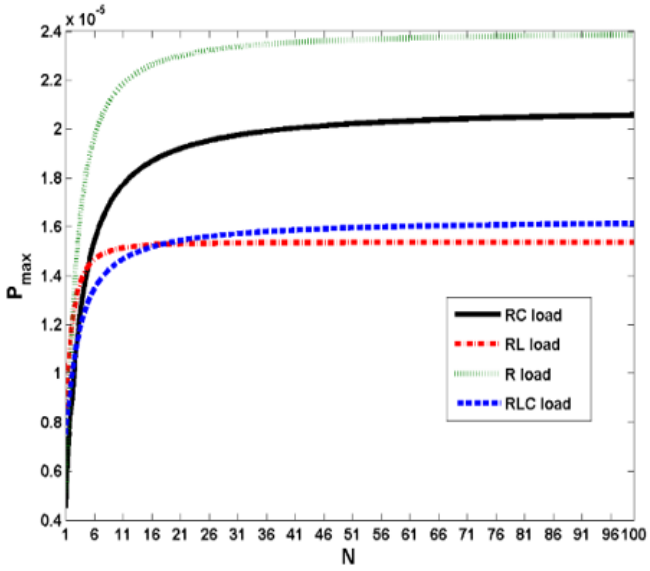

Figure 3.14: Power (Watt) delivered to the R, RL, RLC and RC loads versus the number N of Grudzinski and Zebrowski oscillators, with $\omega_0 = 594228.361$ and the parameters of figure 3.10.

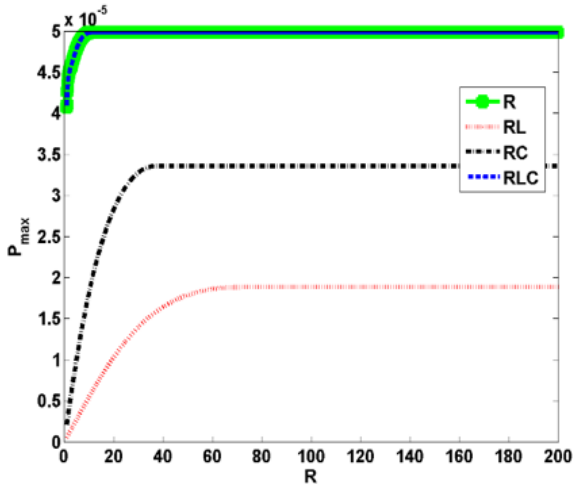

Figure 3.15: Power (Watt) delivered in the load RLC, RL, RC, and R load versus R with $N = 20$, $\omega_0 = 594228.361$ and with the parameters of figure 3.10.

We observe that no matter the load (RLC, RL, RC, and R), the power increases and reaches a value then after this maximum value, it remains constant with the evolution of the resistance. This variation is different from that which we obtained in the case of the study of the oscillator of Van der Pol where the power increases and reaches the maximum value, then it decrease and finally remains almost constant around zero with the evolution resistance.

3.3.4 Synchronization of the Grudzinski and Zebrowski oscillators subjected to the RC load

In this section, one considers the situation where all the Grudzinski-Zebrowski oscillators are mutually coupled to each other by a capacitor and indirectly coupled to the RC load. In this subsection, direct coupling, is about the coupling between neighboring oscillators one after the other by a capacitor while forming a ring (oscillator network). When this oscillator network is coupled to a load by a capacitor, we are in the presence of an indirect coupling. Figure 3.16 presents the system under consideration. Each oscillator is directly coupled to its nearest neighbors through a capacitor. At the same time, all the oscillators are indirectly coupled to the RC load, generating therefore an indirect coupling between the oscillators. We chose a ring for the reason that it is due to periodic boundary

conditions since in reality the system is assumed to have a large number of cells. Moreover, the direct coupling is a biological mechanism by which cells communicate through gap junctions.

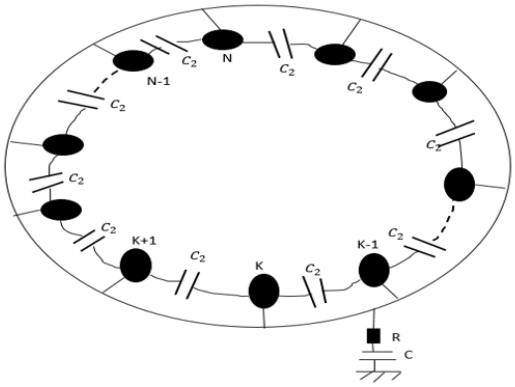

Figure 3.16: Ring of N mutually coupled Grudzinski-Zebrowski oscillators coupled indirectly by a RC load.

Using the electric laws, one finds that the voltages in Figure 3.16 are described by the following set of differential equations:

$$\begin{cases} \frac{d^2x_k}{dt^2} + \frac{3b}{V_0\omega_0 C_1}\left({x_k}^2 + \frac{i_0 x_k}{3b} - \frac{a}{3b} + \frac{i_0}{3b} + \frac{R_1 V_0 C_1}{3bL_1}\right)\frac{dx_k}{dt} + x_k + \frac{R_1 i_0 {x_k}^2}{2L_1\omega_0^2 C_1 V_0} \\ + \frac{R_1 b {x_k}^3}{L_1\omega_0^2 C_1 V_0} + K_2\ddot{y}_k + \frac{R_1 K_2}{L_1\omega_0}\dot{y}_k = K_1\left(\ddot{x}_{k-1} - 2\ddot{x}_k + \ddot{x}_{k+1}\right) + \frac{R_1 K_1}{L_1\omega_0}\left(\dot{x}_{k-1} - 2\dot{x}_k + \dot{x}_{k+1}\right) \\ \sum_{P=1}^{N}\left(\dot{y}_P + \frac{1}{R\omega_0 C}y_P\right) = \frac{1}{R\omega_0 C_0}(x_k - y_k) \end{cases} \tag{3.21}$$

Where the dimensionless quantities are given below:

$$x_k = \frac{V_k}{V_0}; \mathrm{y}_k = \frac{u_k}{V_0}; \mathrm{K}_2 = \frac{C_0}{C_1}; K_1 = \frac{C_2}{C_1}; t_{ref} = \frac{1}{\omega_0}; \omega_0 = \sqrt{\frac{-a + 2i_0}{L_1 i_0 C_1}} \tag{3.22}$$

The direct coupling coefficient is K_1 and the indirect coupling coefficient is K_2 .
Three concerns arise from the model. The first one is to see how the mutually coupled oscillators behave when they are not coupled to the load. In other words, for which value of the mutual coupling coefficient a full synchronization can be achieved? The second one is to understand how the indirect coupling affects the synchronization limits. The third concern is to find out how the mutual coupling coefficient affects the power in the RC load.

Referring to Enjieu et al. [23], numerical simulations have been conducted in search of the coupling coefficient leading to full synchronization as a function of the number of Grudzinski and Zebrowski oscillators. Considering the system of figure 3.16 without the RC load, equation (3.23) repeats the set of dimensionless equations under consideration here

$$\begin{aligned}&\frac{d^2x_k}{dt^2}+\frac{3b}{V_0\omega_0C_1}\left({x_k}^2+\frac{i_0x_k}{3b}-\frac{a}{3b}+\frac{i_0}{3b}+\frac{R_1V_0C_1}{3bL_1}\right)\frac{dx_k}{dt}+x_k+\frac{R_1i_0{x_k}^2}{2L_1\omega_0^2C_1V_0}\\&+\frac{R_1b{x_k}^3}{L_1\omega_0^2C_1V_0}=K_1\left(\ddot{x}_{k-1}-2\ddot{x}_k+\ddot{x}_{k+1}\right)+\frac{R_1K_1}{L_1\omega_0}\left(\dot{x}_{k-1}-2\dot{x}_k+\dot{x}_{k+1}\right)\end{aligned}\tag{3.23}$$

When one considers two Grudzinski and Zebrowski oscillators described by the same equations and starting with different initial conditions, one observes that they present the same behaviour but with a phase difference. Finding the synchronization domain is to look for N and the coupling coefficient K_1 leading to the disappearance of the phase difference so that the oscillators are phase locked with phase difference equal to 0. Figure 3.17 presents the synchronization domains in the $(N, \mathrm{K_1})$ plane. It is seen that the full synchronization domains (FS) are not linearly delineated from the domains where there is no synchronization (NS). The figure 3.17 was made by fixing each time the number of oscillators and by varying the value of the coupling coefficient in order to find the values of the coupling coefficient where there is a total synchronization of its oscillators fixed at the start. The difference of the average value between two positions of two oscillators must be 0.01 for there to be synchronization. For the case $N = 16$, |x (16) -x(13)| < 0.01 and |x(16)-x(12) |< 0.01 so that there is synchronization.

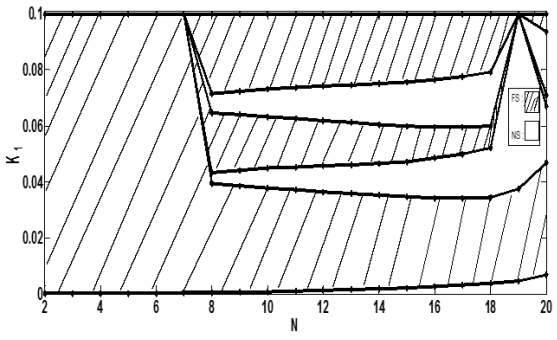

Figure 3.17: Boundaries for full synchronization (FS) and no-synchronization (NS) in the parametric plane $(N, \mathrm{K_1})$ with $\omega_0 = 594228.361$ and with the parameters of figure 3.10.

In order to show the accuracy of the synchronization diagram, we took a couple of

values (N, K_1) where there is synchronization and where there is no synchronization according to figure 3.17, and plotted there time traces for these cases. From the temporal traces, it emerges that for the parameters for which there is synchronization, the temporal traces are in phase and in the contrary case they are out of phase (see figure 3.18 and figure 3.19).

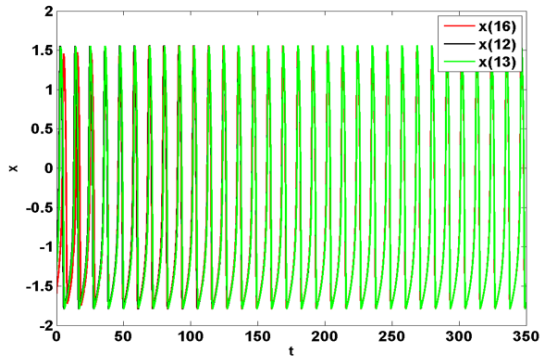

Figure 3.18: Time traces of the oscillations in case there is no synchronization with $K_1 = 0.04$ and parameters of figure 3.10.

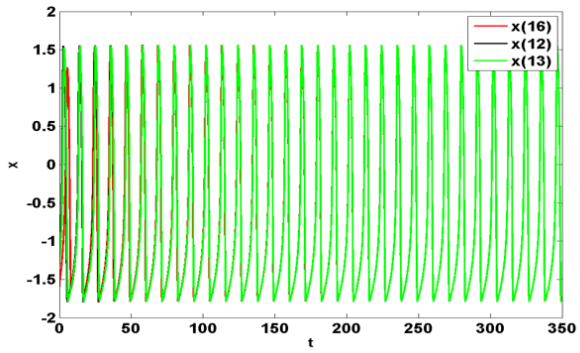

Figure 3.19: Time traces of the oscillations in case of full synchronization with $K_1 = 0.1$ and parameters of figure 3.10.

When the load is taken into account, the power delivered by the array of self-sustained oscillators is given as follows:

$$P = R(NC_0\dot{y}_k V_0\omega_0)^2 \tag{3.24}$$

It is rewritten according to the mutual coupling

$$P = R\left(N\left(\frac{C_0 * C_2}{K_1 * C_1}\right)\dot{y}_k V_0\omega_0\right)^2 \tag{3.25}$$

In figure 3.20, the variation of the power in the load is presented as a function of the number of oscillators for three values of the mutual coupling coefficient. One observes that, the power decreases with the increase in the mutual coupling coefficient. In addition, one also observes a succession of decrease and increase in the amplitudes of the power with the increase in the number of oscillators. For some values of N, the power is equal to zero. This is an indication of lost of synchronization in the oscillators dynamics.

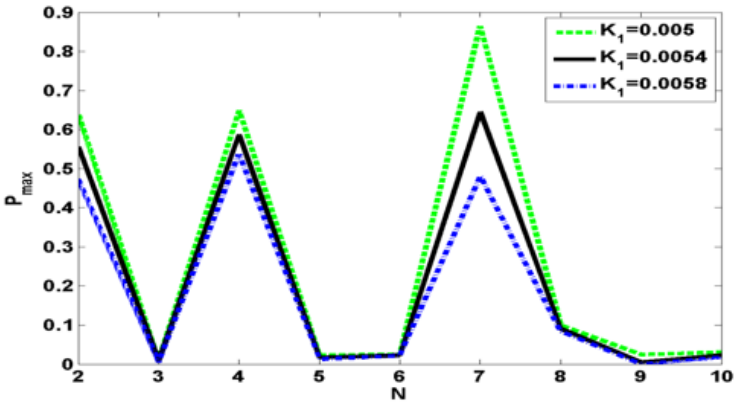

Figure 3.20: Power (Watt) in the load RC load versus the number of Grudzinski-Zebrowski oscillators for different values of K_1 with $\omega_0 = 594228.361$ and parameters of figure 3.10.

3.3.5 Power at load output when synchronization is reached

When the full synchronization is reached, the power in the RC load is plotted versus the mutual coupling coefficient in figure 3.21. The power first decreases and reaches the value 5.107×10^{-4}, then increases till the value 6.402×10^{-3} and finally decreases when the mutual coupling increases.

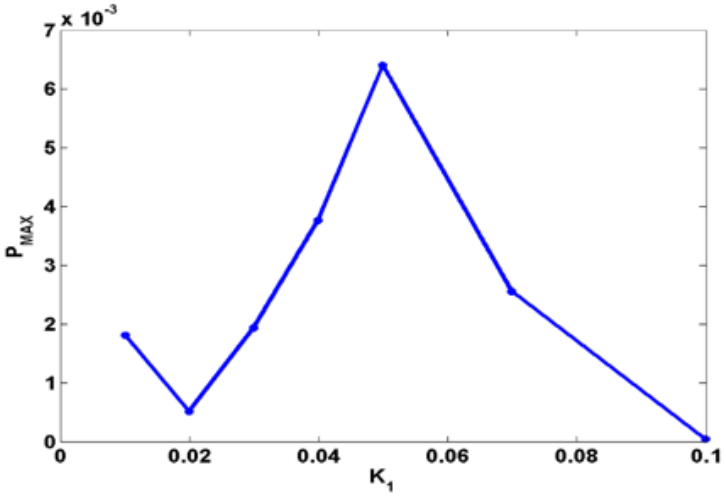

Figure 3.21: Power (Watt) in the RC load versus the mutual coupling coefficient with $N = 10$, $\omega_0 = 594228.361$ and parameters of figure 3.10.

3.4 Response of a Hindmarsh-Rose oscillator array coupled to an RLC load

In this part, the Van der Pol oscillator is replaced by the Hindmarsh-Rose oscillator. The Hindmarsh-Rose oscillator is a self-sustained biological oscillator whose dynamics is based on the overall behavior of neurons [17,18] as explained in chapter 1. The Hindmarsh-Rose model presents good properties and is commonly used to study behavior of interacting neurons [19]. It is described by the following three coupled ordinary differential equations

$$\begin{cases} \dot{x} = -x^3 + w + a_1 x^2 + I - z \\ \dot{w} = 1 - dx^2 - w \\ \dot{z} = \gamma \left(s \left(x - a_0 \right) - z \right) \end{cases} \tag{3.26}$$

where the variable x is the membrane potential, the variables w and z model the transport rate of sodium, potassium ions and other ions across the membrane through fast and slow ion channels respectively. a_1 indicates the qualitative behavior of the oscillator. a_0 is the resting potential of the system. I is the external current injected in the oscillator. d is a positive constant while S and γ are constants of small values.

Figure 3.22 opposite shows us the signal generated by the Hindmarsh-Rose oscillator given by the differential equation (3.26), it is the bursting.

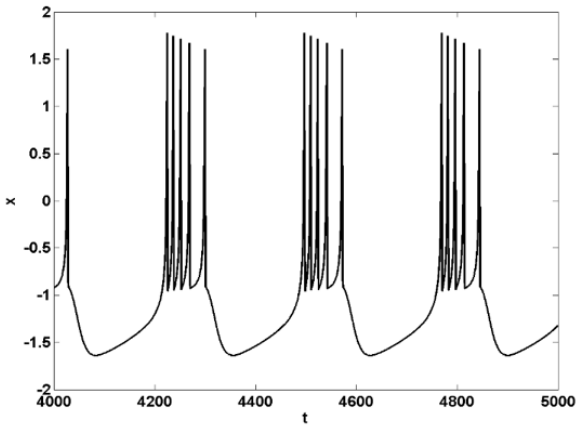

Figure 3.22: Signal generated by the HR oscillator with the following parameters: $I = 1.5, d = 5, a_0 = 3, a_1 = -1.5, S = 4, \gamma = 0.0021$

3.4.1 Voltage variation across each oscillator and across the load

We model the dynamics of an array of N Hindmarsh-Rose oscillators coupled to a RLC circuit by the set of equations (3.27) assuming that the x variable is coupled to the load.

$$\begin{cases} \dot{x}_j = -x_j^3 + w_j + a_1 x_j^2 - z_j + I + \alpha \ddot{y}_j \\ \dot{w}_j = 1 - w_j - d x_j^2 \\ \dot{z}_j = \gamma \left[s \left(x_j - a_0 \right) - z_j \right] \\ \sum_{k=1}^{N} \left(\ddot{y}_k + \lambda \dot{y}_k + \mu y_k \right) = \beta \left(x_j - y_j \right) \end{cases} \tag{3.27}$$

Figure 3.23 opposite shows us the signal generated by the Hindmarsh-Rose oscillator coupled to the RLC charge given by the differential equation (3.27). This corresponds to a spiking signal. So because of the coupling to the load, the bursting oscillations are transformed to spiking oscillations.

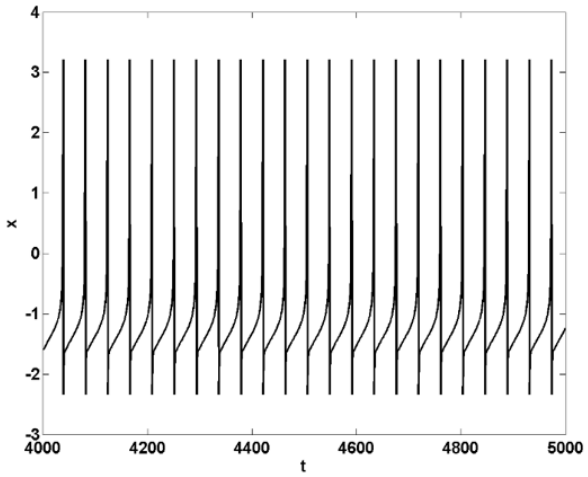

Figure 3.23: Signal generated by the HR oscillator coupled to the RLC load with the following parameters: $a_1 = 3, d = 5, I = 1.5, s = 4, \gamma = 0.0021, \beta = 10, \lambda = 2, \alpha = 0.6, \mu = 0.85, a_0 = -1.5$

Due to the complexity of the set of equations (3.27), it has not been possible to find analytical expressions as in the case of the Van der Pol oscillators. We thus rely on numerical simulations. In Figure 3.24, we plot for different values of the coupling coefficient α , the voltage amplitudes of the signals across the HR oscillator and across the RLC circuit. It is found that the voltage amplitudes across the HR oscillators and across the RLC circuit decrease with the increase of the number of HR oscillators. This is contrary to what was obtained in the case of an array of VdP oscillators. With the increase of the coupling coefficient α , one notes that these amplitudes decrease across the RLC circuit, but increase across the HR oscillator. We also remark that, depending of the coupling parameter α , there is a critical value of the number of HR oscillators under which there is no signal in the oscillator and no transmission of signal to the RLC circuit.

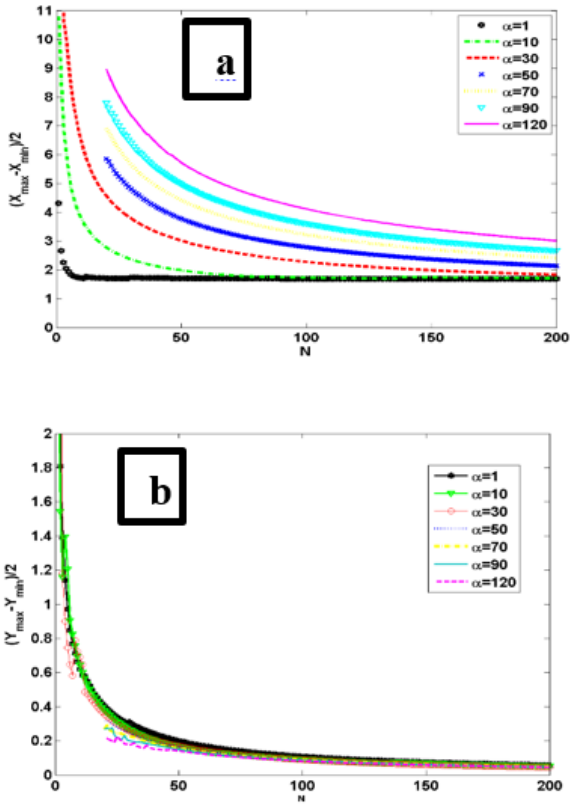

Figure 3.24: Voltage amplitudes response as a function of N (number of Hindmarsh-Rose oscillators): (a) Hindmarsh-Rose oscillator; (b) RLC oscillator, for the following parameters: $a_1 = 3, d = 5, I = 1.5, s = 4, \gamma = 0.0021, \beta = 10, \lambda = 2, \mu = 0.85, a_0 = -1.5$

3.4.2 Effect of the variation of the coupling coefficient

Plotting the variation of the amplitudes versus the coupling coefficient α , one finds that the system generates different types of dynamical behaviors as it appears in the bifurcation diagrams of Figure 3.26 with the variation of the Lyapunov exponent. With the increase of the coupling α , there is an increase of the amplitude across the HR oscillator and a decrease of the voltage amplitude across the RLC load (Figure 3.25). But, this decrease is irregular (non-monotonic) when the value of the coupling is in the range [40-120] (see Figure 3.25). Indeed, when the coupling coefficient α increases from 40 to 100, there is an alternating appearance of two dynamics in the load, namely chaotic (can be manifested by the appearance of spikes and bursting in an aperiodic way with also a sensitivity to the initial conditions) and quasi-periodic (is the signature of the combination of two signals of incommensurable frequencies (ratio different from an integer or the inverse of an integer.))

(Figure 3.26).

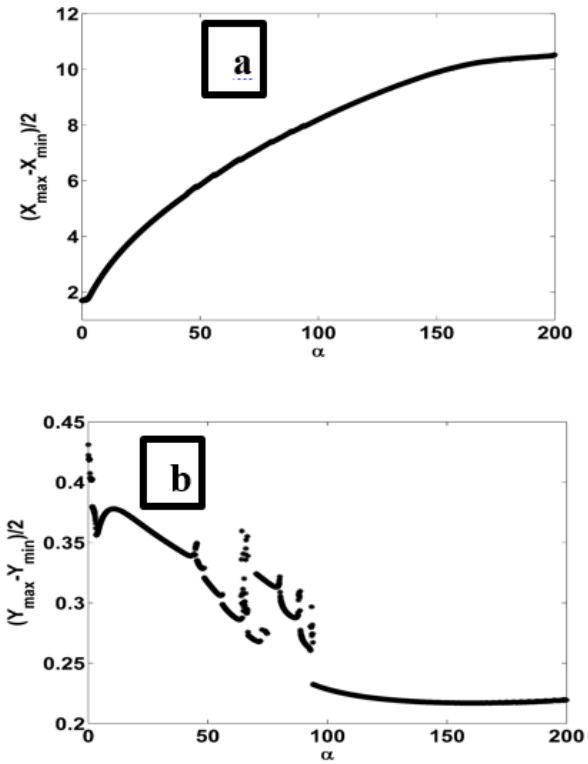

Figure 3.25: Voltage amplitudes responses versus the coupling coefficient α : (a) across the Hindmarsh-Rose oscillator; (b) across the RLC load for the following parameters: $a_1 = 3, d = 5, I = 1.5, s = 4, \gamma = 0.0021, \beta = 10, \lambda = 2, \mu = 0.85, a_0 = -1.5, N = 20$

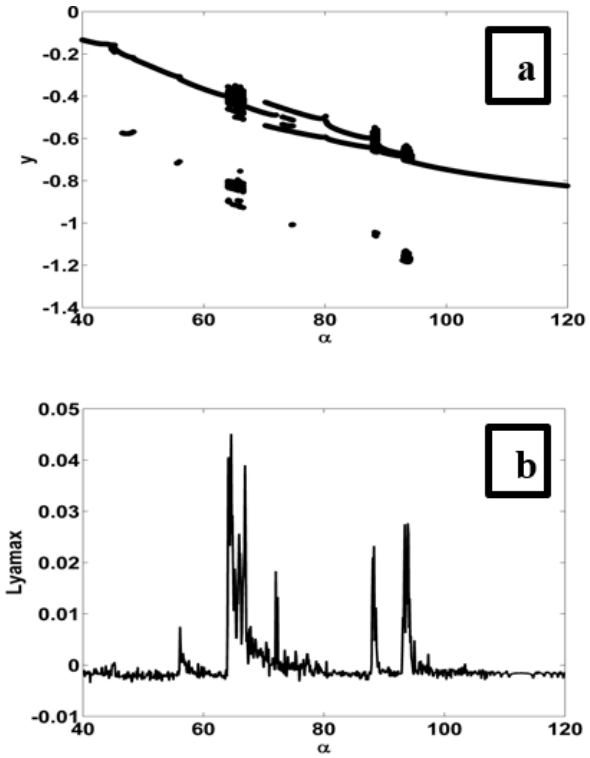

Figure 3.26: (a) Bifurcation diagram and (b) Lyapunov exponent (Lyamax) versus the coupling coefficient in RLC oscillator for these parameters $a_1 = 3, d = 5, I = 1.5, s = 4, \gamma = 0.0021, \beta = 10, \lambda = 2, \mu = 0.85, a_0 = -1.5, N = 20$

Simulation of Hindmarsh-Rose neuron showing typical neuronal bursting with this parameters.

3.5 Oscillations of the concentrations of chemical species in cyanobacteria

3.5.1 Case of the monomer

a) In vitro model

As presented in chapter 2 (section 2.3), the kinetics of the concentration of the different forms of the $KaiC$ protein in the monomer structure obeys the following set of differential equations

$$\begin{cases} \frac{dT}{dt} = k_{UT}(S) * U + k_{DT}(S) * D - k_{TU}(S) * T - k_{TD}(S) * T \\ \frac{dD}{dt} = k_{TD}(S) * T + k_{SD}(S) * S - k_{DT}(S) * D - k_{DS}(S) * D \\ \frac{dS}{dt} = k_{US}(S) * U + k_{DS}(S) * D - k_{SU}(S) * S - k_{SD}(S) * S \\ k_{XY}(S) = k^0_{XY} + \frac{k^A_{XY} * A(S)}{k_{\frac{1}{2}} + A(S)} \\ A(S) = \max\{0, [KaiA] - 2 * S\} \end{cases} \tag{3.28}$$

The numerically simulation of equations (3.28) led to figure 3.27 with the parameters taken from the litterature given in Table 3.2.

Table 3.2: The values of the parameter K^0_{XY} , K^A_{XY} with X, Y = U, T, D, S

$K_{1/2} = 43/100\ \mu M$	$K^0_{UT} = 0\ h^{-1}$	$K^0_{TD} = 0\ h^{-1}$	$K^0_{US} = 0\ h^{-1}$
$K^0_{SD} = 0\ h^{-1}$	$K^0_{DS} = 0.31\ h^{-1}$	$K^0_{DT} = 0\ h^{-1}$	$K^0_{TU} = 0.21\ h^{-1}$
$K^0_{SU} = 0.11\ h^{-1}$	$K^A_{SD} = 0.4791\ h^{-1}$	$K^A_{TD} = 0.2129\ h^{-1}$	$K^A_{US} = 0.0532\ h^{-1}$
$K^A_{SD} = 0.5\ h^{-1}$	$K^A_{DS} = -0.3194\ h^{-1}$	$K^A_{DT} = 0.173\ h^{-1}$	$K^A_{TU} = 0.0798\ h^{-1}$
$K^A_{SU} = -0.1331\ h^{-1}$			

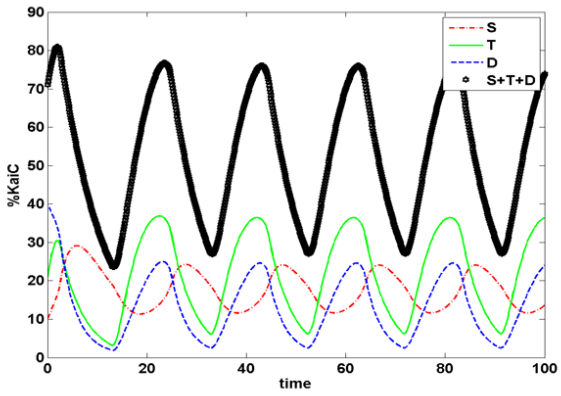

Figure 3.27: Percentages of the different forms of the phosphorylated $KaiC$ protein as a function of time (hours) with the parameters cited in Table 3.2.

We realize that all the protein form oscillate, so phosphorylation of $KaiC$ take place. In this figure, the curve in black, the green and the curve in blue are materialized by a double alternation behavior. Approximately, the oscillations period is $20h$.

b) In vivo model

As presented in chapter 2 (section 2.3), the kinetics of the concentration of the different forms of the $KaiC$ protein in the monomer form in the *in vivo* state obeys the following set of differential equations:

$$\begin{cases} \frac{dU}{dt} = k_{TU} * T + k_{SU} * S - k_{UT} * U - k_{US} * U - V * \frac{U}{K+U} - V_d * U + K_s * M \\ \frac{dT}{dt} = k_{UT}(S) * U + k_{DT}(S) * D - k_{TU}(S) * T - k_{TD}(S) * T - V * \frac{T}{K+T} - V_d * T \\ \frac{dD}{dt} = k_{TD}(S) * T + k_{SD}(S) * S - k_{DT}(S) * D - k_{DS}(S) * D - V * \frac{D}{K+D} - V_d * D \\ \frac{dS}{dt} = k_{US}(S) * U + k_{DS}(S) * D - k_{SU}(S) * S - k_{SD}(S) * S - V * \frac{S}{K+S} - V_d * S \\ \frac{dM}{dt} = V_s * \frac{K_i^n}{K_i^n + C_r^n} - V_m * \frac{M}{K_m + M} \end{cases} \tag{3.29}$$

Where $C_r = C_U * U + C_T * T + C_S * S + C_D * D$

The numerically simulation of equations (3.29) led to figure 3.28 with the parameters taken from the literature are given in Table 3.2 above and Table 3.3.

Table 3.3: The values of the parameters of the system.

$V = 0.0078\ \mu M.h^{-1}$	$K = 0.1\ \mu M$	$K_i = 1\mu M$ $n = 4$	$V_S = 2\ \mu M.h^{-1}$
$K_S = 2.7\ h^{-1}$	$V_d = 0.02\ h^{-1}$	$C_U = 0.9$	$C_T = 0.5$
$C_D = 0.3$	$C_S = 1$	$V_m = 0.2\ \mu M.h^{-1}$	$K_m = 0.2\ \mu M$

These results indicate also oscillations meaning the circadian clock. The U concentration, which is new curve, oscillates and approaches the value of 80; the T and D concentration curves have the same behavior as before. The concentration curve of S is periodic with a period of $20h$. It admits a half-wave behavior because it oscillates in only one direction.

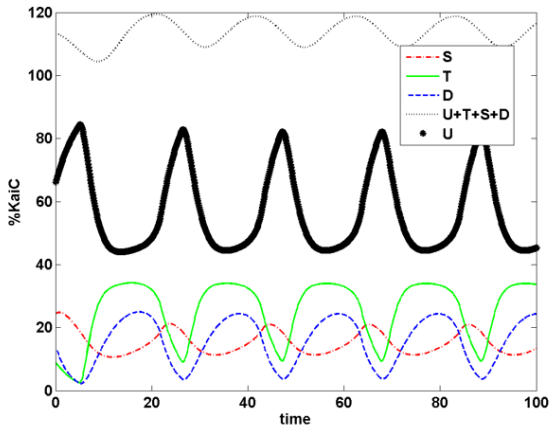

Figure 3.28: Percentage of the different form of the phosphorylated $KaiC$ protein function of time (h) *in vivo* with the parameters of Tables 3.2 and 3.3

c) Stability of the oscillations

In this part, the question that interests us is to see if the oscillations present in the system appear in a wide range of the system parameter values. This corresponds to check the stability of the phosphorylation necessary for the circadian clock. This was done for all parameters and the parameter K_{TU}^{A} caught our attention. Thus, we opt to plot the bifurcation diagram as K_{TU}^{A} varies (because this is the parameter that had the widest range of values where we can see the oscillations arise). Figure 3.29 and figure 3.30 presents respectively the bifurcation diagram of the *in-vitro* model and the bifurcation diagram of the *in vivo* model. One observes of its two figures that oscillations are presents in wide range of K_{TU}^{A}. An interesting fact is that the oscillations amplitude in the *in vivo* form is very small in comparison to the amplitude obtained in the *in-vitro* form. Moreover, one finds that the range of stability is smaller in the *in vivo* form. But as indicated above, there is a large range of K_{TU}^{A} in which the circadian clock manifests itself.

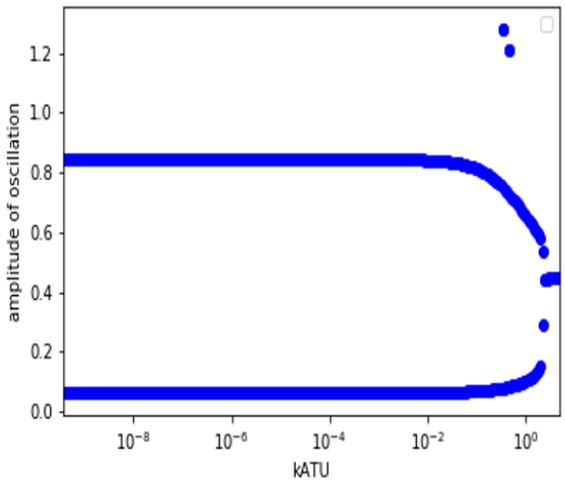

Figure 3.29: Bifurcation diagram of the *in vitro* model of the amplitude of the oscillations as a function of the parameter K_{TU}^{A} (the maximal influence of $KaiA$ on that rate constant for the transition from state T to state U) with the parameter cited in Tables 3.2

3.5.2 Oscillations in the hexamer structure

a) Oscillations in the vitro model

As presented in chapter 2, in the hexamer structure, the concentration of the $KaiC_{i,j,k}$ and $KaiB * KaiC_{i,j,k}$ are described by the set of differential equations in (2.8).
The initial conditions used for the numerical simulations are:

$$\begin{aligned} &KaiC_{000} = 3.6 * 0.552/2; KaiC_{100} = 3.6 * 0.186/2; \\ &KaiC_{010} = 3.6 * 0.085/2; KaiC_{001} = 3.6 * 0.177/2 \\ &KaiC_{600} = 3.6 * 0.186/2; \\ &KaiC_{060} = 3.6 * 0.085/2; KaiC_{006} = 3.6 * 0.177/2 \end{aligned} \tag{3.30}$$

For the equations at the boundaries of i,j and k (($i = 0$ ou$i = 6$); ($j = 0$ ou $j = 6$) ; ($k = 0$ ou $k = 6$)) the following scheme has been used:

$$\begin{aligned} &KaiC_{0,i,j} = 0; KaiC_{6,i,j} = 0; KaiC_{i,0,k} = 0; KaiC_{i,6,k} = 0; \\ &KaiC_{i,j,0} = 0; KaiC_{i,j,6} = 0; KaiB * KaiC_{0,i,j,} = 0; \\ &KaiB * KaiC_{6,i,j} = 0; KaiB * KaiC_{i,0,k} = 0; \\ &KaiB * KaiC_{i,6,k} = 0; KaiB * KaiC_{i,j,0} = 0; KaiB * KaiC_{i,j,6} = 0 \end{aligned} \tag{3.31}$$

The values of some parameters used for the simulations taken from the literature are given in table 3.4.

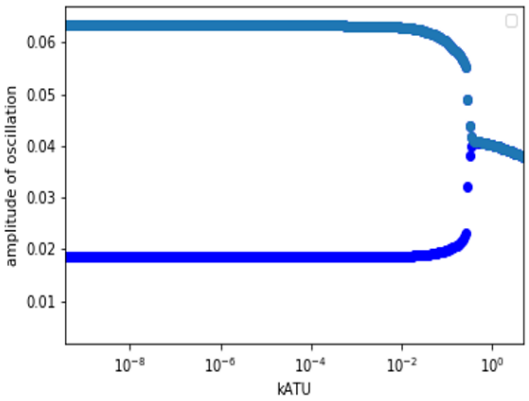

Figure 3.30: Bifurcation diagram of the *in vivo* model of the amplitude of the oscillations as a function of the parameter K^A_{TU} (the maximal influence of $KaiA$ on that rate constant for the transition from state T to state U) with the parameter cited in Tables 3.2 and Tables 3.3

Table 3.4: The values of the parameter K^0_{XY} ,K^{Act}_{XY}, with $\mathrm{X, Y = U, T, D, S}$.

$K^{Act}_{SU} = 0\ h^{-1}$	$K^0_{UT} = 0\ h^{-1}$	$K^0_{TD} = 0\ h^{-1}$	$K^0_{US} = 0\ h^{-1}$
$K^0_{TU} = 0\ h^{-1}$	$K^0_{SU} = 0.11\ h^{-1}$	$K^{Act}_{UT} = 0.4791\ h^{-1}$	$K^{Act}_{TD} = 0.2129\ h^{-1}$
$K^{Act}_{US} = 0.0532\ h^{-1}$	$K^{Act}_{SD} = 0.5\ h^{-1}$	$K^{Act}_{DS} = 0\ h^{-1}$	$K^{Act}_{DT} = 0.173\ h^{-1}$
$K^{Act}_{TU} = 0.29\ h^{-1}$	$K^0_{DT} = 0\ h^{-1}$	$K^0_{SD} = 0\ h^{-1}$	$K^0_{DS} = 0.31\ h^{-1}$
$K_{on,B} = 0.15\ h^{-1}$	$K_{off,B} = 0.33\ h^{-1}$	$V_{spr} = 2.7\ \mu M.h^{-1}$	

With the above, we have succeeded in getting oscillations as it appears in figure 3.31 for mean value of $KaiC_{i,j,k}$. These oscillations indicate that the hexamer structure also lead to phosphorylation and thus entertains the circadian clock. The above figure illustrates the periodic behavior of 40h periods of $KaiCs$ and the oscillations amplitude is about 0.49. Each period is materialized by two behaviors: one part is characterized by the sudden variation (increase) in $KaiC$ and the other by an exponential decrease.

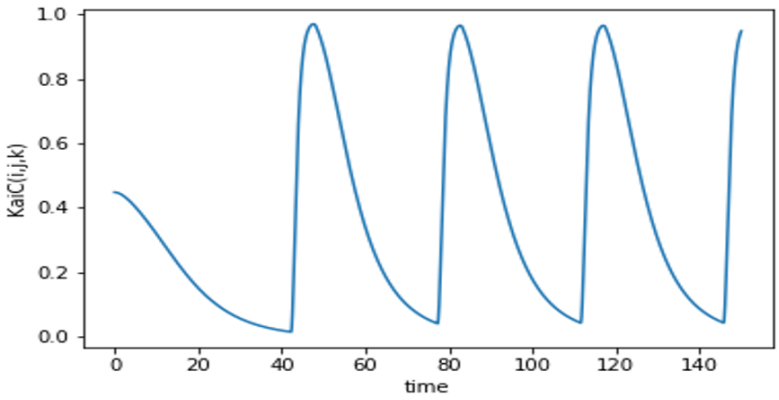

Figure 3.31: Percentage of phosphorylated $KaiC$ as a function of time (hours) *in vitro* with parameter of Table 3.4.

b) Oscillations in the vivo model

As in the case of monomer, an extension has also been conducted in the vivo state in which the hexamer configuration is described by the following set of equations (equation 3.32).

$$
\begin{cases}
\frac{d\left[KaiC_{i,j,k}\right]}{dt} = k_{UT}^{i,j,k}\left(7-(i+j+k)\right)\left[KaiC_{i-1,j,k}\right] + \\
k_{US}^{i,j,k}\left(7-(i+j+k)\right)\left[KaiC_{i,j-1,k}\right] + \\
k_{TD}^{i,j,k}\left(i+1\right)\left[KaiC_{i+1,j,k-1}\right] + k_{TU}^{i,j,k}\left(i+1\right)\left[KaiC_{i+1,j,k}\right] + \\
k_{DT}^{i,j,k}\left(k+1\right)\left[KaiC_{i-1,j,k+1}\right] + \\
k_{DS}^{i,j,k}\left(k+1\right)\left[KaiC_{i,j-1,k+1}\right] + k_{SD}^{i,j,k}\left(j+1\right)\left[KaiC_{i,j+1,k-1}\right] + \\
k_{SU}^{i,j,k}\left(j+1\right)\left[KaiC_{i,j+1,k}\right] - \\
\left(\begin{array}{l}(6-i-j-k)*k_{UT}^{i+1,j,k} + (6-i-j-k)*k_{US}^{i,j+1,k} + i*k_{TD}^{i-1,j,k+1} + \\ i*k_{TU}^{i-1,j,k} + k*k_{DT}^{i+1,j,k-1} + k*k_{DS}^{i,j+1,k-1} \\ +j*k_{SD}^{i,j-1,k+1} + j*k_{SU}^{i,j-1,k} + k_{on,B}*F_B^{i,j,k}\end{array}\right)*\left[KaiC_{i,j,k}\right] \\
+k_{off,B}*\left[KaiB*KaiC_{i,j,k}\right] - \frac{V\times KaiC_{i,j,k}}{K+KaiC_{i,j,k}} - V_d\times KaiC_{i,j,k} \\
\frac{d\left[KaiB*KaiC_{i,j,k}\right]}{dt} = k_{UT}^{i,j,k}\left(7-(i+j+k)\right)\left[KaiB*KaiC_{i-1,j,k}\right] + \\
k_{US}^{i,j,k}\left(7-(i+j+k)\right)\left[KaiB*KaiC_{i,j-1,k}\right] + \\
k_{TD}^{i,j,k}\left(i+1\right)\left[KaiB*KaiC_{i+1,j,k-1}\right] + k_{TU}^{i,j,k}\left(i+1\right)\left[KaiB*KaiC_{i+1,j,k}\right] + \\
k_{DT}^{i,j,k}\left(k+1\right)\left[KaiB*KaiC_{i-1,j,k+1}\right] + \\
k_{DS}^{i,j,k}\left(k+1\right)\left[KaiB*KaiC_{i,j-1,k+1}\right] + k_{SD}^{i,j,k}\left(j+1\right)\left[KaiB*KaiC_{i,j+1,k-1}\right] + \\
k_{SU}^{i,j,k}\left(j+1\right)\left[KaiB*KaiC_{i,j+1,k}\right] - \\
\left(\begin{array}{l}(6-i-j-k)*k_{UT}^{i+1,j,k} + (6-i-j-k)*k_{US}^{i,j+1,k} + i*k_{TD}^{i-1,j,k+1} + \\ i*k_{TU}^{i-1,j,k} + k*k_{DT}^{i+1,j,k-1} + k*k_{DS}^{i,j+1,k-1} \\ +j*k_{SD}^{i,j-1,k+1} + j*k_{SU}^{i,j-1,k} + k_{off,B}*F_B^{i,j,k}\end{array}\right)* \\
\left[KaiB*KaiC_{i,j,k}\right] \\
+k_{on,B}*\left[KaiC_{i,j,k}\right] - \frac{V\times KaiB*KaiC_{i,j,k}}{K+KaiB*KaiC_{i,j,k}} - V_d\times KaiB*KaiC_{i,j,k} \\
\frac{dM}{dt} = Vs\frac{K_i^4}{K_i^4+\left(\sum_{j\neq 0} KaiB*KaiC_{i,j,k}\right)} - \frac{V_m\times M}{K_m+M} \\
\frac{d[KaiC_{0,0,0}]}{dt} = \frac{d[KaiC_{0,0,0}]}{dt} + K_s\times \mathrm{M} - \frac{V\times KaiC_{0,0,0}}{K+KaiC_{0,0,0}} - V_d\times KaiC_{0,0,0}
\end{cases}
\tag{3.32}
$$

With $0 \leq i,j,k \leq 6$

The numerical simulation has also shown the oscillatory behavior of $KaiC_{i,j,k}$ fraction in phosphorylated form as it is presented in Figure 3.32. The oscillations period is about $22h$. The shape of the oscillations is similar to the one observed in the *in vitro* model. However, the oscillations amplitude equal to 0.435 is very small compare to the *in vitro* form due to the presence of dilution, degradation and production parameters.

Each period is materialized by two behaviors: one part is characterized by the sudden variation (increase) in $KaiC$ and the other by exponential decrease. Therefore, one can conclude that even the hexamer model in the *in vivo* state also generates oscillations and thus maintains the circadian clock.

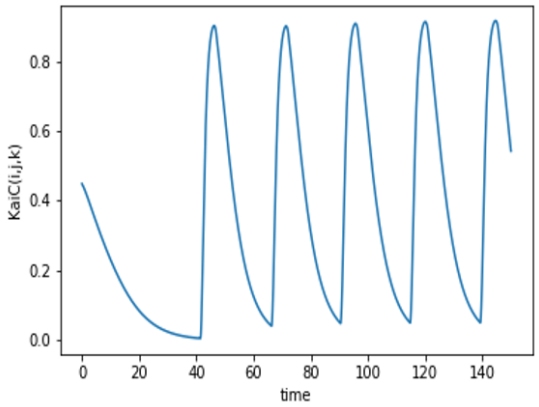

Figure 3.32: Percentage of phosphorylated $KaiC$ as a function of time (hours) *in vivo* with the parameters cited in Tables 3.3 and 3.4

As in [73], we consider on top of the wild type (WT) cyanobacterial circadian clock described above, the case of a mutant cyanobacteria lacking the transcriptional feedback. This is simply done by replacing the production term of $mRNA$ by a constant production rate V_{sptr}. This mutant is referred to as post-transcriptional (PTR) mutant while the WTR clock has a transcriptional translational regulation (TTR). We analyzed the sensitivity to parameter changes of the PTR mutant and showed that model does not requires fine tuning to generated oscillations, see figure 3.33. We observe that the main change between the WTR cyanobacteria and the mutants lacking the TTR circuit is that the WTR bacteria are more robust to changes in the translation rate. However, the TTR circuit is not crucial for the clock to be robust against changes in the dilution rate.

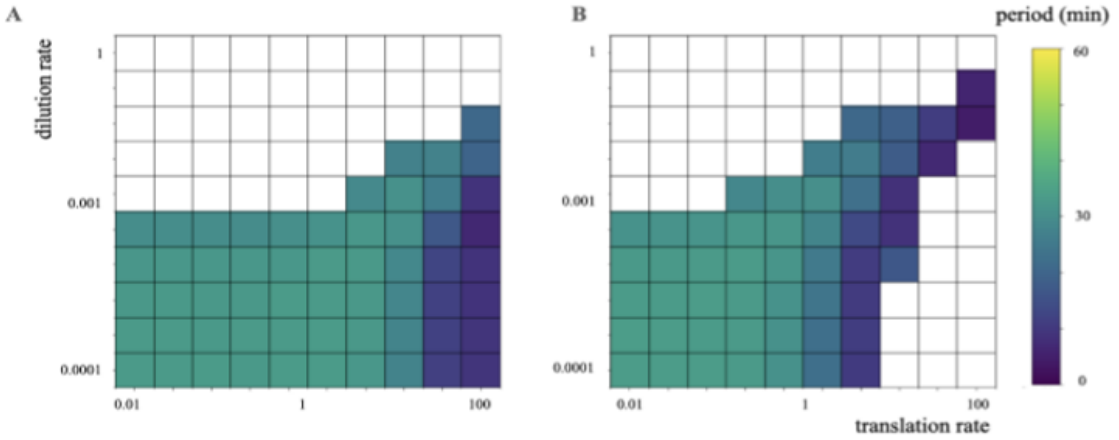

Figure 3.33: Robustness analysis of the wild type model (panel A) and the model for the mutant lacking the transcriptional regulation (panel B) over parameter changes. We varied both the translation rate K_S and the dilution rate V_d over 4 orders of magnitudes.

3.6 Conclusion

In this chapter, we have presented and discussed the results obtained.

In section 2, we have presented the system of the array of Van der Pol oscillator coupled to the load in which the powering an electrical load by an array of Van der Pol oscillators and the voltages variation across the load and oscillator are analyzed. It appeared from our analysis that the power increases versus the number of oscillators and when the number of oscillator is less than a critical value, there is no generation of voltages in the system. We showed that the high order nonlinearity affects the voltages by increasing their values.

In section 3, an equivalent electric circuit model of the Grudzinski and Zebrowski oscillator was proposed and subsequently a set of this oscillator coupled with the load was presented. The voltages variation across the load and the oscillator and the power in an electrical load were analyzed. We showed that the power increases versus the resistance and with the number of oscillators.The study of the synchronization of the Grudzinski and Zebrowski oscillators coupled to a load led to a map on a plane where we can have the range of values where there is synchronization and the range of values where there is no synchronization. The power in case of synchronization was analyzed.

In section 4, the response of coupled Hindmarsh-Rose oscillator is considered where the effect of the variation of the coupling coefficient is analyzed and we showed that when the coupling coefficient increases, there is an alternating appearance of two dynamics in the load (chaotic and quasi- periodic dynamics).

In section 5, the oscillations of the concentrations of chemical species in cyanobacteria have been considered where we showed in the case of monomer the range of the value of the parameter K_{TU}^{A} where the oscillation was presented and we propose a revisited version of the *in vivo* model of the cyanobacterial circadian clock, our model is able to reproduce oscillatory behavior for the mutant, as observed experimentally, without finely tuned parameters.

General conclusion

In this thesis, we were concerned by four problems.

The first problem was to analyze the response of several heart cells modeled by the Van der Pol oscillator when they are coupled to a biological organ (load) and the influence of the high order of the nonlinearity of the Van der Pol oscillator on the variation of the electric power in the load. Our analysis has shown that the power in the load is equal to zero when the number of the oscillators is below a critical value. Above this critical value, the power increases with the number of the oscillators. A resonance phenomenon is observed in the variation of the power in the load versus the resistance with the number of Van der Pol oscillators fixed. Moreover, the higher order of nonlinearity in the damping of the Van der Pol oscillator increases the voltage amplitude response and thereby the output power in the load.

The second problem was to do a similar study as that done on the Van der Pol oscillator but instead using the Grudzinsky-Zebrowski oscillator and to propose an electrical circuit whose equation is similar to the self-sustained oscillator model presented by Grudzinski-Zebrowski. Our analysis has shown that the RL load consumes more power than RLC load while the pure resistive load consumes the highest power whereas the power consumed by the RC load is at the intermediate level. Considering a direct coupling of all the oscillators, the synchronization domains were delimited as a function of the number of oscillators and the coupling coefficient. The variation of the coupling parameter and the dissipation coefficient shows that only a periodic dynamic appears. We found that, when the synchronization is reached for a fixed number of Grudzinski-Zebrowski oscillators in the system (direct coupling of the N oscillator coupled to the load), the power delivered to the load decreases and reaches a value,then begins to increases and reaches a value, and finally decreases. It decreases again according to the increase of the coefficient of mutual. It is observed that, when the mutual coupling coefficient increases, the power decreases when the number of oscillators increases. The shape of the power curve is a succession of decay and growth as the number of Grudzinski-Zebrowski oscillator's increases.

The third problem was to replace the Van der Pol oscillator with the Hindmarsh-Rose oscillator and redo the same study as done previously on the Van der Pol oscillator. Our analysis has shown that the increase of the number of the HR oscillators and the coupling coefficient α results in an increase of voltage amplitudes across the HR oscillators and

a decrease of the voltage amplitude across the RLC load. Moreover, it has been found that varying the coupling coefficient leads to the appearance of quasi-periodic and chaotic dynamics in the system.

The fourth problem was to investigate the existence of the circadian clock in cyanobacteria and to study the stability of this clock in the case of cyanobacteria taken as a monomer and to extend in the vivo state of the cyanobacteria taken as a hexamer. Our analysis has shown that in the case of monomer the parameter K_{TU}^{A} had a wide range of values for which there was oscillation and therefore phosphorylation of $KaiC$ which implied a good functioning of its circadian clocks. In case of hexamer, we propose a revisited version of the *in vivo* cyanobacterial clock which is in agreement with current experiments. We expect that the synchronization properties of the clock will also be enhanced by TTR regulation.

Following this thesis,

- We intend to carry out a synchronization study of a set of Van der Pol oscillators coupled to the load RC.
- An experimental study based on the generation of pulsatile and chaotic behaviors from the electrical equivalent of the Grudzinski and Zebrowki oscillator is awaited.
- For the cyanobacterial circadian clock, our work showed that the role of the transcriptional regulation is not key for robustness as suggested before. In the future, we should develop a stochastic model to study the desynchronization of the clocks in a population of cyanobacteria (Gillespie algorithm).

Appendix

Appendix 1

The first law which states that the sum of the incoming currents is equal to the sum of the outgoing currents at $J-th$ oscillator.

$$i_{v_j} + i_{L_{v_j}} + i_{C_{v_j}} + i_j = 0 \tag{3.33}$$

With $i_{v_j} = -a\left(\frac{v_j}{V_0}\right) + b\left(\frac{v_j}{V_0}\right)^3; i_{L_{v_j}} = \frac{1}{L_v}\int v_j dt; i_{C_{v_j}} = C_v\frac{dv_j}{dt}; i_j = C_0\frac{du_j}{dt}$

$$\Rightarrow -a\left(\frac{v_j}{V_0}\right) + b\left(\frac{v_j}{V_0}\right)^3 + \frac{1}{L_v}\int v_j dt + C_v\frac{dv_j}{dt} + C_0\frac{du_j}{dt} = 0 \tag{3.34}$$

The second law which states that the algebraic sum of the voltages in a closed circuit is zero. Therefore we have to consider the first oscillator and the $j-j-th$ oscillator to have a closed circuit. On a step:

$$u_1 - v_1 + v_j - u_j = 0 \tag{3.35}$$

We can still find this relation by saying that in a parallel assembly the tension is the same in all the branches. So we have this:

$$v_j - u_j = v_1 - u_1; 2 \leq j \leq N \tag{3.36}$$

Thereafter, by considering the mesh which connects the load to the first oscillator and applying in the same way the law of the meshs on this last circuit. We then have the following relation:

$$u_1 - v_1 + u_C + u_L + u_R = 0 \tag{3.37}$$

$$\Rightarrow u_1 - v_1 + \frac{1}{C}\int i dt + L\frac{di}{dt} + Ri = 0 \tag{3.38}$$

Now at node S, we have:

$$i_j + i_N + i_1 = i \tag{3.39}$$

By replacing each expression of (3.39) by its expression, we thus have the relation (3.40) which will be replaced in (3.38), we will have thereafter the relation (3.41)

$$i = C_0\frac{du_j}{dt} + C_0\frac{du_N}{dt} + C_0\frac{du_1}{dt} = C_0\sum_{k=1}^{N}\frac{du_k}{dt} \tag{3.40}$$

$$\frac{1}{C}\int C_0 \sum_{k=1}^{N} \frac{du_k}{dt}dt + L\frac{d}{dt}\left(C_0 \sum_{k=1}^{N} \frac{du_k}{dt}\right) + RC_0 \sum_{k=1}^{N} \frac{du_k}{dt} = v_1 - u_1 \tag{3.41}$$

By integrating the expression (3.41) with respect to time, we have:

$$\sum_{k=1}^{N}\left[\frac{1}{C}\int u_k dt + L\frac{du_k}{dt} + Ru_k\right] = \frac{1}{C_0}\int (v_1 - u_1)dt \tag{3.42}$$

In order to be able to have another form of equations (3.34), (3.36), and (3.42) we will derive these different equations. We successively obtain the equations (3.43), (3.44) and (3.45) given by:

$$C_v\ddot{v}_j - \left[-a - 3b\left(\frac{v_j}{V_0}\right)^2\right]\frac{\dot{v}_j}{V_0} + C_0\ddot{u}_j + \frac{1}{L_v}v_j = 0 \tag{3.43}$$

$$\dot{v}_j - \dot{u}_j = \dot{v}_1 - \dot{u}_1 \tag{3.44}$$

$$\sum_{k=1}^{N}\left(L\ddot{u}_k + R\dot{u}_k + \frac{1}{C}u_k\right) = \frac{1}{C_0}(v_1 - u_1) \tag{3.45}$$

Subsequently to have the characteristic Van der Pol equation coupled to the load, we will proceed by a change of variable, which induces a normalization of the voltage as $x_j = \frac{v_j}{V_0}$ and $y_j = \frac{u_j}{V_0}$ with time which is also normalized in the form $t_{ref} = \frac{1}{\omega_0}$. Where $\omega_0 = \frac{1}{\sqrt{L_v C_v}}$ is the natural frequency of the electric oscillator.

By replacing each term by its normalized value in equations (3.43), (3.44) and (3.45) we obtain the system of equations (3.46) describing the dynamics of the system

$$\begin{cases} \ddot{x}_j + \alpha\ddot{y}_j - d\left[1 - x_j^2 + bx_j^4\right]\dot{x}_j + x_j = 0; 1 \leq j \leq N \\ \sum_{k=1}^{N}\left(\ddot{y}_k + \lambda\dot{y}_k + \mu y_k\right) = \beta\left(x_1 - y_1\right) \end{cases} \tag{3.46}$$

where $\lambda = \frac{R}{L\omega_0}$, $\mu = \frac{L_v C_v}{LC}$, $\beta = \frac{L_v C_v}{LC_0}$, $\alpha = \frac{C_0}{C_v}$, $d = \frac{a}{C_v V_0 \omega_0}$

Appendix 2

The hexameric form was used in order to want to generalize the $KaiC$ protein which has been studied previously in the simplest form (monomer). Knowing that each $KaiC$ hexamer has ($n = 6$) subunits (monomer) where n is the number of subunits, each of them containing two sites. Each site can phosphorylate or dephosphorylate, therefore each $KaiC$ hexamer can progress to a total of 12 possible reactions which will increase or decrease i, j, k by 1. So for each combinatorial composition of phosphorylated subunits in a $KaiC$ hexamer (where the order is assumed not to be important), we parameterize the hexamer state as follows:

i= number of subunits pT (phosphorylated to T)

j= number of subunits pS (phosphorylated to S)

k= number of subunits $pSpT$ (doubly phosphorylated to T and to S)

u= number of non-phosphorylated subunits= $6 - (i + j + k)$

with $0 \leq i, j, k \leq 6$

Therefore, consider the following kinetic reaction (3.47) describing the phosphorylation of the hexamer $KaiC$ and the binding of $KaiB$ under the near-steady state approximations used.

$$\begin{aligned} &KaiC^{B}_{i,j,k} \rightleftarrows KaiC^{A}_{i,j,k} \rightleftarrows KaiC^{*}_{i,j,k} \\ &\uparrow k_{off} \downarrow k_{on} \\ &KaiB * KaiC^{B}_{i,j,k} \rightleftarrows KaiB * KaiC^{A}_{i,j,k} \rightleftarrows KaiB * KaiC^{*}_{i,j,k} \end{aligned} \tag{3.47}$$

Where:

$KaiC^{A}_{i,j,k}$ is the protein that interacted with $KaiC_{i,j,k}$;

$KaiC^{*}$ is the active protein;

$KaiC^{B}_{i,j,k}$ is the protein that interacted with $KaiC_{i,j,k}$

The equations thus describing the dynamics of our system with $KaiC$ as hexamer is given by the equations below (3.48)

$$
\begin{aligned}
&\tfrac{d[KaiC_{i,j,k}]}{dt} = k_{UT}^{i,j,k}\,(7-(i+j+k))\,[KaiC_{i-1,j,k}] + \\
&k_{US}^{i,j,k}\,(7-(i+j+k))\,[KaiC_{i,j-1,k}] + \\
&k_{TD}^{i,j,k}\,(i+1)\,[KaiC_{i+1,j,k-1}] + k_{TU}^{i,j,k}\,(i+1)\,[KaiC_{i+1,j,k}] + \\
&k_{DT}^{i,j,k}\,(k+1)\,[KaiC_{i-1,j,k+1}] + \\
&k_{DS}^{i,j,k}\,(k+1)\,[KaiC_{i,j-1,k+1}] + k_{SD}^{i,j,k}\,(j+1)\,[KaiC_{i,j+1,k-1}] + \\
&k_{SU}^{i,j,k}\,(j+1)\,[KaiC_{i,j+1,k}] - \\
&\left(\begin{array}{l}(6-i-j-k)*k_{UT}^{i,j,k} + (6-i-j-k)*k_{US}^{i,j,k} + i*k_{TD}^{i,j,k} + \\ i*k_{TU}^{i,j,k} + k*k_{DT}^{i,j,k} + k*k_{DS}^{i,j,k} \\ +j*k_{SD}^{i,j,k} + j*k_{SU}^{i,j,k} + k_{on,B}*F_B^{i,j,k}\end{array}\right)*[KaiC_{i,j,k}] \\
&+k_{off,B}*[KaiB*KaiC_{i,j,k}]
\end{aligned}
\tag{3.48}
$$

By assuming $KaiC$ in a complex $KaiB*KaiC$, the latter can be activated by free $KaiA$, therefore an equation similar to the equation (3.48) is given in (3.49).

$$
\begin{aligned}
&\tfrac{d[KaiB*KaiC_{i,j,k}]}{dt} = k_{UT}^{i,j,k}\,(7-(i+j+k))\,[KaiB*KaiC_{i-1,j,k}] + \\
&k_{US}^{i,j,k}\,(7-(i+j+k))\,[KaiB*KaiC_{i,j-1,k}] + \\
&k_{TD}^{i,j,k}\,(i+1)\,[KaiB*KaiC_{i+1,j,k-1}] + k_{TU}^{i,j,k}\,(i+1)\,[KaiB*KaiC_{i+1,j,k}] + \\
&k_{DT}^{i,j,k}\,(k+1)\,[KaiB*KaiC_{i-1,j,k+1}] + \\
&k_{DS}^{i,j,k}\,(k+1)\,[KaiB*KaiC_{i,j-1,k+1}] + k_{SD}^{i,j,k}\,(j+1)\,[KaiB*KaiC_{i,j+1,k-1}] + \\
&k_{SU}^{i,j,k}\,(j+1)\,[KaiB*KaiC_{i,j+1,k}] - \\
&\left(\begin{array}{l}(6-i-j-k)*k_{UT}^{i,j,k} + (6-i-j-k)*k_{US}^{i,j,k} + i*k_{TD}^{i,j,k} + \\ i*k_{TU}^{i,j,k} + k*k_{DT}^{i,j,k} + k*k_{DS}^{i,j,k} \\ +j*k_{SD}^{i,j,k} + j*k_{SU}^{i,j,k} + k_{off,B}\end{array}\right)*[KaiB*KaiC_{i,j,k}] \\
&+k_{on,B}*F_B^{i,j,k}\,[KaiC_{i,j,k}]
\end{aligned}
\tag{3.49}
$$

For each $KaiB$ molecule, we assume that one $KaiA$ dimer can be sequestered (thus $m=2$ below), hence the amount of $KaiA$ in a system dependent on $[KaiB*KaiC_{i,j,k}]$ is given in the folowing path:

$$
[KaiA] = \max\left(0, [KaiA]_0 - m*6\,[KaiB*KaiC_{i,j,k}]\right), m=2 \tag{3.50}
$$

Where $[KaiA]_0$ is the initial amount of $KaiA$ in the system. This describes the limit where the equilibrium of the constant association between $KaiA$ and $KaiB*KaiC$ is

asymptotically zero. The overall control of $KaiA$ concentration by the titration molecule mechanism allows for the synchronized negative feedback on $KaiA$ activity which leads to stable oscillations in this model.

The free energy contribution of each subunit is determined by its state of phosphorylation. There are four possible subunit states and each of them is assigned to one ΔG that we treat as an unknown parameter during model optimization. So the difference in free energy between the two allosteric states depends on the number of each form of monomer in a given $KaiC$ hexamer:

$$\Delta G_{hexamere} = \Delta G_{i,j,k} = i*\Delta G_{pT}+j*\Delta G_{pS}+k*\Delta G_{pSpT}+(6-(i+j+k))*\Delta G_U \quad (3.51)$$

And at equilibrium, we have:

$$\Delta G_{i,j,k} = -K_B * T \ln\left(K_A^{i,j,k}\right) \quad (3.52)$$

Which implies:

$$K_A^{i,j,k} = e^{-\frac{\Delta G_{i,j,k}}{K_B * T}} \quad (3.53)$$

Where $K_A^{i,j,k} = \frac{KaiC^B_{i,j,k}}{KaiC^A_{i,j,k}}$ is defined as.

The fraction of $KaiC$ in the autokinase state of $KaiA$ activated (knowing that only $KaiC^A$ can be activated by $KaiA$) is given by (3.54):

$$F_A = \frac{[KaiC^*]}{[KaiC^B]+[KaiC^A]+[KaiC^*]} = \frac{[KaiA]}{[KaiA]+K_m*K_A+K_m} \quad (3.54)$$

Knowing that $\left[KaiC^B\right] = K_A * \left[KaiC^A\right]$ and $[KaiC^*] = \frac{\left[KaiC^A\right][KaiA]}{K_m}$ with $K_m^{eff} = K_m*(1+K_A)$

The kinetic rates for phosphorite transitions $(X \to Y)$, where X is the subunit of the phosphorylation state reagent and Y is the subunit of the phosphorylation state product are a set as described below:

$$K_{xy}^{i,j,k} = F_A^{i,j,k} * k_{xy}^{act} + \left[1 - F_A^{i,j,k}\right] * k_{xy}^0 \quad (3.55)$$

Where $F_A^{i,j,k}$ depends on the composition of the hexamer subunit (i,j,k) which determines $K_A^{i,j,k}$.

Finally, in the absence of $KaiA$, the fraction of $KaiC$ a specific configuration of the phosphate (i,j,k) in the competent state of the binding $KaiB$ is given above:

$$F_B = \frac{KaiC^B_{i,j,k}}{KaiC_{i,j,k}} = \frac{KaiC^B_{i,j,k}}{KaiC^B_{i,j,k}+KaiC^A_{i,j,k}} = \frac{1}{1+\frac{1}{\mathrm{K_A}}+\frac{[KaiA]}{K_m*K_A^{i,j,k}}} \quad (3.56)$$

The concentrations of the $KaiC_{i,j,k}$ ($KaiC$ hexamer) and $KaiB * KaiC_{i,j,k}$ (the complex of $KaiC$ hexamer with $KaiB$) are described by the following set of differential equations (3.57)

$$
\left\{
\begin{array}{l}
\frac{d\left[KaiC_{i,j,k}\right]}{dt} = k_{UT}^{i,j,k}\left(7-(i+j+k)\right)\left[KaiC_{i-1,j,k}\right] + k_{US}^{i,j,k}\left(7-(i+j+k)\right)\left[KaiC_{i,j-1,k}\right] + \\
k_{TD}^{i,j,k}\left(i+1\right)\left[KaiC_{i+1,j,k-1}\right] + k_{TU}^{i,j,k}\left(i+1\right)\left[KaiC_{i+1,j,k}\right] + k_{DT}^{i,j,k}\left(k+1\right)\left[KaiC_{i-1,j,k+1}\right] + \\
k_{DS}^{i,j,k}\left(k+1\right)\left[KaiC_{i,j-1,k+1}\right] + k_{SD}^{i,j,k}\left(j+1\right)\left[KaiC_{i,j+1,k-1}\right] + k_{SU}^{i,j,k}\left(j+1\right)\left[KaiC_{i,j+1,k}\right] - \\
\left(\begin{array}{l}
(6-i-j-k) * k_{UT}^{i+1,j,k} + (6-i-j-k) * k_{US}^{i,j+1,k} + i * k_{TD}^{i-1,j,k+1} + i * k_{TU}^{i-1,j,k} + \\
k * k_{DT}^{i+1,j,k-1} + k * k_{DS}^{i,j+1,k-1} \\
+j * k_{SD}^{i,j-1,k+1} + j * k_{SU}^{i,j-1,k} + k_{on,B} * F_B^{i,j,k}
\end{array}\right) * \left[KaiC_{i,j,k}\right] \\
+k_{off,B} * \left[KaiB * KaiC_{i,j,k}\right] \\
\frac{d\left[KaiB*KaiC_{i,j,k}\right]}{dt} = k_{UT}^{i,j,k}\left(7-(i+j+k)\right)\left[KaiB * KaiC_{i-1,j,k}\right] + \\
k_{US}^{i,j,k}\left(7-(i+j+k)\right)\left[KaiB * KaiC_{i,j-1,k}\right] + \\
k_{TD}^{i,j,k}\left(i+1\right)\left[KaiB * KaiC_{i+1,j,k-1}\right] + k_{TU}^{i,j,k}\left(i+1\right)\left[KaiB * KaiC_{i+1,j,k}\right] + \\
k_{DT}^{i,j,k}\left(k+1\right)\left[KaiB * KaiC_{i-1,j,k+1}\right] + \\
k_{DS}^{i,j,k}\left(k+1\right)\left[KaiB * KaiC_{i,j-1,k+1}\right] + k_{SD}^{i,j,k}\left(j+1\right)\left[KaiB * KaiC_{i,j+1,k-1}\right] + \\
k_{SU}^{i,j,k}\left(j+1\right)\left[KaiB * KaiC_{i,j+1,k}\right] - \\
\left(\begin{array}{l}
(6-i-j-k) * k_{UT}^{i,j,k} + (6-i-j-k) * k_{US}^{i,j,k} + i * k_{TD}^{i,j,k} + i * k_{TU}^{i,j,k} + \\
k * k_{DT}^{i,j,k} + k * k_{DS}^{i,j,k} \\
+j * k_{SD}^{i,j,k} + j * k_{SU}^{i,j,k} + k_{off,B}
\end{array}\right) * \left[KaiB * KaiC_{i,j,k}\right] \\
+k_{on,B} * F_B^{i,j,k}\left[KaiC_{i,j,k}\right]
\end{array}
\right. \tag{3.57}
$$

with $0 \leq i, j, k \leq 6$

Bibliography

Bibliography

[1] Usha, K. (2019). Hindmarsh Rose neuron model with menristors. *Biosystems* 178, 1-9

[2] Jalife, J. (1984). Mutual entrainment and electrical coupling as mechanisams for synchronous firing of rabbit sinoatrial pacemaker cells. *The Journal of physiology* 356(1), 221-243.

[3] Walors, F. Aarabi, Ardalan, and al. (2008). Inverse coupling between respiratory and cardiac oscillators in a life threatening event in a neonate automatic neuroscience. *Basic and clinical* 143, 79-82.

[4] Bub, G., Glass, L. (1995). Bifurcations in a discontinuous circle map: a theory for a chaotic cardiac arrhythmia: a theory for a chaotic cardiac arrhythmia. *International Journal of Bifurcation and Chaos* 5(02), 359-371.

[5] Grudzinski, K., Zebrowski, J. J. (2004). Modeling cardiac pacemakers with relaxation oscillators. *Physica A: statistical Mechanics and its Applications* 336(1-2), 153-162.

[6] Zebrowski, J. J., Grudzinski, K., Buchner, T., Kuklik, P., Gac, J., Gielerak, G., ... Baranowski, R. (2007). Nonlinear oscillator model reproducing various phenomena in the dynamics of the conduction system of the heart. *Chaos: An Interdisciplinary Journal of Nonlinear Science* 17(1), 015121.

[7] Grudzinski, K., Zebrowski, J. J., Baranowski, R. (2006). Model of the sino-atrial and atrio-ventricular nodes of the conduction system of the human heart. *Biomedical Engineering/Biomedizinische Technik* 51(4), 210-214.

[8] Raja, M. A. Z., Shah, F. H., Syam, M. I. (2018). Intelligent computing approach to solve the nonlinear Van der Pol system for heartbeat model. *Neural Computing and Applications* 30(12), 3651-3675.

[9] El-Chami, M. F., Al-Samadi, F., Clementy, N., Garweg, C., Martinez-Sande, J. L., Piccini, J. P., Roberts, P. R. (2018). Updated performance of the Micra transcatheter pacemaker in the real-world setting: a comparison to the investigational study and a transvenous historical control. *Heart Rhythm* 15(12), 1800-1807.

[10] Hodgkin, A. L., Huxley, A. F. (1952). The components of membrane conductance in the giant axon of Loligo. *The Journal of physiology* 116(4), 473-496.

[11] Van Der Pol, B., Van Der Mark, J. (1928). LXXII. The heartbeat considered as a relaxation oscillation, and an electrical model of the heart. *The London, Edinburgh, and Dublin Philosophical Magazine and Journal of Science* 6(38), 763-775.

[12] Katholi, C. R., Urthaler, F., Macy Jr, J., James, T. N. (1977). A mathematical model of automaticity in the sinus node and AV junction based on weakly coupled relaxation oscillators. *Computers and Biomedical Research* 10(6), 529-543.

[13] Kaiser, F. (1988). Theory of non-linear excitations. *In Biological coherence and response to external stimuli* (pp. 25-48). Springer, Berlin, Heidelberg.

[14] Behnia, S., Ziaei, J., Ghiassi, M., Akhshani, A. (2015). Nonlinear dynamic approach of heartbeats based on the Grudzinski-Zebrowski's model. *Chin. J. Phys,* 53, 120702.

[15] Ferreira, B. B., de Paula, A. S., Savi, M. A. (2011). Chaos control applied to heart rhythm dynamics. *Chaos, Solitons Fractals* 44(8), 587-599.

[16] Nana, B., Woafo, P. (2008). Power delivered by an array of Van der Pol oscillators coupled to a resonant cavity. *Physica A: Statistical Mechanics and its Applications* 387(13), 3305-3313.

[17] Hindmarsh, J. L., Rose, R. M. (1984). A model of neuronal bursting using three coupled first order differential equations. Proceedings of the Royal society of London. Series B. *Biological sciences,* 221(1222), 87-102.

[18] Kazemi, A., Ahmadi, A., Gomar, S. (2014, May). A digital synthesis of Hindmarsh-Rose neuron: A thalamic neuron model of the brain. *In 2014 22nd Iranian Conference on Electrical Engineering (ICEE)* (pp. 238-241). IEEE.

[19] Selverston, A. I., Rabinovich, M. I., Abarbanel, H. D., Elson, R., Szücs, A., Pinto, R. D., ... Varona, P. (2000). Reliable circuits from irregular neurons: a dynamical approach to understanding central pattern generators. *Journal of Physiology-Paris* 94(5-6), 357-374.

[20] Pikovsky, A. S., Rosenblum, M., Kurths, J. (2001). Synchronization-A unified approach to nonlinear science. *Cambridge University Press, Cambridge* 7(8).

[21] Boccaletti, S., Kurths, J., Osipov, G., Valladares, D. L., Zhou, C. S. (2002). The synchronization of chaotic systems. *Physics reports* 366(1-2), 1-101.

[22] Boccaletti, S., Latora, V., Moreno, Y., Chavez, M., Hwang, D. U. (2006). Complex networks: Structure and dynamics. *Physics reports,* 424(4-5), 175-308.

[23] Enjieu Kadji, H. G., Chabi Orou, J. B., Woafo, P. (2007). Spatiotemporal dynamics in a ring of N mutually coupled self-sustained systems. *Chaos: An Interdisciplinary Journal of Nonlinear Science* 17(3), 033109.

[24] Nana, B., Woafo, P. (2006). Synchronization in a ring of four mutually coupled van der Pol oscillators: theory and experiment. *Physical Review E* 74(4), 046213.

[25] Goldbeter, A. (1997). Biochemical oscillations and cellular rhythms: the molecular bases of periodic and chaotic behaviour. *Cambridge university press.*

[26] Moore-Ede, M. C., Sulzman, F. M., Fuller, C. A. (1982). The clocks that time us: physiology of the circadian timing system. *Harvard Univ Pr.*

[27] Hardin, P. E., Hall, J. C., Rosbash, M. (1990). Feedback of the Drosophila period gene product on circadian cycling of its messenger RNA levels. *Nature,* 343(6258), 536-540.

[28] Grima, B., Chelot, E., Xia, R., Rouyer, F. (2004). Morning and evening peaks of activity rely on different clock neurons of the drosophila brain. *Nature* 431, 869-73.

[29] Huang, T. C., Grobbelaar, N. (1995). The circadian clock in the prokaryote Synechococcus RF-1. *Microbiology* 141(3), 535-540.

[30] Huang, T. C., Lin, R. F. (2009). Circadian Rhythm of Cyanothece RF-1 (Synechococcus RF-1). *In Bacterial Circadian Programs* (pp. 39-61) Springer, Berlin, Heidelberg.

[31] Sweeney BM, nad Borgese MB (1989), a circadian rhythm in cell division in a prokaryotes , the cyanobacterium synechococcus WH7803. J. *Phycol* 25:pp183-186

[32] Van der Pol, B. (1926). LXXXVIII. On 'relaxation-oscillations'. *The London, Edinburgh, and Dublin Philosophical Magazine and Journal of Science* 2(11), 978-992.

[33] Nagumo, J., Arimoto, S., Yoshizawa, S. (1962). An active pulse transmission line simulating nerve axon. *Proceedings of the IRE* 50(10), 2061-2070.

[34] Nygren, A., Fiset, C., Firek, L., Clark, J. W., Lindblad, D. S., Clark, R. B., Giles, W. R. (1998). Mathematical model of an adult human atrial cell: the role of K+ currents in repolarization. *Circulation research* 82(1), 63-81.

[35] Noble, D. (1962). A modification of the Hodgkin-Huxley equations applicable to Purkinje fibre action and pacemaker potentials. *The Journal of physiology* 160(2), 317-352.

[36] Di Francesco, D., Noble, D. (1985). A model of cardiac electrical activity incorporating ionic pumps and concentration changes. *Philosophical Transactions of the Royal Society of London. B, Biological Sciences* 307(1133), 353-398.

[37] Luo, C. H., Rudy, Y. (1994). A dynamic model of the cardiac ventricular action potential. II. After depolarizations, triggered activity, and potentiation. *Circulation research* 74(6), 1097-1113.

[38] Luo, C. H., Rudy, Y. (1994). A dynamic model of the cardiac ventricular action potential. I. Simulations of ionic currents and concentration changes. *Circulation research* 74(6), 1071-1096.

[39] Ten Tusscher, K. H., Noble, D., Noble, P. J., Panfilov, A. V. (2004). A model for human ventricular tissue. *American Journal of Physiology-Heart and Circulatory Physiology* 286(4), H1573-H1589.

[40] Van der Pol, B., Van der Mark, M. (1928). The beating of the heart considered as relaxation oscillation and an electric model of the heart. *L'onde électrique* 7, 365-392.

[41] Gois, S. R., Savi, M. A. (2009). An analysis of heart rhythm dynamics using a three-coupled oscillator model. *Chaos, Solitons Fractals* 41(5), 2553-2565.

[42] di Bernardo, D., Signorini, M. G. (1998). A model of two nonlinear coupled oscillators for the study of heartbeat dynamics. *International journal of Bifurcation and Chaos* 8(10), 1975-1985.

[43] dos Santos, A. M., Lopes, S. R., Viana, R. R. L. (2004). Rhythm synchronization and chaotic modulation of coupled Van der Pol oscillators in a model for the heartbeat. *Physica A: Statistical Mechanics and its Applications* 338(3-4), 335-355.

[44] Ferreira, B. B., Savi, M. A., de Paula, A. S. (2014). Chaos control applied to cardiac rhythms represented by ECG signals. *Physica Scripta* 89(10), 105203.

[45] Sato, S., Doi, S., Nomura, T. (1994). Bonhoeffer-van der Pol oscillator model of the sino-atrial node: a possible mechanism of heart rate regulation. *Methods of information in medicine* 33(01), 116-119.

[46] Honerkamp, J. (1983). The heart as a system of coupled nonlinear oscillators. *Journal of Mathematical Biology* 18(1), 69-88.

[47] Makouo,L., and Woafo,P. (2017). Experimental observation of bursting patterns in Van der Pol oscillators. *Chaos,Solitons and Fractals* 94, 95-101.

[48] Ryzhii, E., Ryzhii, M. (2014). A heterogeneous coupled oscillator model for simulation of ECG signals. *Computer methods and programs in biomedicine* 117(1), 40-49.

[49] Cardarilli, G. C., Di Nunzio, L., Fazzolari, R., Re, M., Silvestri, F. (2019). Improvement of the Cardiac Oscillator Based Model for the Simulation of Bundle Branch Blocks. *Applied Sciences* 9(18), 3653.

[50] Lopez-Chamorro, F. M., Arciniegas-Mejia, A. F., Imbajoa-Ruiz, D. E., Rosero-Montalvo, P. D., García, P., Castro-Ospina, A. E., ... Peluffo-Ordóñez, D. H. (2018, April). Cardiac Pulse Modeling Using a Modified van der Pol Oscillator and Genetic Algorithms. *In International Conference on Bioinformatics and Biomedical Engineering* (pp. 96-106). Springer, Cham.

[51] Izhikevich, E. M. (2004). Which model to use for cortical spiking neurons ?. *IEEE transactions on neural networks* 15(5), 1063-1070.

[52] Izhikevich, E. M. (2007). Dynamical systems in neuroscience. *MIT press.*

[53] Morris, C., Lecar, H. (1981). Voltage oscillations in the barnacle giant muscle fiber. *Biophysical journal* 35(1), 193-213.

[54] FitzHugh, R. (1961). Impulses and physiological states in theoretical models of nerve membrane. *Biophysical journal* 1(6), 445-466.

[55] Hindmarsh, J. L., Rose, R. M. (1982). A model of the nerve impulse using two first-order differential equations. *Nature* 296(5853), 162-164.

[56] Françoise, J. P. (2005). Oscillations en biologie: analyse qualitative et modèles (Vol. 46). *Springer Science Business Media.*

[57] Izhikevich, E. M. (2000). Neural excitability, spiking and bursting. *International journal of bifurcation and chaos* 10(06), 1171-1266.

[58] Corson, N., Aziz-Alaoui, M. (2009, March). Couplages de neurones de type Hindmarsh-Rose: de la synchronisation à l'émergence de propriétés. *12e Rencontre du Non-Lineaire Paris*, p-47.

[59] Corson, N., Aziz-Alaoui, M. (2009). Asymptotic dynamics of Hindmarsh-Rose neuronal system. *Dynamics of continuous, Discrete and Impulsive Systems, series B: Applications and Algorithms*, (16) p-535.

[60] Ginoux, J. M., Rossetto, B. (2006). Slow manifold of a neuronal bursting model. *In Emergent properties in natural and artificial dynamical systems* (pp. 119-128). Springer, Berlin, Heidelberg.

[61] Storace, M., Linaro, D., de Lange, E. (2008). The Hindmarsh-Rose neuron model: bifurcation analysis and piecewise-linear approximations. *Chaos: An Interdisciplinary Journal of Nonlinear Science* 18(3), 033128.

[62] Najjar,R.P, Zeizer, J.M.(2017).Anatomy and physiology of the circadian system. *Sleep and neurologic disease* , 29-53. Academy Press.

[63] Reddy, S., Reddy, V., Sharma, S. (2020). Physiology, Circadian Rhythm. *StatPearls [internet].*

[64] Potter, G.D., Skene, D.J., Arendt, J., Cde, J. E., Grant, P.J., and al. Hardie, L.J. (2016). Circadian Rhythm and sleep disruption: causes, metabolic consequence and countermeasures. *Endocrine reviews* 37(6), 584-608.

[65] Marchant, J. (1729) .Observation botanique. *Histoire de l'Académie Royale des Sciences* , Paris ,35-36

[66] Schmidt, A.M, Jacoby, T.B. (1996). Herbs to orchids: *biotamical illustration in the nineteenth century.*

[67] Frisch,K.V,(1920). Uber den einfluss der bodenfarbe auf die fleckenzeichnung des feuersalamanders. *Verlay Von Georg Thieme* .

[68] Hardin, P. E., Hall, J. C., Rosbash, M. (1990). Feedback of the Drosophila period gene product on circadian cycling of its messenger RNA levels. *Nature* 343(6258), 536-540.

[69] Rouyer, F. (2005). Des horloges du matin et du soir dans le cerveau de la drosophile. *M/S: médecine sciences* 21(10), 808-810.

[70] Shearman, L. P., Sriram, S., Weaver, D. R., Maywood, E. S., Chaves, I., Zheng, B., Reppert, S. M. (2000). Interacting molecular loops in the mammalian circadian clock. *Science* 288(5468), 1013-1019.

[71] Nakajima, M., Imai, K., Ito, H., Nishiwaki, T., Murayama, Y., Iwasaki, H., Oyama, T., Kondo, T. (2005). Reconstitution of circadian oscillation of cyanobacterial KaiC phosphorylation in vitro. *Science* 308: 414.

[72] Rust, M. J., Markson, J. S., Lane, W. S., Fisher, D. S., O'Shea, E. K. (2007). Ordered Phosphorylation Governs Oscillation of a Three-Protein Circadian Clock. *Science* 318, 809.

[73] Teng, S. W., Mukherji, S., Moffitt, J. R., De Buyl, S., O'shea, E. K. (2013). Robust circadian oscillations in growing cyanobacteria require transcriptional feedback. *Science* 340(6133), 737-740.

[74] Lin, J., Chew, J., Chockanathan, U., Rust, M. J. (2014). Mixtures of opposing phosphorylations within hexamers precisely time feedback in the cyanobacterial circadian clock. *Proceedings of the National Academy of Sciences*, 111(37), E3937-E3945.

[75] Kitayama, Y., Nishiwaki-Ohkawa, T., Sugisawa, Y., Kondo, T. (2013). KaiC intersubunit communication facilitates robustness of circadian rhythms in cyanobacteria. *Nature communications*4(1), 1-13.

[76] Https: //fr.m.wikepedia.org/cyanobacteria (consultate the 08/09/21 at 12h).

[77] Lin, J., Chew, J., Chockanathan, U., Rust. M.J. (2014). Supporting Appendix for: Mixtures of opposing phosphorylations within hexamers precisely time feedback in the cyanobacterial circadian clock. *PNAS*, E3937-E3945.

[78] Hayashi, C. (1964). Forced Oscillations in Physical Systems. *McGraw-Hill Book Co*, p.392 (1964).

[79] Nayfeh, A. H., Mook, D. T.,Holmes, P.(1980). Nonlinear oscillations. *John Willey and Sons, New York*, 305, p 692-692.

[80] Pecora, L. M., Carroll, T. L. (1991). Driving systems with chaotic signals. *Physical Review A* 44(4), 2374.

[81] Frolkovic, P. (1990). Numerical recipes: The art of scientific computing. *Acta Applicandae Mathematica* 19(3), 297-299.

[82] Press, W. H., Teukolsky, S. A., Vetterling, W. T., Flannery, B. P. (2007). Numerical recipes 3rd edition: The art of scientific computing. *Cambridge university press.*

[83] Kepseu, W. D., Woafo, P., Sepulchre, J. A. (2010). Dynamics of the transition to pathogenicity in Erwinia chrysanthemi. *Journal of Biological Systems* 18(01), 173-203.

[84] Youmbi Fouego, D., Dongmo, E. D., Woafo, P. (2017). Powering RLC load by an array of self-sustained oscillators. *Chaos, Solitons Fractals* 104, 222-227.

[85] Youmbi Fouego, D., Dongmo, E. D., Woafo, P. (2021). Voltages responses and synchronization of an array of Grudzinski and Zebrowski oscillators coupled to an electrical load. *Chaos, Solitons Fractals* 146,110848.

List of publications

1- **Youmbi Fouego, D.**, Dongmo, E. D., Woafo, P. (2017). Powering RLC load by an array of self-sustained oscillators. *Chaos, Solitons Fractals* 104, 222-227.

2- **Youmbi Fouego, D.**, Dongmo, E. D., Woafo, P. (2021). Voltages responses and synchronization of an array of Grudzinski and Zebrowski oscillators coupled to an electrical load. *Chaos, Solitons Fractals* 146,110848.

3- **Youmbi Fouego, D.**, de Buyl, S. (2022). On the robustness of the in vivo cyanobacterial circadian clock. *Preprint on Arxiv*.

Collection of the published papers

Chaos, Solitons and Fractals 104 (2017) 222–227

Contents lists available at ScienceDirect

Chaos, Solitons and Fractals

Nonlinear Science, and Nonequilibrium and Complex Phenomena

journal homepage: www.elsevier.com/locate/chaos

Powering RLC load by an array of self-sustained oscillators

D. Youmbi Fouego[a], E.D. Dongmo[a], P. Woafo[a,b,*]

[a] Laboratory of Modelling and Simulation in Engineering, Biomimetics and Prototypes, and TWAS Research Unit, Department of Physics, Faculty of Science, P. O. Box 812, Yaoundé, Cameroon

[b] Applied Physics Research Group (APHY), Vrije Universiteit Brussel, Pleinlaan 2, 1050 Brussels, Belgium

ARTICLE INFO

Article history:
Received 14 April 2017
Revised 20 July 2017
Accepted 21 August 2017

Keywords:
Biological oscillators
Array of Van de Pol oscillators
Array of Hindmarsh–Rose oscillators
Power generation
RLC load
Chaos

ABSTRACT

This work deals with the analysis of the voltage amplitude generated in a linear load by an array of Van der Pol (VDP) and Hindmarsh–Rose (HR) oscillators. For the array of Van der Pol oscillators, it is found that after a threshold number of oscillators under which the power is equal to zero, the power increases with the size of the array. A high order nonlinearity in the damping of the Van der Pol oscillator increases the power. In the case of the array of HR oscillators, it is shown that varying the coupling coefficient leads to the appearance of chaotic dynamics in the system. Contrary to the case of the VDP oscillators, it is found that the voltage amplitudes decrease when the size of the array of the HR oscillators increases. These results can be linked to the mechanism of biological oscillators powering biological organs.

1. Introduction

The study of the dynamical behavior of single or coupled mechanical and electrical systems powered by self-sustained and bio-inspired oscillators is a subject that has attracted the attention of various scientists [1–5]. Coupled oscillators are of interest both for physical and biological systems as they describe interactions between different nodes and lead to special dynamics including full synchronization, partial synchronization, spatial chaos and spatio-temporal chaos [6]. Van der Pol oscillators [7], Rayleigh oscillators [8] and Hindmarsh–Rose oscillators, which are representative models of biological oscillators [9], are some of the most studied self-sustained oscillators. Coupling such oscillators of the electrical nature to a load (such as RLC load) can be interesting as this can be used as a representative model to analyze the effects of biological signals on biological organs, e.g., an ensemble of cells constituting the pacemaker acting on the heart or the image of an ensemble of neurons acting on a muscle. Moreover, this can represent the powering of some man made devices, the RLC load representing the electric image of the rest of the device. Furthermore, for biomimetic purpose, research is currently under way in view of constructing artificial oscillators behaving as the natural biological oscillators [10–12]. We would like to mention that there is no direct link between Van der Pol oscillator and the Hindmarsh–Rose oscillator apart the fact they are models describing (different) biological cells activities. Each one has its own dynamics.

But, one of the major problems met in those systems is the low magnitude of the output voltage amplitude and output power in the load and the determination of the number of oscillators capable of generating electrical signal in the load. This problem was considered in Ref. [13] with an array of classical Van der Pol oscillators coupled to a RLC load. And it was shown that there is a critical value of the number of oscillators under which no power is generated. Above this critical value, the output voltage and output power increase with the number of Van der oscillators. Kaiser showed in Ref. [14] that the modified Van Der Pol oscillator equation seems to be more appropriate to describe some biological processes better than the classical Van Der Pol oscillator. Moreover, the modified Van der Pol oscillator has proved to be more flexible as in some cases it leads to bistability which can have some biological implications [see Ref. 1]. Thus the first goal of this work is to complement the results reported in Ref [13] by analyzing the effects of higher order nonlinearity in the nonlinear damping of the Van der Pol oscillator. Secondly, we extend the analysis by considering the cases of RL, RC and R loads. The third goal is to extend the analysis to another biologically inspired self-sustained oscillator, namely the Hindmarsh–Rose oscillator which models neuronal activities [15,16].

The structure of the work is as follows. The voltage amplitudes and power due to the array of VDP oscillators are analyzed in Section 2, considering RLC, RL, RC and R loads. In Section 3, the Van der Pol oscillator is replaced by the Hindmarsh–Rose

* Corresponding author.
E-mail addresses: pwoafo@lamsebp.org, pwoafo1@yahoo.fr (P. Woafo).

http://dx.doi.org/10.1016/j.chaos.2017.08.018
0960-0779/

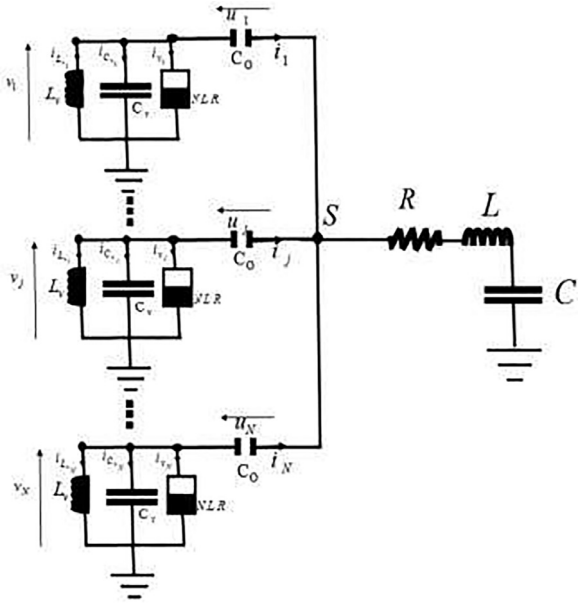

Fig. 1. An array of N Van der Pol oscillators coupled to a RLC oscillator.

oscillator and the voltage amplitude response is also analyzed. Section 4 summarizes the work.

2. Voltage amplitude and power generated by an array of Van der Pol oscillators in electrical loads

2.1. The system and equations

The studied system is shown in Fig. 1. This is a set of N Van der Pol oscillators coupled to a resonant RLC oscillator (full case). The coupling between the Van der Pol oscillators is indirect as it is through the load and the strength of the coupling depends on the values of the capacitance C_0. Each Van der Pol oscillator is constituted of an inductor of inductance L_v, a capacitor of capacitance C_v and a nonlinear resistance (NLR), all in parallel. Van der pol and Van der mark suggested that VDP oscillator can be used to model the beating of human heart and since then it has been a favorite choice in modeling biological phenomena [17]. The current–voltage characteristic of the nonlinear resistance is defined as follows:

$$i_{v_j} = -a\left(\frac{v_j}{V_0}\right) + a_1\left(\frac{v_j}{V_0}\right)^3 - a_2\left(\frac{v_j}{V_0}\right)^5 \tag{1}$$

where a, a_1,a_2 and V_0 are positive parameters.

Using Kirchhoff's laws and appropriate dimensionless variables, one obtains the following set of equations:

$$\begin{cases} \ddot{x}_j + \alpha\ddot{y}_j - d\left[1 - x_j^2 + bx_j^4\right]\dot{x}_j + x_j = 0 \qquad 1 \le j \le N & \text{(2a)} \\ \sum_{k=1}^{N} (\ddot{y}_k + \lambda\dot{y}_k + \mu y_k) = \beta(x_1 - y_1) & \text{(2b)} \end{cases}$$

where $x_j = \frac{v_j}{V_0}$, $y_j = \frac{u_j}{V_0}$, $\lambda = \frac{R}{L\omega_0}$, $\mu = \frac{L_v C_v}{LC}$, $\beta = \frac{L_v C_v}{LC_0}$ and $\alpha = \frac{C_0}{C_v}$

In the case of a RL load, the term μy_k is removed from equation (2b) while in the case of a RC load, the term $\ddot{y}_k$ is removed from equation (2b). But in this case, the coefficients λ, β and μ are replaced respectively by 1, λ_1 and λ_2 defined as:

$$\lambda = 1; \lambda_1 = \frac{1}{CR\omega_0} \text{ and } \lambda_2 = \frac{1}{C_0 R\omega_0}.$$

In this case of a simple R load, the terms $\ddot{y}_k$ and μy_k are removed from equation (2b). But in this last case, the coefficient β is replaced by β_1 defined as $\beta_1 = \frac{1}{C_0 R\omega_0}$.

The power in the load is consumed in the resistor and is given by the following expression

$$P = R \prec i \succ^2 \tag{3}$$

where $\prec i \succ$ is the effective current through the load. The current in the load is given by:

$$i = \sum_{k=1}^{N} C_0 \frac{du_k}{dt} \tag{4}$$

Let us assume that all the Van der Pol oscillators are synchronized. When the nonlinear coefficient d and the coupling coefficients α and β are small, the analytical solution of equations (2) can be found using the harmonic balance method which considers that the solutions are in the form of (5).

$$\begin{cases} x = A\cos(t + \phi) \\ y = B\cos(t + \varphi) \end{cases} \tag{5}$$

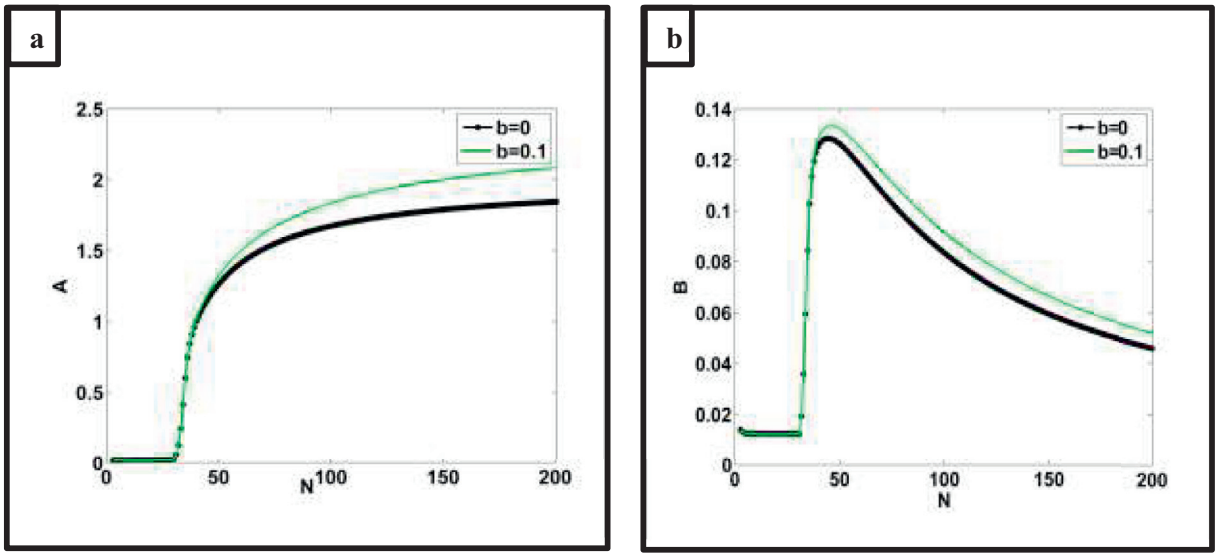

Fig. 2. Effect of the parameter b on the voltage amplitudes -response curves: (a) Van der Pol oscillator; (b) the coupling capacitance C_0, for $\alpha = 0.6$, $\beta = 10$, d = 0.1, $\lambda = 2$ and $\mu = 0.85$.

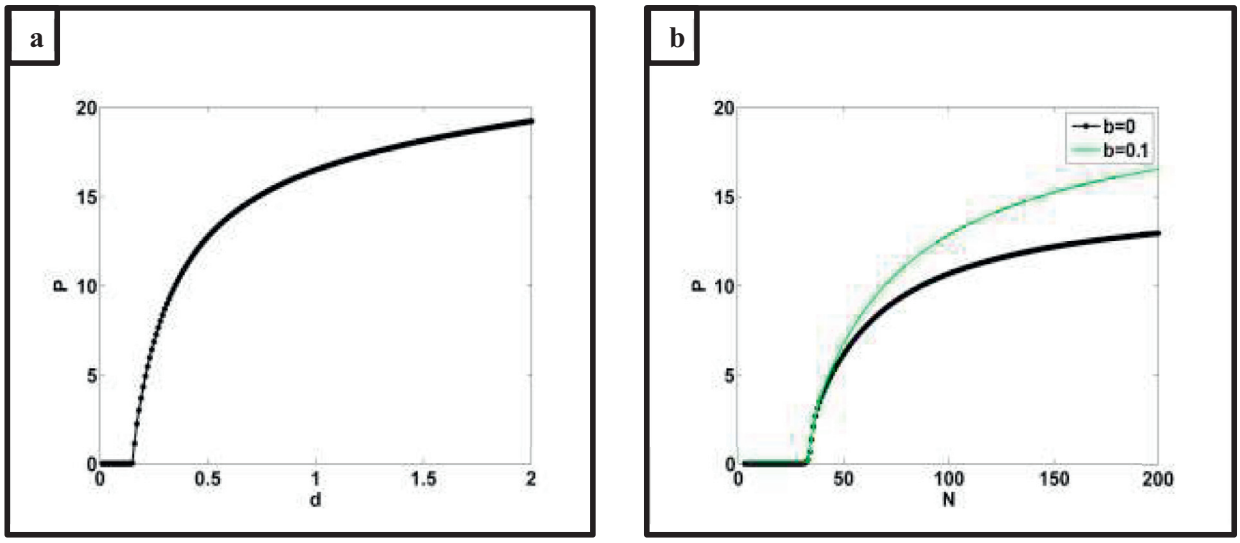

Fig. 3. Power in the RLC load versus d with $b = 0.1$ (Fig. 6a) and versus N for two different value of b with $d = 0.1$ (Fig. 6b) for $\alpha = 0.6$, $\beta = 10$, $\lambda = 2$, $\mu = 0.85$ and $R = 156\ \Omega$.

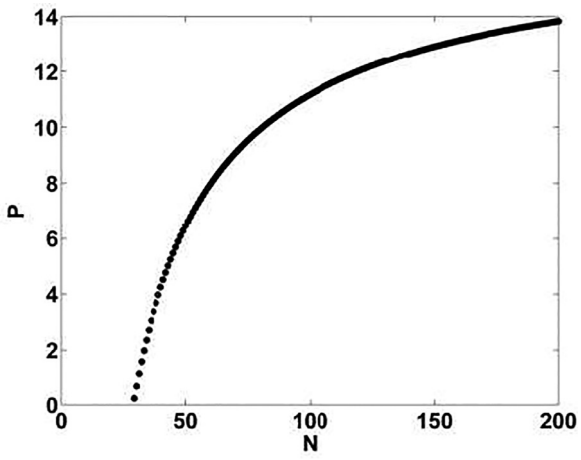

Fig. 4. Power in the RL load versus the number of oscillators in the array for $\alpha = 0.6$, $\beta = 10$, b = 0.1, $\lambda = 2$, d = 0.1 and $R = 156\ \Omega$.

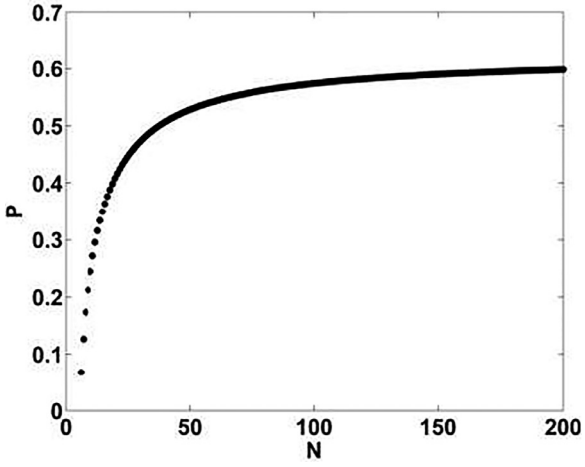

Fig. 6. Power in the R load versus the number of oscillators in the array for $\alpha = 0.6$, $\beta 1 = 0.86$, $b = 0.1$, $d = 0.1$ and $R = 156\ \Omega$.

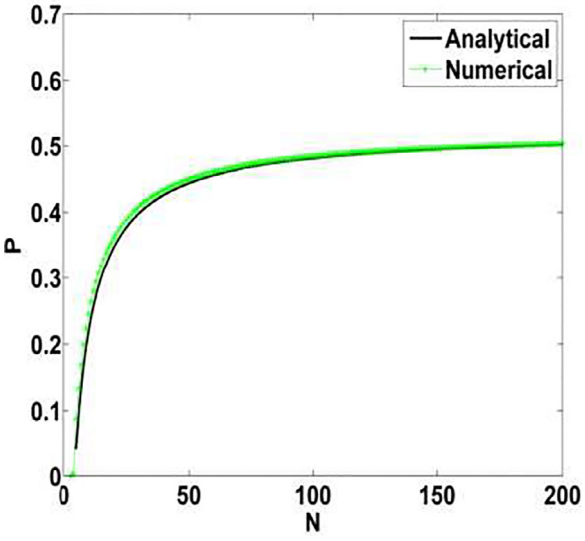

Fig. 5. Power in the RC load versus the number of oscillators in the array for $\lambda_1 = 0.44$, $\lambda_2 = 0.86$, d = 0.1, b = 0.1, $\alpha = 0.6$ and R = 156Ω.

where A and B are voltage amplitudes and, ϕ and φ are the phases of the voltages across the Van der Pol oscillators and the coupling capacitor respectively. Inserting these expressions in the equations, one obtains the voltage amplitudes A and B as

$$A = \sqrt{\frac{\frac{1}{4} - \sqrt{\frac{1}{16} - \frac{b}{2}\left(1 - \frac{\beta\alpha}{d\sqrt{(\mu N - N + \beta)^2 + \lambda^2 N^2}}\right)}}{\frac{b}{4}}} \tag{6}$$

and

$$B = \frac{\beta A}{\sqrt{(\mu N - N + \beta)^2 + \lambda^2 N^2}} \tag{7}$$

The voltage amplitude A exists under the following conditions

$$\begin{cases} N \in]N_1,\ N_{11}[\cup]N_{22},\ N_2[& \text{if } b > 1/8 \\ N \in]0,\ N_1[\cup]N_2,\ +\infty[& \text{if } 0b < 1/8 \end{cases} \tag{8}$$

where N_1, N_2, N_{11} and N_{22} are given below:

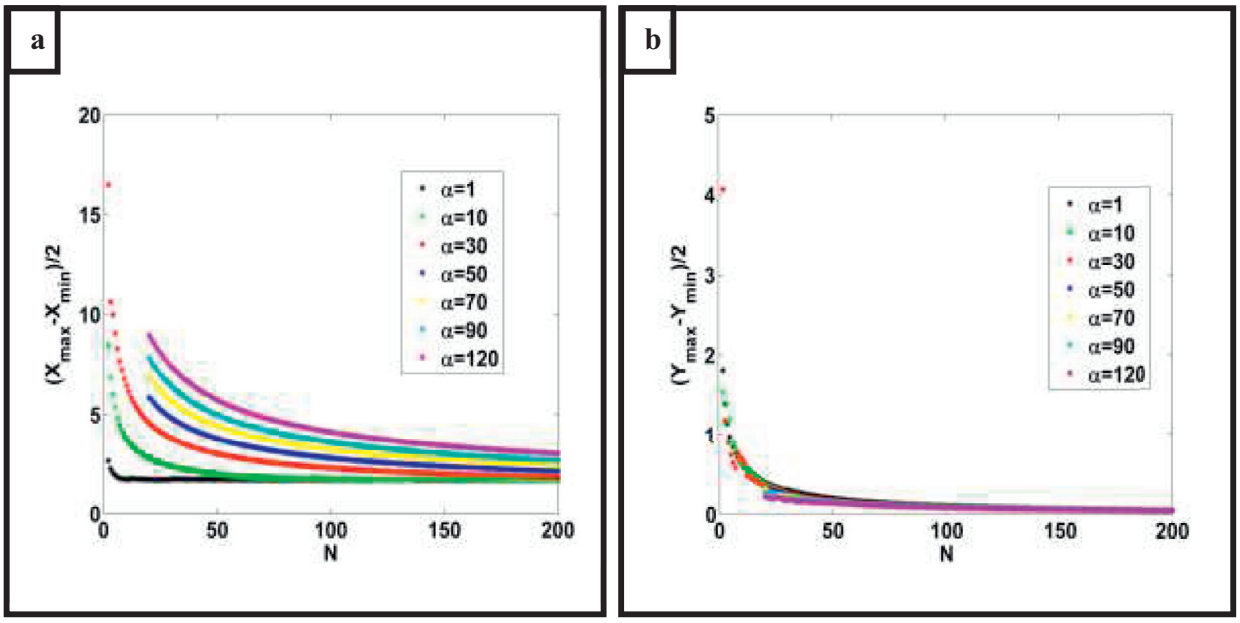

Fig. 7. Voltage amplitudes response: (a) Hindmarsh–Rose oscillator; (b) RLC oscillator, as a function of N (number of Hindmarsh–Rose oscillators), for the following parameters: $a_1 = 3, d = 5, I = 1.5, s = 4, \gamma = 0.0021, \beta = 10, \lambda = 2, \alpha = 0.6, \mu = 0.85, a_0 = -1.5$.

$$N_1 = \frac{(-2\mu\beta + 2\beta) - \sqrt{Q}}{2\left(\mu^2 + 1 - 2\mu + \lambda^2\right)},\ N_2 = \frac{(-2\mu\beta + 2\beta) + \sqrt{Q}}{2\left(\mu^2 + 1 - 2\mu + \lambda^2\right)},$$

$$N_{11} = \frac{(-2\mu\beta + 2\beta) - \sqrt{S}}{2\left(\mu^2 + 1 - 2\mu + \lambda^2\right)},\ \text{and}\ N_{22} = \frac{(-2\mu\beta + 2\beta) + \sqrt{S}}{2\left(\mu^2 + 1 - 2\mu + \lambda^2\right)},$$

with

$$S = \frac{4\beta^2\alpha^2}{d^2}\left(\mu^2 + 1 - 2\mu + \lambda^2\right) - 4\lambda^2\beta^2 \text{ and}$$

$$Q = \frac{4\beta^2\alpha^2}{d^2\left(1 - \frac{1}{8b}\right)^2}\left[\mu^2 + 1 - 2\mu + \lambda^2\right] - 4\lambda^2\beta^2$$

The expression of the power in the resistor is thus:

$$P = \frac{RN^2 w_0^2 C_v^2 V_0^2 \alpha^2 \beta^2 A^2}{2\left(\lambda^2 N^2 + (\mu N - N + \beta)^2\right)} \tag{9}$$

In what follows, the voltage amplitudes A and B and the power P are plotted versus N, b and d. The curves obtained from the analytical calculations are compared to those obtained from the direct numerical simulation of the set of differential equations (2). It has been found that for small values of nonlinear coefficients, there is a good agreement between the curves obtained from Eqs. (6), (7) and (9) and those obtained from the direct numerical simulation. The numerical simulation is therefore used only to present curves related to the case where the values of the nonlinear coefficients are not small enough to warrant the validity of the analytical results.

Fig. 2 presents the variations of A and B versus the number of the oscillators. When the number of oscillators is less than 29, there is no generation of voltage in the system. The Van der Pol oscillators are death because of the indirect coupling. After this critical value of N, the voltage in the Van der Pol oscillator increases with N and saturates at a value equal to 2 for large value of N. In its side, B increases with N and attains a maximal value (at $N = 50$) after which it decreases with N. This behavior of B versus N indicates that there is an optimal value of the size of the array leading to higher voltage in the load.

As it also appears in Fig. 2, the quartic nonlinear coefficient b affects the voltages by increasing their values. The analysis of the voltage amplitudes versus the d, for fixed value of N, has presented a voltage shape (for both the VDP oscillator and the RLC load) similar to what is observed in Fig. 2a. As d increases, the voltage amplitudes remain equal to zero until a threshold value of d after which they increase rapidly, then slowly with d and finally attain a plateau.

The fact that there are threshold values of the size of the array and of the nonlinear coefficient d can be related to the development of the heart pacemaker at its early stage. Indeed, it is known that, after its formation, the heart pacemaker remains silent and starts firing electrical signal after some days. A sort of quorum sensing phenomenon where the system starts its activity after a certain size, depending on the environment, is attained [18].

Now considering the power delivered to the load by the array of Van der Pol oscillators, Fig. 3 presents its variation versus the control parameters N, d and b. It is seen that the power increases with N after the critical value of N below which the power in the load is equal to zero (see Fig. 3b). The power begins to exist from $N = 30$ and increases until the value of $P = 16.53$ for $N = 200$ for $b = 0$. As for the voltage amplitudes, the power increases with d (Fig. 3a) and with b (Fig. 3b).

2.2. Power in the RL, RC and R loads

In the case of RL load, the critical value of N below which there is no power in the load is 29 and that power increases until the value of $P = 13.84$ for $N = 200$ (Fig. 4) while in the case of the RC load, that critical value of N is 3 and the power increases until the value of $P = 0.503$ for $N = 200$ (Fig. 5). In the case of the R load, that critical value of N is 6 and the power increases until the value of $P = 0.5983$ for $N = 200$ (Fig. 6). According to Fig. 5, a good agreement is found between the analytical and the numerical results. This has been also the case for other figures.

Comparing Figs. 3 to 6, one can note that for load with inductance, the number of oscillators necessary to activate the load is higher than in the case of loads without inductance. Moreover,

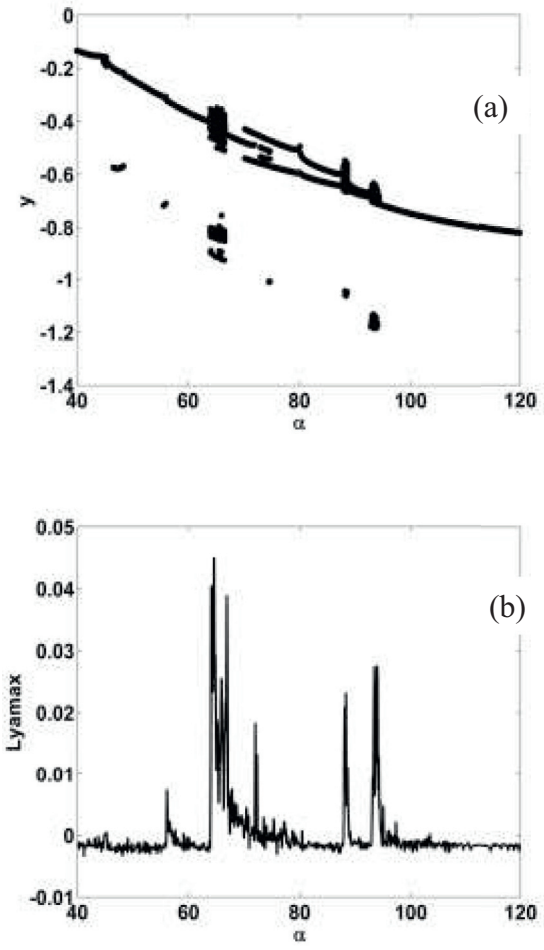

Fig. 8. (a) Bifurcation diagram and (b) Lyapunov exponent Lyamax versus the coupling coefficient α for these parameters: $a_1 = 3, d = 5, I = 1.5, s = 4, \gamma = 0.0021, \beta = 10, \lambda = 2, \mu = 0.85, a_0 = -1.5, N = 20$.

the power increase in load the load is also high when the inductance is taken into account (note that the values of the power at $N = 200$ are 16.53 and 13.84 for RLC and RL loads respectively. The case of the RC load appears as the one consuming less power and thus more favorable in terms of metabolic requirements. This could have more biological implications as the RC loads are representative of most biological systems.

3. Voltage amplitudes in the case of array of Hindmarsh–Rose oscillators

In this section, the Van der Pol oscillator is replaced by the Hindmarsh–Rose oscillator. The Hindmarsh–Rose oscillator is a self-sustaining biological oscillator whose dynamics is based on the overall behavior of neurons [9,19]. The Hindmarsh–Rose model presents good properties and is commonly used to study behavior of interacting neurons [20]. It is described by the following three coupled ordinary differential equations

$$\begin{cases} \dot{x} = -x^3 + w + a_1 x^2 + I - z \\ \dot{w} = 1 - dx^2 - w \\ \dot{z} = \gamma\,(s(x - a_0) - z) \end{cases} \tag{10}$$

where the variable x is the membrane potential, the variables w and z model the transport rate of sodium, potassium ions and other ions across membrane through fast and slow ion channels respectively. a_1 indicates the qualitative behavior of the oscillator. a_0 is the resting potential of the system. I is the external current injected in the oscillator. d is a positive constant while s and γ are constants of small values.

We model the dynamics of an array of N Hindmarsh–Rose oscillators coupled to a RLC circuit by the set of Eq. (11) assuming that the x variable is coupled to the load.

$$\begin{cases} \dot{x}_j = -x_j^3 + w_j + a_1 x_j^2 - z_j + I + \alpha \ddot{y}_j \\ \dot{w}_j = 1 - w_j - d x_j^2 \\ \dot{z}_j = \gamma\left[s\left(x_j - a_0\right) - z_j\right] \\ \sum_{k=1}^{N} \left(\ddot{y}_k + \lambda \dot{y}_k + \mu y_k\right) = \beta\left(x_j - y_j\right) \end{cases} \tag{11}$$

Due to the complexity of the set of Eq. (11), it has not been possible to find analytical expressions as in the case of the Van

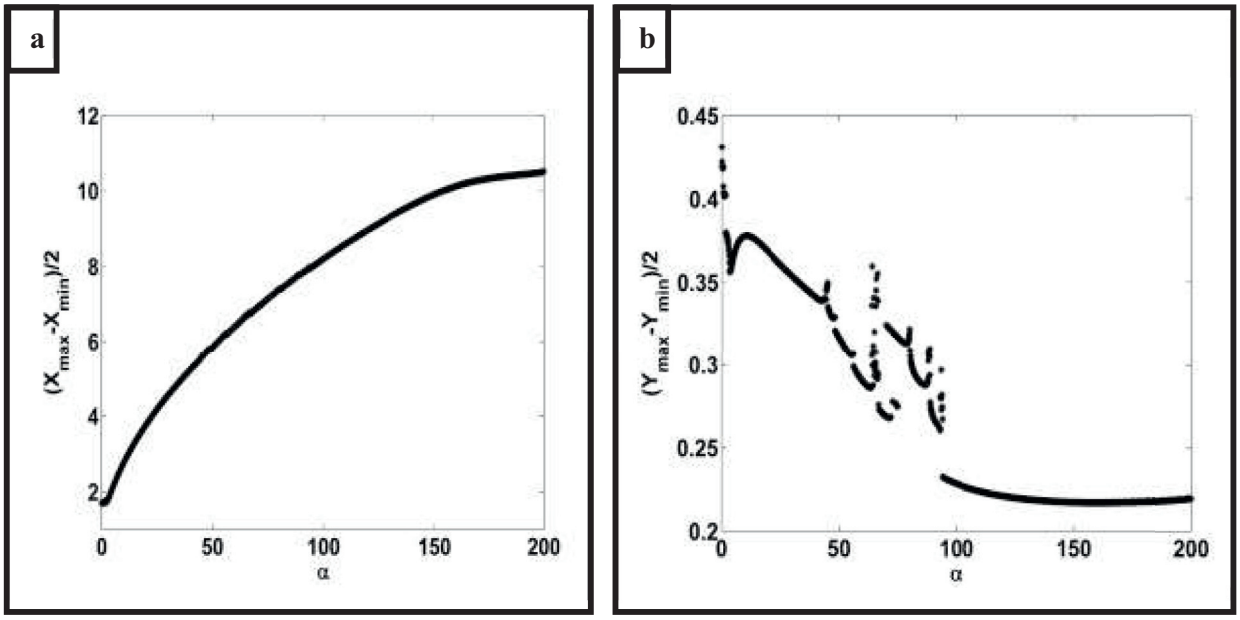

Fig. 9. Voltage amplitudes responses: (a) across the Hindmarsh–Rose oscillator; (b) across the RLC load versus the coupling coefficient α, for the following parameters: $a_1 = 3, d = 5, I = 1.5, s = 4, \gamma = 0.0021, \beta = 10, \lambda = 2, \mu = 0.85, a_0 = -1.5, N = 20$.

der Pol oscillators. We thus rely on numerical simulations. In Fig. 7, we plot for different values of the coupling coefficient α, the voltage amplitudes of the signals across the HR oscillator and across the RLC circuit. It is found that the voltage amplitudes across the HR oscillators and across the RLC circuit decrease with the increase of the number of HR oscillators. This is contrary to what was obtained in the case of an array of VDP oscillators. With the increase of the coupling coefficient α, one notes that these voltage amplitudes decrease across the RLC circuit, but increase across the HR oscillator. We also remark that, depending of the coupling parameterα, there is a critical value of the number of HR oscillators under which there is no signal in the oscillator and no transmission of signal to the RLC circuit.

Comparing Figs. 7 and 3, it appears that the variation of power in terms of the number of oscillators is not qualitatively identical for both types of oscillators. But, a fair comparison cannot be made since the oscillators are different. The idea is just to see how an ensemble of oscillators (representing cardiac pacemakers) acts on a given load (which can be the rest of the heart) and how another ensemble (representing neurons) also act on another given load (which can be a muscle).

Plotting the variation of the voltage amplitudes versus the coupling coefficient α, one finds that the system generates different types of dynamical behaviors as it appears in the bifurcation diagrams of Fig. 8 with the variation of the Lyapunov exponent. A close analysis of this Figure at the places where chaos appears in the system indicates a sudden transition to chaos. With the increase of the coupling α, there is an increase of the voltage amplitude across the HR oscillator and a decrease of the voltage amplitude across the RLC load (Fig. 9). But, this decrease is irregular (non-monotonic) when the value of the coupling is in the range [40–120] (see Fig. 9). Indeed, when the coupling coefficient α increases from 40 to 100, there is an alternating appearance of two dynamics in the load, namely chaotic and quasi-periodic dynamics (Fig. 8).

4. Conclusion

This work has considered the effects of the size of an array of self-sustained oscillators powering an electrical load. Two representatives of the biological oscillators have been considered: the Van der Pol oscillator known as a model for heart pacemaker and the Hindmarsh–Rose oscillator which models the dynamical behavior of neurons. In the case of the Van der Pol oscillators, it has been found that the power in the load is equal to zero when the number of the oscillators is below a critical value. Above this critical value, the power increases with the number of the oscillators. A resonance phenomenon is observed in the variation of the voltage amplitude in the load as one varies the number of the Van der Pol oscillators. Moreover, the higher order of nonlinearity in the damping of the Van der Pol oscillator increases the voltage amplitude response and thereby the output power in the load. In the case of the Hindmarsh–Rose oscillators, the increase of the number of the HR oscillators and the coupling coefficient αresults in an increase of voltage amplitudes across the HR oscillators and a decrease of the voltage amplitude across the RLC load. Moreover, it has been found that varying the coupling coefficient leads to the appearance of quasiperiodic and chaotic dynamics in the system.

References

[1] Chamgoué AC, Yamapi R, Woafo P. Nonl Dynamics 2013;73:2157.
[2] Kitio Kwuimy CA, Nana B, Woafo P. J Sound Vib 2010;329:3137.
[3] Abobda LT, Woafo P. Eur Phys J Special Topics 2014;223:2885.
[4] Simo HP, Woafo P. Mech Res Commun 2011;38:537.
[5] Domguia US, Abobda LT, Woafo P. J Comput Nonl. Dynamics 2016;11:051006.
[6] Peleš S, Wiesenfeld K. Physl Rev E 2003;68:026220.
[7] Barron MA. J Appl Res Technol 2016;14:62.
[8] Guin A, Dandapathak M, Sarkar S, Sarkar BC. Commun Nonl Sci Numer Simul 2017;42:420.
[9] Hindmarsh JL, Rose RM. Proc R Soc London B: Bio Sci 1984;221(1222):87.
[10] Lu J, Kim YB, Ayers J. In: 2011 IEEE 54th International Midwest Symposium,Circuits and Systems (MWSCAS); 2011. p. 1–4.
[11] Lee YJ, Lee J, Kim KK, Kim YB, Ayers J. Neurocomput 2007;71:284.
[12] Jun M, Long H, Zhen-Bo X, Wang C. Commun Nonl Sci Numer Simul 2012;17:2659.
[13] Nana B, Woafo P. Physica A 2008;387:3305.
[14] Kaiser F. In: Fröhlich H, editor. Biological coherence and external stimuli. New York: Springer; 1988. p. 25–48.
[15] Holden AV, Fan Y. Chaos Solitons Fractals 1992;2:349.
[16] Erichsen R Jr, Brunnet LG. Phys Rev.E 2008;78:061917.
[17] Van der pol B, Van der mark J. Philos Mag 1928;7:763.
[18] Kepseu WD, Woafo P, Sepulchre J-A. J Biol Syst 2010;18:173.
[19] Kazemi A, Ahmadi A, Gomar S. In: 2014 22nd Iranian Conference on Electrical Engineering (ICEE); 2014. p. 238–41.
[20] Falcke M, Huerta RA, Rabinovich MI, Abarbanel HDI, Elsons RC, Selverston AI. Bio Cybern 2000;82:517.

Chaos, Solitons and Fractals 146 (2021) 110848

Contents lists available at ScienceDirect

Chaos, Solitons and Fractals

Nonlinear Science, and Nonequilibrium and Complex Phenomena

journal homepage: www.elsevier.com/locate/chaos

Voltages responses and synchronization of an array of Grudzinski and Zebrowski oscillators coupled to an electrical load

Dorota Youmbi Fouego [a,b], Eric Donald Dongmo [a,c,*], Paul Woafo [a,b]

[a] Laboratory of Modelling and Simulation in Engineering, Biomimetics and Prototypes and TWAS Research Unit, Department of Physics, Faculty of Science, University of Yaoundé I, Po. Box 812, Yaoundé, Cameroon

[b] Applied Physics Research Group (APHY), Vrije Universiteit Brussel, Pleinlaan 2, 1050 Brussels, Belgium

[c] Department of Mechanical Engineering, College of Technology, University of Buea, Po. Box 63, Buea, Cameroon

ARTICLE INFO

Article history:
Received 26 June 2020
Revised 1 March 2021
Accepted 2 March 2021

Keywords:
Grudzinski and Zebrowski oscillator
Array of oscillators
Electrical load
Power
Synchronization
Direct coupling
Indirect coupling

ABSTRACT

In this work, we consider a system consisting of an array of Grudzinski and Zebrowski oscillators coupled to an electrical load and analyze the variation of voltages amplitudes and power versus the number of oscillators, the coupling coefficient and the values of the loads. An equivalent electrical circuit of the Grudzinski and Zebrowski oscillator is first proposed. It is then demonstrated that the power in electrical loads (RLC, RL, RC and R) coupled to an array of such oscillator's increases with the number of oscillators till a constant value depending on the types of loads and values of the load parameters. Considering both direct and indirect coupling of an array, synchronization is observed. The synchronization domain is seen to depend on the values of the direct coupling, the value of the indirect coupling and on the number of oscillators in the array.

1. Introduction

In recent years, thanks to the progress in nonlinear dynamics, the modeling followed by mathematical and numerical studies of the electrical conduction system models of the heart has attracted the attention of several researchers [1–6]. Several models to mimic the rhythm of heartbeat were developed, moving from the Hodgkin-Huxley model [7] to the Van der Pol (VdP) model [8]. The VdP model was the pioneer in providing relaxation oscillations. It was also used to qualitatively model heartbeat [9], although it was not very realistic. It is in the challenge of designing an oscillator whose dynamics is closed to the physiologically behavior of the electric signal of heart that the Grudzinski and Zebrowski oscillator was designed [2]. Derived from the classic Van der Pol oscillator, it suitably present signals having the shapes of physiological signals such as the resting potential, refraction time and diastolic period depending on its parameters. However, depending on its initial conditions and the values of its parameters and certain values of external input [10,11], Grudzinski and Zebrowski oscillator (cardiac rhythms) may have periodic (normal) or chaotic (pathological) behavior. The design of its equivalent electrical circuit is still unaddressed in the literature. The coupling of this oscillator to an electrical charge made up of one or more conventional electrical components such as the resistance R, the inductance L and the capacitance C, could be interesting insofar as it would have a behavior closed to that of the pacemaker, feeding the rest of the heart or the rest of the body.

As in an initial work carried out by Nana and Woafo [12], Youmbi et al. [13] considered an array of modified VdP oscillators (with higher non linearity in the damping term) coupled to an RLC load and demonstrated that there is a value of the number of oscillators below which the amplitude of the signal is almost equal to zero, indicating that the system is unpowered. Behnia et al. [10] studied the Grudzinski-Zebrowski oscillator subjected to an external excitation and showed that the change of external factors can alter the heartbeat dynamics.

The dynamics of synchronized oscillators finds its interest in several fields such as engineering, medicine, astronomy, etc. [14]. The phenomenon of synchronization is extremely wide spread in nature as well as in the realm of technology. In the study of several nonlinear dynamical systems, the study of synchronization was made, scientists showed its important role to solve problems in various fields such as in biology, in physics. The effects of synchronization in systems of coupled oscillators nowadays provide a unifying framework for different phenomena observed in nature [15,16]. Enjieu et al. [17] coupled a set of VdP oscillators and

* Corresponding author.
E-mail address: e.dognmo90@yahoo.fr (E.D. Dongmo).

https://doi.org/10.1016/j.chaos.2021.110848
0960-0779/

demonstrated that full synchronization is observed after some critical values of the coupling coefficient and the number of oscillators is reached. Nana and Woafo [18] have investigated different states of synchronization in a ring of four mutually coupled Van der Pol oscillators both in their regular and chaotic states. They were able to obtain the boundaries of the synchronization process when the external force is present and that the accuracy of synchronization becomes reliable for large coupling parameters. In the case of Grudzinski-Zebrowski oscillators, a synchronization study considering both the direct coupling and the indirect coupling is of interest and will be considered in this work.

The present study consists first to design an electrical circuit model of the Grudzinski-Zebrowski oscillator. Then, a set of this equivalent model oscillator is coupled to an electrical load as in references [12] and [13] in order to find out how the power in the load evolves with the number of oscillators and with some parameters of the system. In mind, the goal of this study is to understand in models how the natural pacemaker powers the electrical network of the heart. Indeed, the heart pacemaker is constituted of a set of self-sustained oscillators as the Grudzinski-Zebrowski oscillators working together to sustain its electrical activity. Four types of electrical loads are considered: RLC, RL, RC and R. Finally the synchronization between the oscillators of Grudzinski and Zebrowski is analyzed firstly when they are mutually coupled to each other by a capacitor, and secondly when they are coupled through an indirect coupling by an RC load. The electric power in the load will be evaluated when the total synchronization is reached. Although, the main focus is to describe theoretically the dynamics of an assembly of pacemaker cells, one should have in mind that the system studied here can also have implications in fields of engineering. Indeed the models considered in the study could also be seen as a set of self-sustained electrical oscillators powering a device which is seen electrically as a load (R, RC, RL, RLC).

The structure of the work is as follows. The equivalent electrical model of the Grudzinski-Zebrowski oscillator and its modeling is presented in Section 2. Section 3 considers the dynamical behavior of a set of Grudzinski-Zebrowski oscillators coupled indirectly to an RLC load. The electrical signal amplitudes will be analyzed in terms of the number of oscillators and in terms of the values of the electrical load components. The variation of the power in the different types of load will be presented and analyzed. The analysis of the directly coupled array of oscillators coupled to the electrical load is conducted in Section 4. In that section, we will highlight the ranges of values between the direct coupling coefficient and the number of oscillators for which there is full synchronization. The effect of the indirect coupling will be shown and the electric power in load will be plotted when the total synchronization is reached. Finally, Section 5 deals with the conclusion.

2. The equivalent electrical circuit of the Grudzinski-Zebrowski oscillator

The mathematical equation of the Grudzinski-Zebrowski oscillator [2–4] is given as in Eq. (1), where β is the damping constant.

$$\ddot{x}+\beta\left(x^2-(\theta_1+\theta_2)x+\theta_1\theta_2\right)\dot{x}+x+\frac{(\gamma+\eta)}{\gamma\eta}x^2+\frac{x^3}{\gamma\eta}=0 \qquad (1)$$

According to the literature review, we found that, most of studies done on this Grudzinski-Zebrowski oscillator were essentially based on the mathematical model using numerical simulation. To the best of our knowledge, there is no equivalent electrical circuit composed of discrete electronic components [12] (diodes, resistance, transistors or analog components), as it is in the case of the Van der Pol oscillator. There is therefore, a need of an electrical model for the Grudzinski-Zebrowski oscillator since it will give way for more studies such as the one conducted in this work where loads are coupled to an equivalent electrical circuit of the Grudzinski-Zebrowski oscillator. It is also expected that experimental study can be undertaken using an equivalent electrical which is provided below. After a series of tries and fails, we come out with the electrical model presented in Fig. 1. It consists of 4 branches. The first branch comprises an inductor L_1 and a resistance R_1; the second contains a capacitor C_1; the third is a nonlinear resistance; and the last one has a diode.

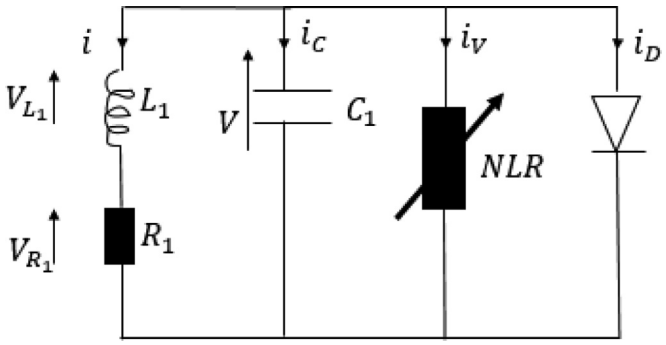

Fig. 1. Equivalent electrical circuit of the Grudzinski-Zebrowski oscillator.

As it is demonstrated in the Appendix A, the equations describing the dynamics of the electrical circuit presented on Fig. 1 lead to the final Eq. (2).

$$\frac{d^2x}{dt^2}+\frac{3b}{V_0\omega_0C_1}\left(x^2+\frac{i_0x}{3b}-\frac{a}{3b}+\frac{i_0}{3bV_0}+\frac{R_1V_0C_1}{3bL_1}\right)\frac{dx}{dt}+x+\frac{R_1i_0x^2}{2L_1\omega_0^2C_1V_0}+\frac{R_1bx^3}{L_1\omega_0^2C_1V_0}=0 \qquad (2)$$

where $x=\frac{V}{V_0}$ represents the dimensionless quantity for the voltage V (see Fig. 1).

In this study, we have fixed the following values for the electrical components: $L_1=200\times10^{-6}H$; $R_1=260\Omega$; $i_0=10^{-4}A$; $V_0=26\times10^{-3}V$; $C_1=1.41\times10^{-8}F$; $a=0.0001$; $b=0.237$

Eq. (2) can thus take the form of Eq. (1) with the following dimensionless coefficients:

$$\beta=3;\ \theta_1+\theta_2=0;\ \theta_1\theta_2=0.6889;\ \frac{1}{\gamma\eta}=0.05;\ \frac{(\gamma+\eta)}{\gamma\eta}=0.5 \qquad (3)$$

Fig. 2 presents the phase portrait and the time trace of the signal delivered by Eq. (1) with the above parameters and the following initial conditions: $x(0)=-0.1$ and $\frac{dx}{dt}(0)=0.025$.

In order to corroborate the numerical results that we obtained with our electrical equivalent circuit of the Grudzinski-Zebrowski oscillator, we introduced multisim emulator to see if the numerical results, qualitatively mesh with the multisim results. Thus, Fig. 3 presents the phase portrait and the temporal trace of the voltage of the circuit built with multisim.

Comparing Fig. 3 and Fig. 2, one notes that they are not coincident. This can be explained by invoking the fact the in the multisim simulation, diodes equivalent are used and the nonlinear term in the original Eq. (1) may differ from the nonlinear characteristics delivered by the diodes in multisim simulation.

3. Array of Grudzinski-Zebrowski oscillators indirectly coupled to electrical loads

3.1. The model and equations

As one indicates above, the Grudzinski-Zebrowski oscillator is a representative of electrical models of heart pacemaker cells. The

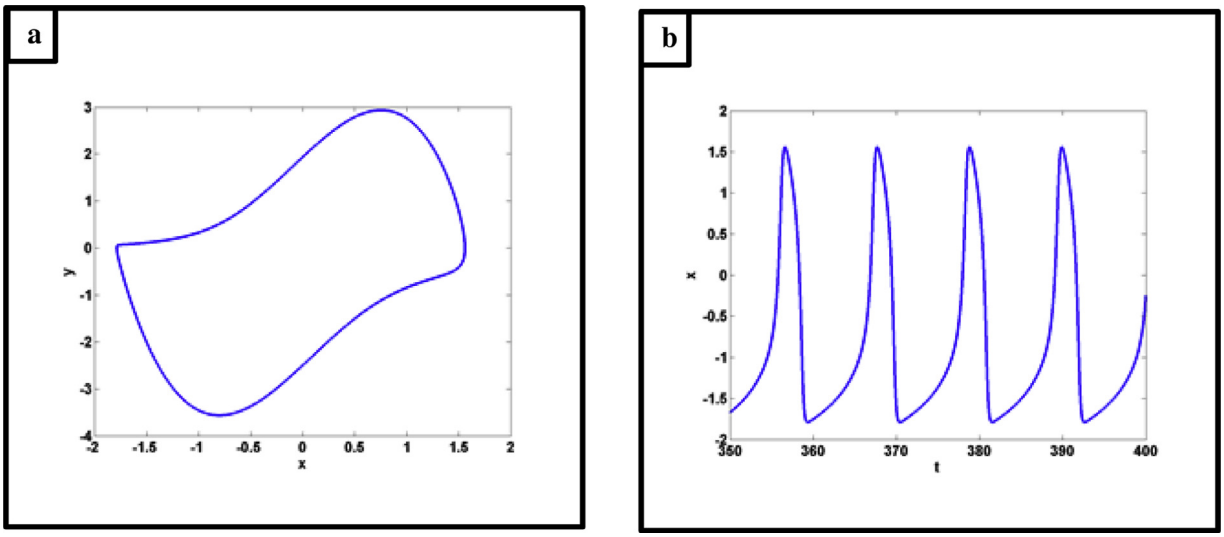

Fig. 2. Signal delivered by Grudzinski-Zebrowski oscillator: a) phase space, b) time history.

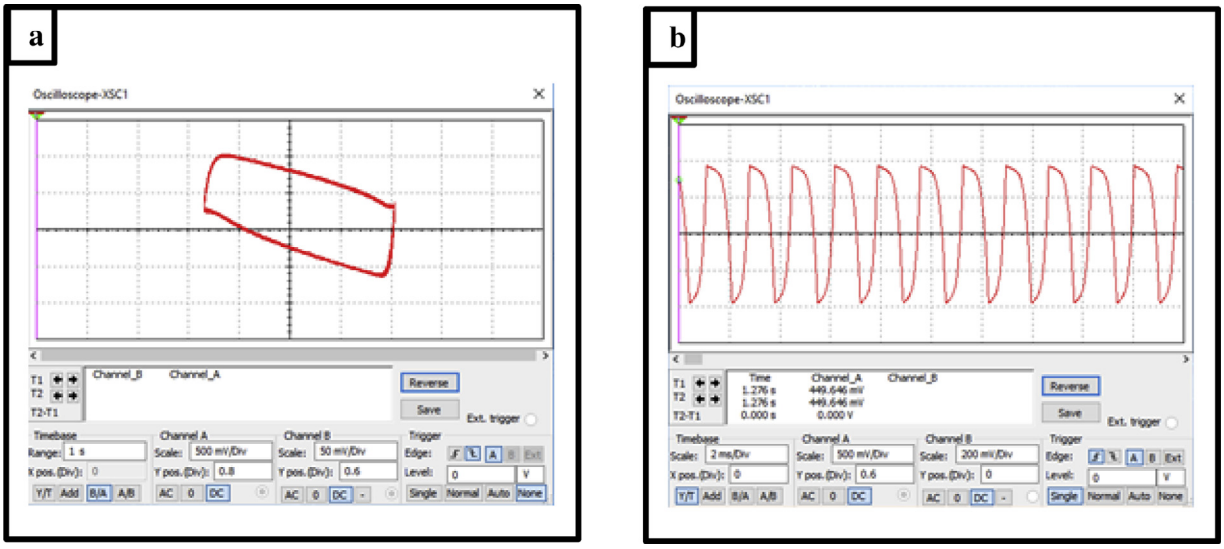

Fig. 3. Signal delivered by Grudzinski-Zebrowski oscillator using multisim: a) phase space, b) time history.

cells can be coupled indirectly through the electrical load representing the rest of the heart or the rest of the cardiovascular system seen by the pacemaker or both directly and indirectly. In the case of the indirect coupling, each cell is coupled to the external load as in references [12,13]. When the direct and indirect coupling take place, each cell is coupled to the external load, but all the cells are coupled together in a diffusive manner with short or long range coupling [18]. We will consider both cases in this work and come out with the behavior of the oscillatory states and the power received by the load. But this section is first devoted to the case of indirect coupling.

In the indirect coupling scheme, the structure is presented in Fig. 4, where we see a set of N Grudzinski-Zebrowski oscillators coupled to an RLC load. The coupling is through the capacitance C_0.

Using Kirchhoff's laws, appropriate dimensionless variables and the same normalization as above and also setting $y_j = \frac{u_j}{V_0}$, one obtains the set of Eq. (4) which describes the variation of voltage x_j across each oscillator and the voltage y_j across the coupling capacitance.

$$\begin{cases} \ddot{x}_j + \mu\left(x_j^2 - 0.6889\right)\dot{x}_j + x_j + 0.5x_j^2 + 0.05x_j^3 + A_1\ddot{y}_j + A_2\dot{y}_j = 0 \quad 2 \le j \le \mathrm{N} & \text{(a)} \\ \sum_{k=1}^{N}\left(\ddot{y}_k + B_1\dot{y}_k + B_2 y_k\right) = B_3(x_1 - y_1) & \text{(b)} \end{cases} \tag{4}$$

$$A_1 = \frac{C_0}{C_1},\ A_2 = \frac{R_1 C_0}{L_1\omega_0 C_1}$$

The dimensionless parameters B_1, B_2 and B_3 are defined in Table 1 for different types of used loads.

3.2. Voltage amplitude versus the number of oscillators

We first analyze the variations of the voltage amplitude as the number of oscillators varies. The initial conditions used for the

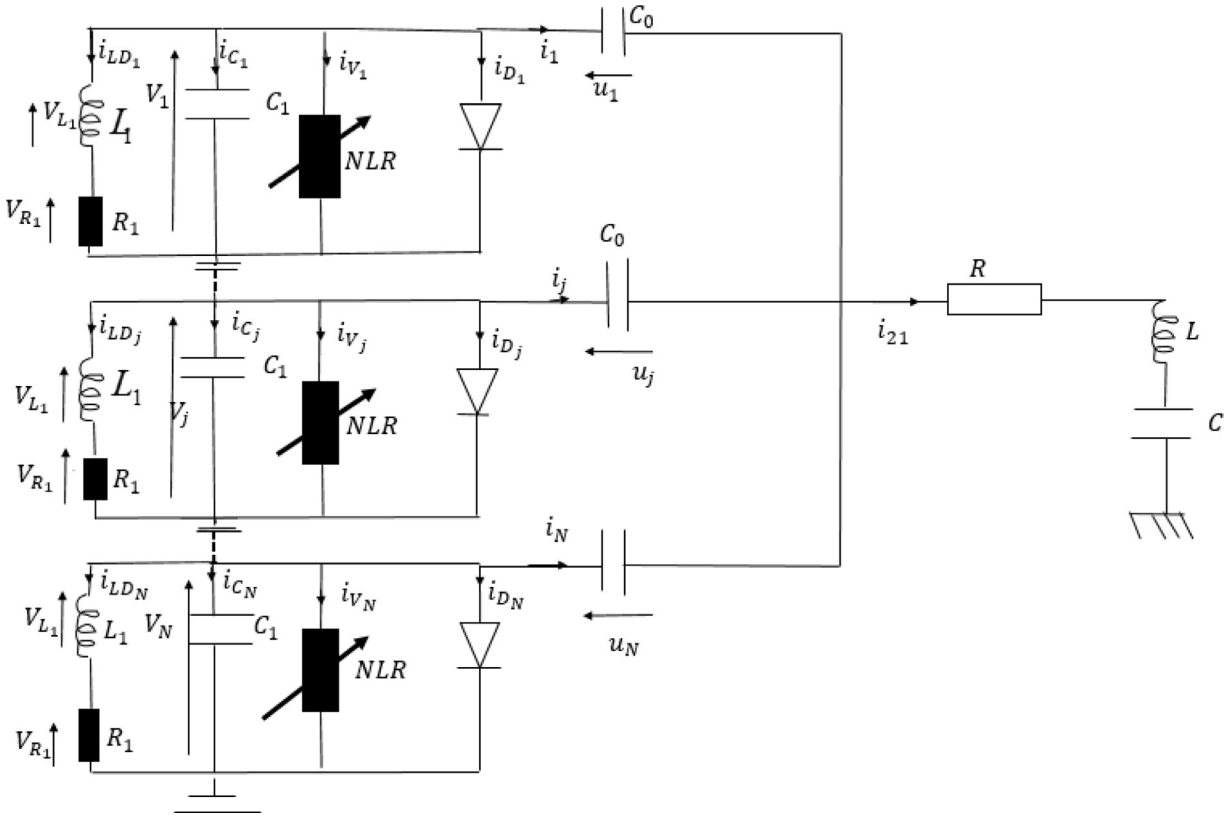

Fig. 4. Array of Grudzinski and Zebrowski oscillators loaded by an RLC circuit.

Table 1
Expressions of the coefficients B_i for each type of electrical load.

Load	B_1	B_2	B_3
RLC load	$\frac{R}{L\omega_0}$	$\frac{1}{LC\omega_0^2}$	$\frac{1}{L\omega_0^2 C_0}$
R load	1	0	$\frac{1}{C_0 R\omega_0}$
RL load	$\frac{R}{L\omega_0}$	0	$\frac{1}{L\omega_0^2 C_0}$
RC load	1	$\frac{1}{R\omega_0 C}$	$\frac{1}{R\omega_0 C_0}$

numerical simulation are $x(0) = -0.1$, $\frac{dx}{dt}(0) = 0.025$, $y_i(0) = 0.025$ and $\frac{dy}{dt}_i(0) = 0.025$.

First considering the RLC load, we use the following values: $R = 156\Omega$, $R_1 = 260\Omega$ $L_1 = 200\times10^{-6}$H, $C = 36.3\times10^{-9}$F and $C_0 = 1.89\times10^{-8}$F. Fig. 5 presents the amplitude of the voltages x_j and y_j versus the number N of the oscillators where $x = \frac{V}{V_0}$ and $y = \frac{u}{V_0}$ are the appropriate dimensionless variables. It is observed that the voltage amplitude increases in each Grudzinski-Zebrowski oscillator with the increase of N (Fig. 5). One remarks that for lower values of N, the voltage is almost equal to zero as for the case of array of Van der Pol oscillator [13]. But at the same time, the voltage amplitude across the capacitance C_0 decreases when N increases.

Considering the other types of loads (RL, RC, and R), we found similar variation as in the case of the RLC load. However quantitatively, it has been observed that the amplitudes is lower in the RC load compare to the other loads (see Fig. 6).

Now, we analyze the influence of the coupling capacitance C_0. In Fig. 7, it is observed that the voltage amplitude across the Grudzinski-Zebrowski oscillator increases while the voltage amplitude across C_0 decreases with the increase of C_0. The effects of the nonlinear damping parameter μ has also been investigated. It is found that the voltage amplitude in each oscillator increases with μ up to the value $\mu = 8.5$. Then, a decrease takes place till $\mu = 84.8$, followed by a second smooth increase. For the voltage across C_0, its amplitude increases with the increase of μ (see Fig. 8).

3.3. Power in the load: Case of indirect coupling

The most interesting quantity in the load is the power delivered by the array of self-sustained oscillators. It is defined by the following equation

$$P = R \times i_{21}^2. \tag{5}$$

where R and i_{21} are respectively the load resistance and the intensity.

Since $i_{21} = \sum_{k=1}^{N} C_0 \frac{du_k}{dt}$, and knowing that $u_k = y_k V_0$, one obtains $i_{21} = NC_0 \dot{y}_k V_0 \omega_0$.

By taking into account the above literal expression of i_{21}, one has the power P which is given by Eq. (6).

$$P = R(NC_0 \dot{y}_k V_0 \omega_0)^2 \tag{6}$$

This expression remains the same for the different types of load, except that the value of the derivative of the component y will be determined according to the load that will be taken into account during the numerical simulations.

Fig. 9 presents the power variation versus N in the R, RL, RLC and RC load. We notice that, the power increases with the increase of N for all types of loads. Quantitatively, one notes that the RL load consumes more power than the RLC load while the pure resistive load consumes the highest power. The power consumed by the RC load (which is more close to biological tissue) is at the intermediate level.

We have also considered the resistance R as a control parameter and plot the power versus R. It has been found that, for all

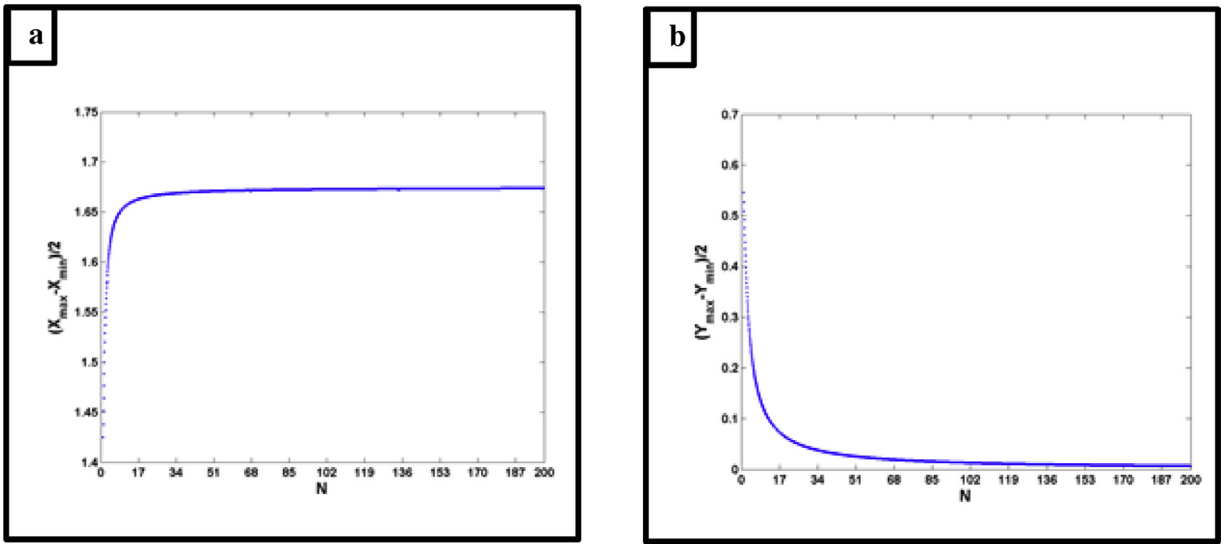

Fig. 5. Voltage amplitudes responses versus the number N of the oscillator: a) in the Grudzinski-Zebrowski oscillator; b) across the coupling capacitance C_0, with the values of parameters listed above and with $\omega_0 = 594228.361\ s^{-1}$ which will be used in the forthcoming figures.

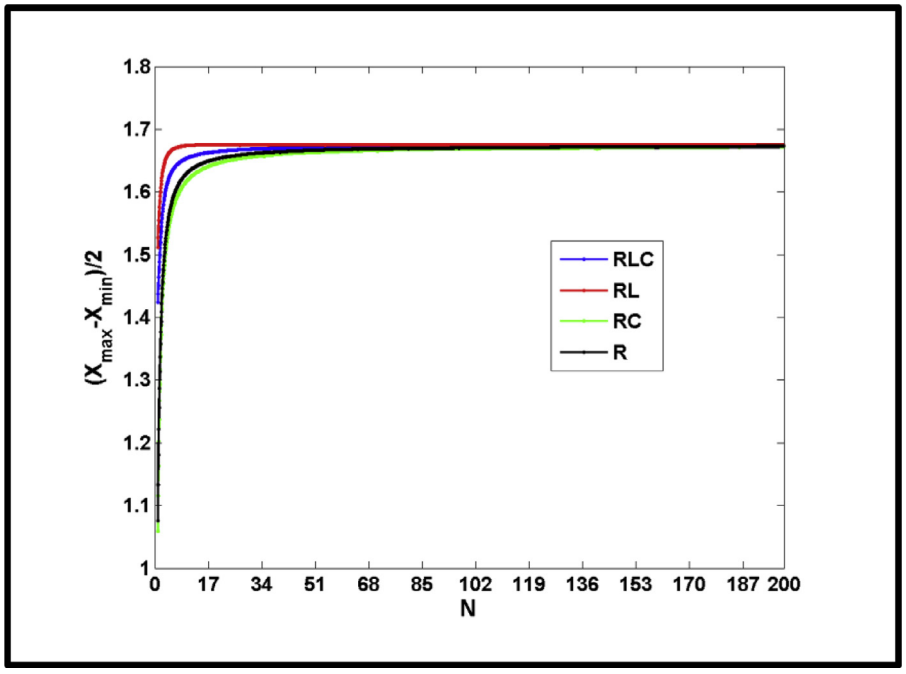

Fig. 6. Voltage amplitudes responses versus the number N of oscillators coupled to RLC, RL, RC and R loads across the Grudzinski-Zebrowski oscillator with the parameters of Fig. 5.

types of load, the power increases with R and attains a saturation level where it remains constant. Such a variation is presented in Fig. 10 for the RLC, RC, RL, and R loads. Let us mention that the curve for the R load and that of the RLC load are almost the same.

4. Directly coupled array of oscillators coupled to the electrical load

4.1. The system

In this section, one considers the situation where all the Grudzinski-Zebrowski oscillators are mutually coupled to each other by a capacitor and indirectly coupled to the RC load. In this subsection, when we talk about mutual or direct coupling, it is about the coupling made between oscillators one after the other by a capacitor while forming a ring (oscillator network). When this oscillator network is coupled to a load by a capacitor, we are in the presence of an indirect coupling. Fig. 11 presents the system under consideration. Each oscillator is directly coupled to its nearest neighbors through a capacitor. At the same time, all the oscillators are indirectly coupled to the RC load, generating therefore an indirect coupling between the oscillators. We chose a ring for the simple reason that it is due to periodic boundary conditions since in reality the system is assumed to have more than thousands of cells.

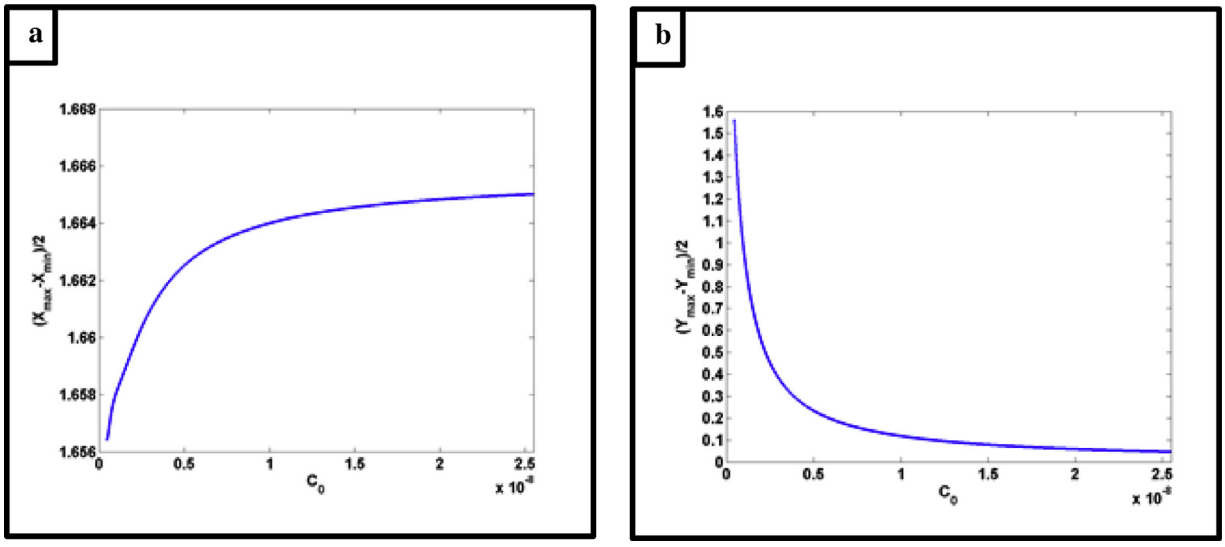

Fig. 7. Voltage amplitudes responses versus the coupling capacitance C_0: a) across the Grudzinski and Zebrowski oscillator; b) across the coupling capacitance with $N = 20$ and with the parameters of Fig. 5.

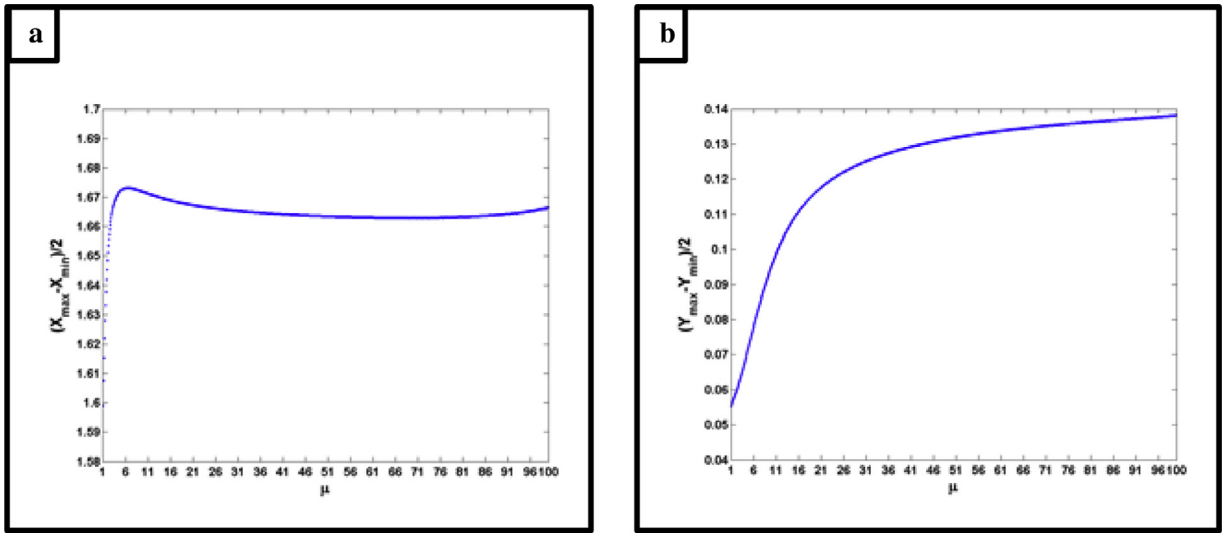

Fig. 8. voltage amplitudes responses versus the coupling coefficient μ: a) across the Grudzinski and Zebrowski oscillator; b) across the coupling capacitor C_0 with $N = 20$ and with the parameters of Fig. 5.

Using the electric laws, one finds that the voltages in Fig. 11 are described by the following set of differential equations:

$$\begin{cases} \frac{d^2x_k}{dt^2} + \frac{3b}{V_0\omega_0 C_1}\left(x_k^2 + \frac{i_0 x_k}{3b} - \frac{a}{3b} + \frac{i_0}{3bV_0} + \frac{R_1 V_0^3 C_1}{3bL_1}\right)\frac{dx_k}{dt} + x_k + \frac{R_1 i_0 x_k^2}{2L_1\omega_0^2 C_1 V_0} \\ + \frac{R_1 b x_k^3}{L_1\omega_0^2 C_1 V_0} + K_2\ddot{y}_k + \frac{R_1 K_2}{L_1\omega_0}\dot{y}_k = K_1(\ddot{x}_{k-1} - 2\ddot{x}_k + \ddot{x}_{k+1}) \\ \quad + \frac{R_1 K_1}{L_1\omega_0}(\dot{x}_{k-1} - 2\dot{x}_k + \dot{x}_{k+1}) \\ \sum_{P=1}^{N}\left(\dot{y}_P + \frac{1}{R\omega_0 C}y_P\right) = \frac{1}{R\omega_0 C_0}(x_k - y_k) \end{cases} \tag{7}$$

where the dimensionless quantities are given below:

$$x_k = \frac{V_k}{V_0};\ y_k = \frac{u_k}{V_0};\ K_2 = \frac{C_0}{C_1};\ K_1 = \frac{C_2}{C_1};\ t_{ref} = \frac{1}{\omega_0};$$
$$\omega_0 = \sqrt{\frac{-a + 2i_0}{L_1 i_0 C_1}} \tag{8}$$

The direct coupling coefficient is K_1 and the indirect coupling coefficient is K_2.

Three concerns arise from the model. The first one is to see how the mutually coupled oscillators behave when they are not coupled to the load. In other words, for which value of the mutual coupling coefficient a full synchronization can be achieved? The second one is to understand how the indirect coupling affects the synchronization limits. The third concern is to find out how the mutual coupling coefficient affects the power in the RC load.

4.2. Full synchronization with no load

Referring to Enjieu et al. [17], numerical simulations have been conducted in search of the coupling coefficient leading to full synchronization as a function of the number of Grudzinski and Zebrowski oscillators. Considering the system of Fig. 11 without RC load, Eq. (9) repeats the set of dimensionless equations under consideration here

$$\frac{d^2x_k}{dt^2} + \frac{3b}{V_0\omega_0 C_1}\left(x_k^2 + \frac{i_0 x_k}{3b} - \frac{a}{3b} + \frac{i_0}{3bV_0} + \frac{R_1 V_0^3 C_1}{3bL_1}\right)\frac{dx_k}{dt} + x_k + \frac{R_1 i_0 x_k^2}{2L_1\omega_0^2 C_1 V_0} + \frac{R_1 b x_k^3}{L_1\omega_0^2 C_1 V_0} = K_1(\ddot{x}_{k-1} - 2\ddot{x}_k + \ddot{x}_{k+1}) + \frac{R_1 K_1}{L_1\omega_0}(\dot{x}_{k-1} - 2\dot{x}_k + \dot{x}_{k+1}) \tag{9}$$

When one considers two Grudzinski and Zebrowski oscillators described by the same equations and starting with different ini-

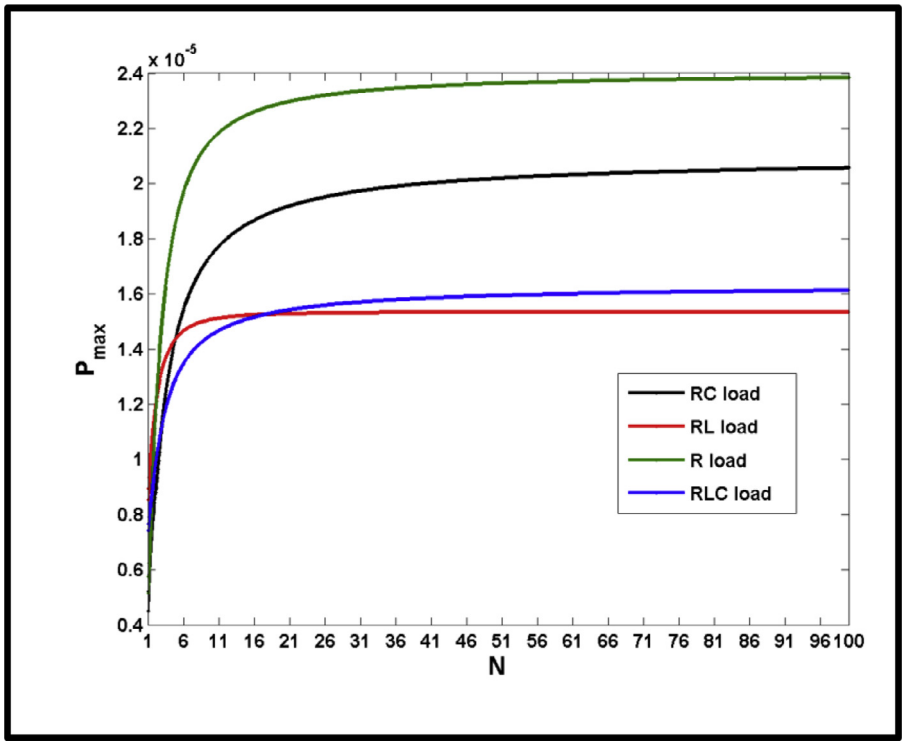

Fig. 9. Power delivered to R, RL, RLC and RC loads versus the number N of Grudzinski and Zebrowski oscillators, using parameters of Fig. 5.

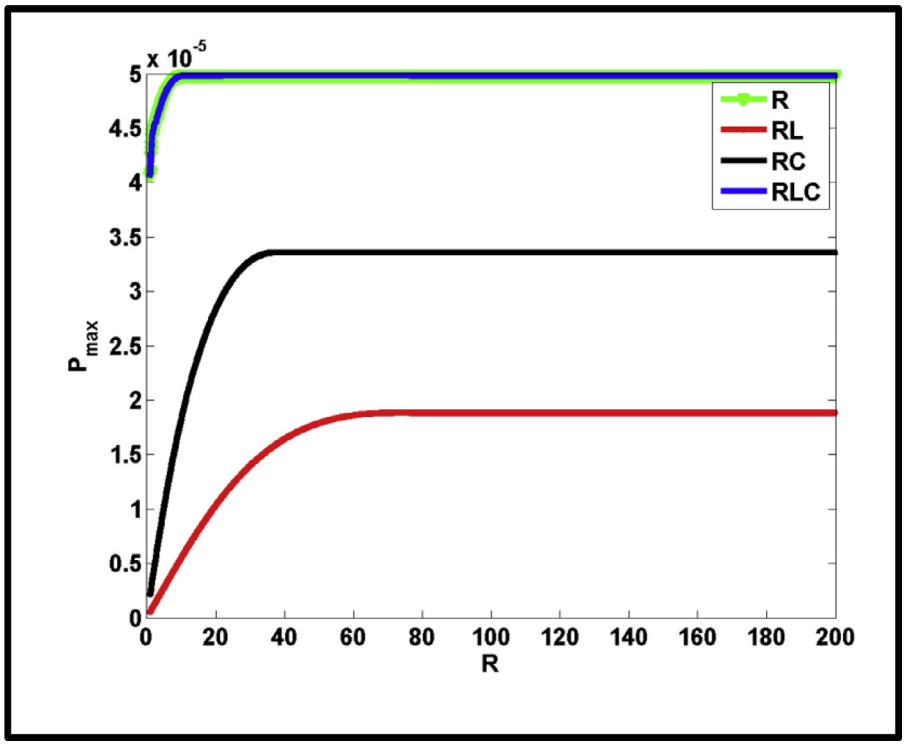

Fig. 10. Power delivered in the load RLC, RL, RC, and R versus R with N= 20 and the parameters of Fig. 5.

tial conditions, one observes that they present the same behaviour but with a phase difference. Finding the synchronization domain is to look for N and the coupling coefficient K_1 leading to the disappearance of the phase difference so that the oscillators are phase locked with phase difference equal to 0. Fig. 12 presents the synchronization domains in (N, K_1) plane. It is seen that the full synchronization domains (FS) are not linearly delineated from the domains where there is no synchronization (NS).

In order to show the veracity of the synchronization diagram, we took a couple of values (N, K_1) where there is synchronization and where there is not according to Fig. 12, and plotted there time traces for these cases. From the temporal traces, it emerges that for

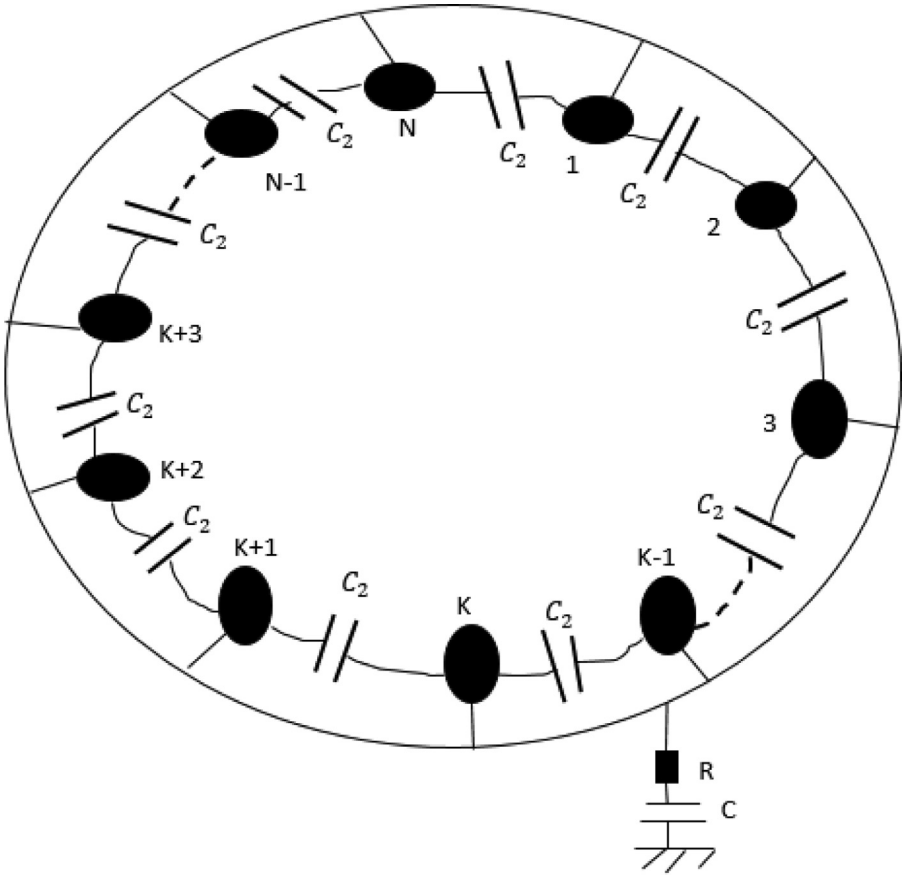

Fig. 11. Ring of N mutually coupled Grudzinski-Zebrowski oscillators coupled indirectly by RC load.

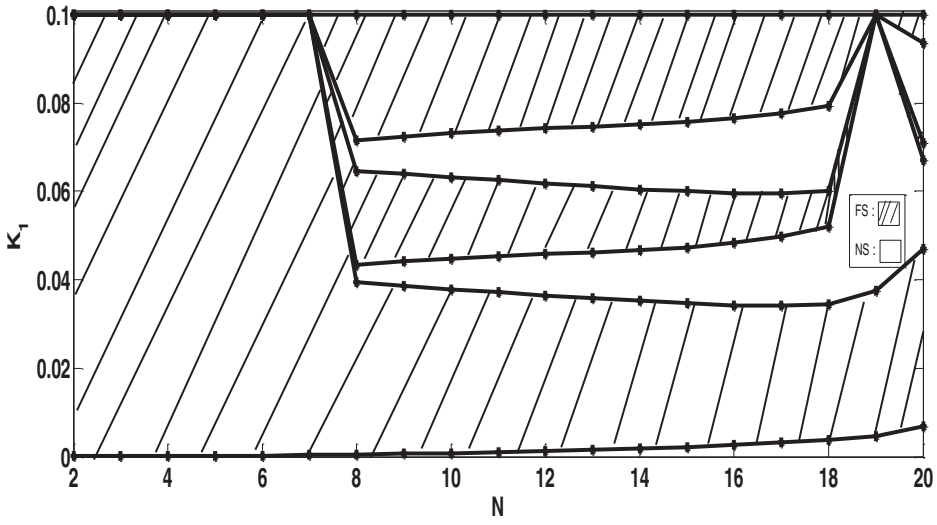

Fig. 12. The boundaries for full synchronization (FS) and no-synchronization (NS) in the parametric plan (N, K_1) with parameters of Fig. 5.

the parameters for which there is synchronization, the temporal traces are in phase and in the contrary case they are out of phase (see Fig. 13) after the transient regime.

4.3. Power in the RC load versus the number of oscillator for different values of the mutual coupling coefficient

When the load is taken into account (see Fig. 11), the power delivered by the array of self-sustained oscillators is given as follows:

$$P = R(NC_0\dot{y}_k V_0\omega_0)^2$$

where this power is rewritten according to the mutual coupling in Eq. (10)

$$P = R\left(N\left(\frac{C_0 * C_2}{K_1 * C_1}\right)\dot{y}_k V_0\omega_0\right)^2 \tag{10}$$

Knowing that the direct coupling $K_1 = \frac{C_2}{C_1}$, the power can be rewritten as follow $P = R(N(\frac{C_0 * K_1}{K_1})\dot{y}_k V_0\omega_0)^2$, and by simplification one

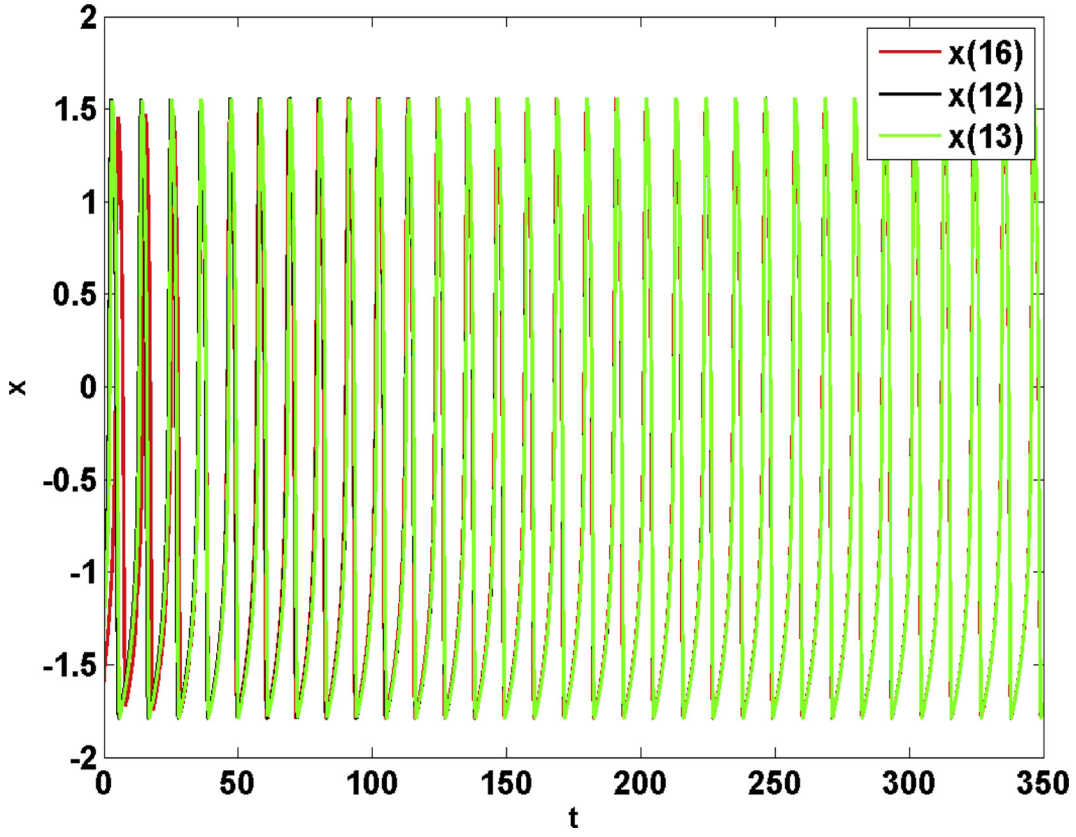

Fig. 13. **a:** evolution of the temporal trace: no synchronization with $K_1 = 0.04$ and parameters of Fig. 5. **b:** evolution of the temporal trace: full synchronization with $K_1 = 0.1$ and parameters of Fig. 5.

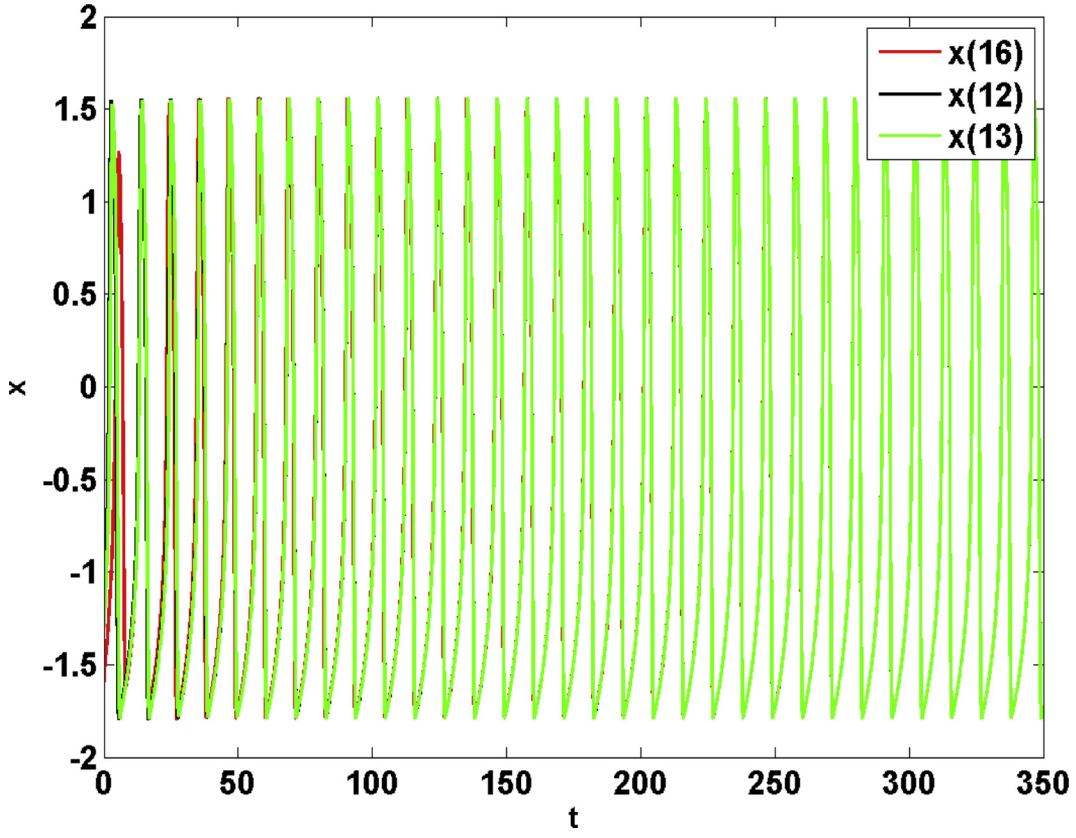

Fig. 13. Continued

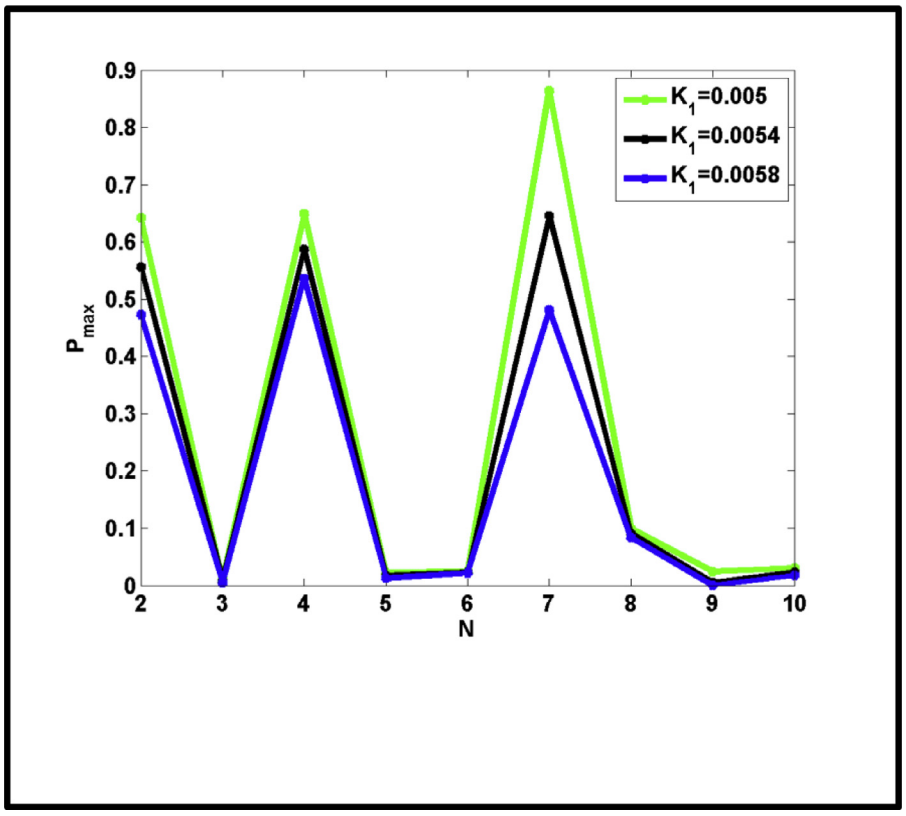

Fig. 14. Power in the load RC load versus the number of Grudzinski-Zebrowski oscillators for different values of K_1 the parameters of Fig. 5.

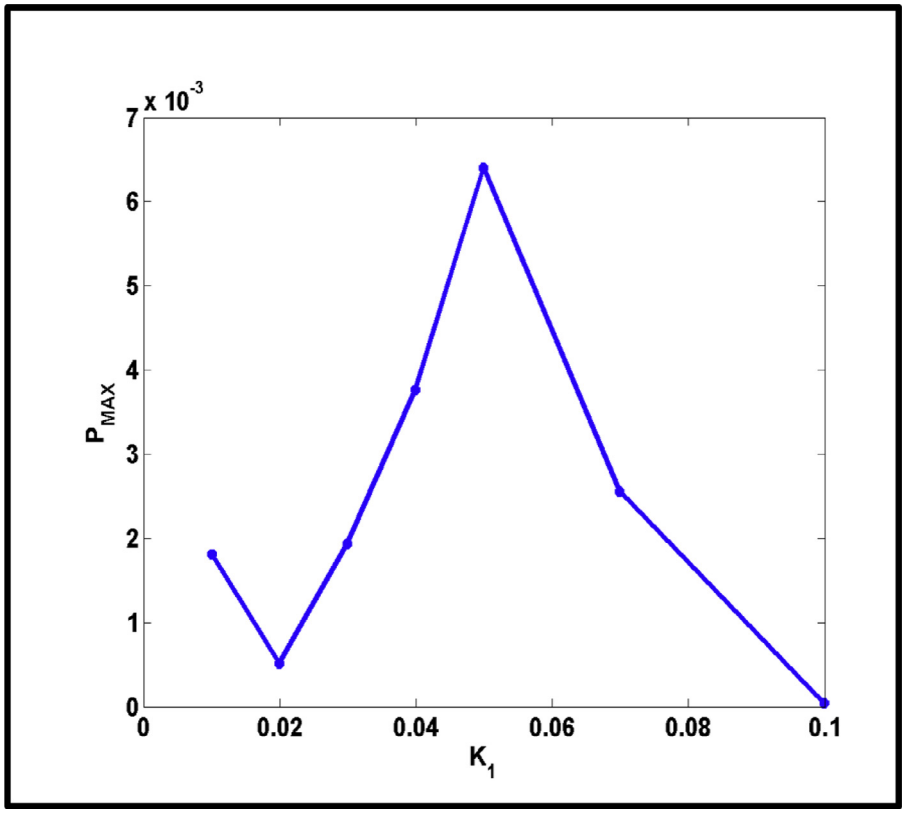

Fig. 15. Power in the load RC load versus the mutual coupling coefficient with $N = 10$ and parameters of Fig. 5.

has $P = R(NC_0\dot{y}_k V_0\omega_0)^2$ which is independent to the direct coupling coefficient K_1.

In Fig. 14, the evolution of the power in the load is presented as a function of the number of oscillators for three values of the mutual coupling coefficient. One observes that, the power decreases with the increase in the mutual coupling coefficient. In addition, one also observes a succession of decrease and increase in the amplitudes of the power with the increase in the number of oscillators.

4.4. Power in the load versus the mutual coupling coefficient

As soon as the full synchronization is reached, the power in the RC load (see the system presented in Fig. 11) is plotted according to the mutual coupling coefficient given in Fig. 15 where the power delivered in the load is decreasing and reaches the value 5.107×10^{-4}, begins to increase and starting from the value 6.402×10^{-3}, it decreases again according to the increase of the coefficient of mutual.

5. Conclusion

In this paper, it was first question to propose an electrical circuit whose equation is similar to the self-sustained oscillator model presented by Grudzinski-Zebrowski. Secondly, to consider an array of Grudzinski-Zebrowski oscillators coupled to an electrical load. The analysis of the signal amplitude was done taking into account the number of oscillators and the coupling parameters. Then, the variation of the power in different types of load was analyzed. One notes that, RL load consumes more power than RLC load while the pure resistive load consumes the highest power whereas the power consumed by the RC load is at the intermediate level. Considering a direct coupling of all the oscillators, the synchronization domains were delimited as a function of the number of oscillators and the coupling coefficient. The variation of the coupling parameter and the dissipation coefficient shows that only a periodic dynamic appears. We found that, when the synchronization is reached for a fixed number of Grudzinski-Zebrowski oscillators in the system (direct coupling of the N oscillator coupled to the load), the power delivered to the load decreases and reaches a value, then a succession of growth and decay follows and finally there is a growth with the increase of the mutual coupling coefficient. It is observed that, when the mutual coupling coefficient increases, the power decreases when the number of oscillators increases. The shape of the power curve is a succession of decay and growth as the number of Grudzinski-Zebrowski oscillator's increases.

Declaration of Competing Interest

The authors declare that they have no known competing financial interests or personal relationships that could have appeared to influence the work reported in this paper.

Appendix A. Modelling of Grudzinski and Zebrowski oscillator from Fig. 1

We assume that the current-voltage (I-V) characteristics of the diode is given by (A1).

$$i = i_0(e^{V/V_0} - 1) \tag{A1}$$

whose after expansion gives $i = i_0(\frac{V}{V_0} + \frac{V^2}{2V_0^2})i_0$ and V_0 are constant coefficients related to the diode.

We also assume that the current-voltage characteristics of the nonlinear resistance NLR is given as follow

$$i = -\frac{aV}{V_0} + \frac{bV^3}{V_0^3}$$

Using the first mesh of the circuit (see Fig. 1), one gets (A2)

$$L_1\frac{di}{dt} + Ri - V = 0 \tag{A2}$$

where i is the current flowing through L_1 and V the voltage across the nonlinear capacitor.

where $V = \frac{q}{C_1}$, which is the voltage across the capacitor.

Considering the nodes law, one gets (A3)

$$i = -\frac{dq}{dt} + \frac{aV}{V_0} - \frac{bV^3}{V_0^3} - \frac{i_0V}{V_0} - \frac{i_0V^2}{2V_0^2} \tag{A3}$$

where q is the electric charge in the capacitor.

By replacing (A3) in (A2), it comes that the voltage V satisfies the following equations (A4):

$$\frac{d^2V}{dt^2} + \frac{3b}{V_0^3C_1}\left(V^2 + \frac{i_0V_0V}{3b} - \frac{V_0^2a}{3b} + \frac{i_0V_0^2}{3b} + \frac{R_1V_0^3C_1}{3bL_1}\right)\frac{dV}{dt} + \frac{R_1bV^3}{V_0^3L_1C_1} + \frac{R_1i_0V^2}{2V_0^2L_1C_1} - \frac{R_1aV}{L_1C_1V_0} + \frac{V}{L_1C_1} + \frac{R_1i_0V}{V_0L_1C_1} = 0 \tag{A4}$$

Setting $x = \frac{V}{V_0}$ and the time t is normalized with respect $t_{ref} = \frac{1}{\omega_0}$ with $\omega_0 = \sqrt{\frac{-a+2i_0}{L_1i_0C_1}}$, one obtains (A5).

$$\frac{d^2x}{dt^2} + \frac{3b}{V_0\omega_0C_1}\left(x^2 + \frac{i_0x}{3b} - \frac{a}{3b} + \frac{i_0}{3bV_0} + \frac{R_1V_0C_1}{3bL_1}\right)\frac{dx}{dt} + x + \frac{R_1i_0x^2}{2L_1\omega_0^2C_1V_0} + \frac{R_1bx^3}{L_1\omega_0^2C_1V_0} = 0 \tag{A5}$$

The following values have been given to the electrical components and parameters:

$$L_1 = 200 \times 10^{-6}\text{H};\ i_0 = 10^{-4}\text{A};\ V_0 = 26 \times 10^{-3}\text{V};$$
$$\frac{1}{C_1} = 70921985,8156\text{F}^{-1};\ a = 0.0001;\ b = 0.237.$$

Eq. (A5) can thus take the form of Eq. (1) with the following dimensionless coefficients:

$$\beta = 3;\ \theta_1 + \theta_2 = 0;\ \theta_1\theta_2 = -0.6889;\ \frac{1}{\gamma\eta} = 0.05;\ \frac{(\gamma+\eta)}{\gamma\eta} = 0.5 \tag{A6}$$

CRediT authorship contribution statement

Dorota Youmbi Fouego: Conceptualization, Methodology, Software, Writing – original draft, Writing – review & editing. **Eric Donald Dongmo:** Conceptualization, Methodology, Software, Writing – original draft, Writing – review & editing. **Paul Woafo:** Supervision, Writing – review & editing.

References

[1] Bub GIL, Glass L. Bifurcations in a discontinuous circle map: a theory for a chaotic cardiac arrhythmia: a theory for a chaotic cardiac arrhythmia. Int J Bifurc Chaos 1995;5(02):359–71.
[2] Grudziński K, Żebrowski JJ. Modeling cardiac pacemakers with relaxation oscillators. Physica A 2004;336(1–2):153–62.
[3] Żebrowski JJ, Grudziński K, Buchner T, Kuklik P, Gac J, Gielerak G, Sanders P, Baranowski R. Nonlinear oscillator model reproducing various phenomena in the dynamics of the conduction system of the heart. Chaos 2007;17(1):015121.

[4] Grudziński K, Żebrowski JJ, Baranowski R. Model of the sino-atrial and atrio-ventricular nodes of the conduction system of the human heart. Biomed Tech 2006;51(4):210–14.
[5] Muhammad AZR, Fiaz HS, Muhammad IS. Intelligent computing approach to solve the nonlinear Van der Pol system for heartbeat model. Neural Comput Appl 2018;30(12):3651–75.
[6] Michael FEC, Faisal AS, Nicolas CCG, Jose L. Updated performance of the micra transcatheter pacemaker in the real- word setting: a comparison to the investigational study and a transvenous historical control. Heart Rhythm 2018;15(12):1800–7.
[7] Hodgkin AL, Huxley AF. A quantitative description of membrane current and its application to conduction and excitation in nerve. J Physiol 1952;117(4):500–44.
[8] Van Der Pol B, Van Der Mark J. LXXII. The heartbeat considered as a relaxation oscillation, and an electrical model of the heart. Lond, Edinb, Dublin Philos Mag J Sci 1928;6(38):763–75.
[9] Katholi CR, Urthaler F, Macy Jr, J, James TN. A mathematical model of automaticity in the sinus node and AV junction based on weakly coupled relaxation oscillators. Comput Biomed Res 1977;10(6):529–43.
[10] Behnia S, Ziaei J, Ghiassi M, Akhshani A. Nonlinear dynamic approach of heartbeats based on the Grudzinski-Zebrowski's model. Chin J Phys 2015;53:120702.
[11] Ferreira BB, de Paula AS, Savi MA. Chaos control applied to heart rhythm dynamics. Chaos, Solitons Fractals 2011;44(8):587–99.
[12] Nana B, Woafo P. Power delivered by an array of Van der Pol oscillators coupled to a resonant cavity. Physica A 2008;387(13):3305–13.
[13] Fouego DY, Dongmo ED, Woafo P. Powering RLC load by an array of self-sustained oscillators. Chaos, Solitons Fractals 2017;104:222–7.
[14] Piovsky A, Rosenblum M, Kurths J. Synchronization- a unified approach to nonlinear science, 7. Cambridge: Cambridge University press; 2001.
[15] Boccaletti S, Kurths J, Osipov G, Valladares DL, Zhou CS. The synchronization of chaotic systems. Phys Rep 2002;366(1–2):1–101.
[16] Boccaletti S, Latora V, Moreno Y, Chavez M, Hwang DU. Complex networks: structure and dynamics. Phys Rep 2006;424(4–5):175–308.
[17] Enjieu Kadji HG, Chabi Orou JB, Woafo P. Spatiotemporal dynamics in a ring of N mutually coupled self-sustained systems. Chaos 2007;17(3):033109.
[18] Nana B, Woafo P. Synchronization in a ring of four mutually coupled van der Pol oscillators: theory and experiment. Phys Rev E 2006;74:046213.

On the robustness of the *in vivo* cyanobacterial circadian clock

Dorota Youmbi Fouego[♮,♢] and Sophie de Buyl [♢,♭*]
[♮] *Laboratory of Modelling and Simulation in Engineering, Biomimetics and Prototypes and TWAS Research Unit, Department of Physics, Faculty of Science, University of Yaoundé I, Po. Box 812, Yaoundé, Cameroon*
[♢] *Applied Physics Research Group, Physics Department, Vrije Universiteit Brussel, Brussels 1050, Belgium and*
[♭] *Interuniversity Institute of Bioinformatics in Brussels, Brussels 1050, Belgium*
(Dated: March 29, 2022)

We propose a revisited version of the *in vivo* model of the cyanobacterial circadian clock. Our aim is to address the lack of robustness predicted for the mutant cyanobacteria without transcriptional regulation of the original model. For this, we rely on an *in vitro* model of the clock describing explicitly the hexameric structure of the core protein of the clock. Our model is able to reproduce oscillatory behavior for the mutant, as observed experimentally, without finely tuned parameters.

I. INTRODUCTION

Circadian clocks are endogenous oscillators allowing organisms to synchronize their physiological activities and behavior with the time of the day [1, 2]. They play a role in most living organisms from bacteria to humans. Cyanobacteria possess one of the simplest known circadian clock and serve as one of the model organisms to study mechanisms leading to endogenous oscillations of about 24 hours. One particularly beautiful property of the cyanobacterial circadian clock is that it can be reconstituted in a test tube. If one mixes adenosine triphosphate (ATP) with the three key proteins of the clock, namely KaiC, KaiB and KaiA, autonomous oscillations with a period of about 24 hours are observed during several days [3–6]

The mechanism of the clock is essentially an ensemble of phosphorylation/dephosphorylation reactions of KaiC which is the core protein of the clock. The phosphorylation state of KaiC contains the information about the phase of the clock. More specifically, the structure of KaiC is a homo-hexamer in the shape of a double-doughnut which can be phosphorylated on two residus on each monomer. The role of KaiA is to promote phosphorylation while KaiB, when bound to KaiC, inhibits phosphorylation by sequestring KaiA. Those phosphorylation/dephosphorylation reactions can be reproduced in the test tube. An additional mechanism comes at play *in vivo* as KaiC autoregulates its own production via a negative feedback on its own mRNA production. There are therefore two oscillatory processes underlying the functioning of the clock, the post-translational regulation (PTR) which is observed *in vitro*, and the transcriptional translational regulation (TTR) consisting of the negative feedback on mRNA production.

A mathematical model of the *in vitro* clock relying on careful experiments measuring all kinetic rates and concentrations of proteins involved was proposed in [5]. This simple model beautifully reproduces oscillations with a period of about 24 hours, without any parameter space exploration as all parameters have been measured.

In [7], we proposed an extension to the *in vivo* case. This model showed that PTR regulation is sufficient to generate oscillations, as observed in the experiments with mutant cyanobacteria lacking the TTR regulation. It also showed that the transcriptional regulation helps maintaining synchrony in a population of growing cyanobacteria. However, the model requires finely tuned parameters to lead to oscillatory behavior of the mutant cyanobacteria lacking the transcriptional regulation. The *in vitro* model it is based on did not explicitly described the hexameric structure of the KaiC protein. More recently, a more realistic model of the *in vitro* clock has been proposed in [8]. It describes explicitly the hexameric nature of KaiC and the binding of KaiB to KaiC. We propose here to build an *in vivo* model based on this more realistic *in vitro* model. Our model is able to produce robust oscillations for the wild type cyanobacteria as well as for the mutants lacking transcriptional regulation.

The structure of the work is as follows. We first briefly introduce the *in vitro* model of [8] for completeness and to introduce notations. Then we describe our *in vivo* model of the cyanobacterial circadian clock. We analyze the robustness of our model with respect to parameter variations, and compare it with the model proposed in [7]. We end with a short discussion on the role of transcriptional regulation.

II. THE *IN VITRO* HEXAMERIC MODEL

The hexameric model of the clock describes the interconversions of the different phosphoforms of KaiC as well as the binding and unbinding of KaiC to KaiB. When KaiC is bound to KaiB, it forms the KaiB.KaiC complex which can undergo to same (de)phosphorylation reactions as KaiC. The nonlinearity in the system comes from the fact that the reaction rates depend on the state of the system. When KaiA is bound to KaiC, it enhances the auto-kinase activity of KaiC. Although KaiA is not

* sdebuyl@vub.be

described explicitly, it impacts the (de)phosphorylation rates as KaiC binds differentially to KaiA in its different phosphoforms. Similarly, KaiB is implicitly taken into account and antagonizes the effect of KaiA in a KaiC phosphoform dependent manner. Essentially, when KaiC subunits are in the S form, KaiB will bind to KaiC and sequestrate KaiA, thereby repressing phosphorylation. More details are provided in the appendix. A scheme of the model is depicted in Fig. 1. Each subunit of KaiC

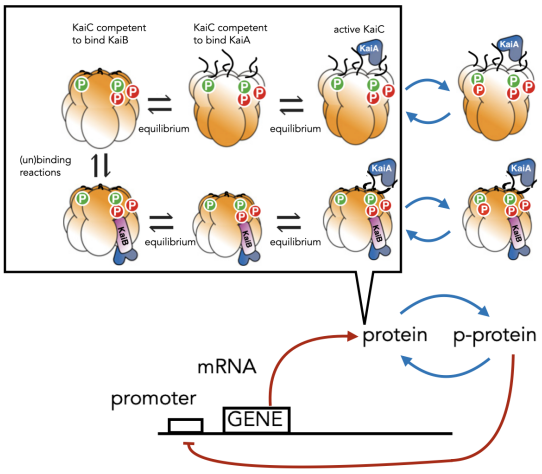

FIG. 1: Schematic representation of the model, adapted from [8]. The representation of the configuration of the active form of KaiB.KaiC is speculative.

undergoes independent autokinase and autophosphatate reactions at two sites, serine 431 (S) and threonine 432 (T) which can be phosphorylated or not. Therefore, each subunit can be in four forms, namely: the phosphorylated form at S, the phosphorylated form at T, the doubly phosphorylated form at S and T (denoted D), and the U form which is the non-phosphorylated form. The different phosphoforms are denoted by KaiC_{ijk} where i represents the number of subunits phosphorylated at T only, j represents the number of phosphorylated subunits at S only and k represents the number of doubly phosphorylated subunits. By construction, the variables $KaiC_{ijk}$ which are physical have indices obeying $0 < i, j, k < n$ and the number of unphosphoryated subunits is given by $n - (i + j + k)$. For the hexamer model $n = 6$, but to study theoretically the effect of changing the number of KaiC subunits, the model was constructed with an arbitrary number subunits denoted by n. For instance, the unphosphorylated KaiC is $KaiC_{000}$ and the fully doubly phosphorylated form is $KaiC_{00n}$. One should note that the dynamical variables constructed by assuming that the different subunits of the hexamer are indistinguishable. KaiC can undergo potentially (de)phosphorylation reactions which will increase or decrease the values of i, j, k by one unit. Additionally, $KaiC_{i,j,k}$ can bind to KaiB, forming the complex $KaiB.KaiC_{i,j,k}$ which undergoes the same (de)phosphorylation reactions. The model is given by Eqs. (1). The dependence of the reaction rates on the KaiC phosphoforms are given in the appendix, see Eqs. A1 and A2.

$$
\begin{aligned}
\left.\frac{d\mathrm{KaiC}_{i,j,k}}{dt}\right|^{in\ vitro} &= k_{UT}^{i-1,j,k}(n+1-(i+j+k))\mathrm{KaiC}_{i-1,j,k} + k_{US}^{i,j-1,k}(n+1-(i+j+k))\mathrm{KaiC}_{i,j-1,k} \\
&+ k_{TD}^{i+1,j,k-1}(i+1)\mathrm{KaiC}_{i+1,j,k-1} + k_{TU}^{i+1,j,k}(i+1)\mathrm{KaiC}_{i+1,j,k} \\
&+ k_{DT}^{i-1,j,k+1}(k+1)\mathrm{KaiC}_{i-1,j,k+1} + k_{DS}^{i,j-1,k+1}(k+1)\mathrm{KaiC}_{i,j-1,k+1} \\
&+ k_{SD}^{i,j+1,k-1}(j+1)\mathrm{KaiC}_{i,j+1,k-1} + k_{SU}^{i,j+1,k}(j+1)\mathrm{KaiC}_{i,j+1,k} \\
&- ((n-i-j-k)\,(k_{UT}^{i,j,k} + k_{US}^{i,j,k}) + i\,k_{TD}^{i,j,k} + i\,k_{TU}^{i,j,k} + k\,k_{DT}^{i,j,k} + k\,k_{DS}^{i,j,k} + j\,k_{SD}^{i,j,k} + j\,k_{SU}^{i,j,k})\mathrm{KaiC}_{i,j,k} \\
&- k_{\mathrm{on},B}F_B^{i,j,k}\,\mathrm{KaiC}_{i,j,k} \\
&+ k_{\mathrm{off},B}\,\mathrm{KaiB.KaiC}_{i,j,k} \\
\left.\frac{d\mathrm{KaiB.KaiC}_{i,j,k}}{dt}\right|^{in\ vitro} &= k_{UT}^{i-1,j,k}(n+1-(i+j+k))\mathrm{KaiB.KaiC}_{i-1,j,k} + k_{US}^{i,j-1,k}(n+1-(i+j+k))\mathrm{KaiB.KaiC}_{i,j-1,k} \\
&+ k_{TD}^{i+1,j,k-1}(i+1)\mathrm{KaiB.KaiC}_{i+1,j,k-1} + k_{TU}^{i+1,j,k}(i+1)\mathrm{KaiB.KaiC}_{i+1,j,k} \\
&+ k_{DT}^{i-1,j,k+1}(k+1)\mathrm{KaiB.KaiC}_{i-1,j,k+1} + k_{DS}^{i,j-1,k+1}(k+1)\mathrm{KaiB.KaiC}_{i,j-1,k+1} \\
&+ k_{SD}^{i,j+1,k-1}(j+1)\mathrm{KaiB.KaiC}_{i,j+1,k-1} + k_{SU}^{i,j+1,k}(j+1)\mathrm{KaiB.KaiC}_{i,j+1,k} \\
&-((n-\ i\ -j-k)\,(k_{UT}^{i,j,k} + k_{US}^{i,j,k}) + i\,k_{TD}^{i,j,k} + i\,k_{TU}^{i,j,k} + k\,k_{DT}^{i,j,k} + k\,k_{DS}^{i,j,k} + j\,k_{SD}^{i,j,k} + j\,k_{SU}^{i,j,k})\,\mathrm{KaiB.KaiC}_{i,j,k} \\
&- k_{\mathrm{off},B}\,\mathrm{KaiB.KaiC}_{i,j,k} \\
&+ k_{\mathrm{on,B}}F_B^{i,j,k}\,\mathrm{KaiC}_{i,j,k}
\end{aligned}
\tag{1}
$$

III. THE *IN VIVO* HEXAMERIC MODEL

To construct an *in vivo* model, we rely on the *in vitro* model of [8] described in the section above and add terms for production, degradation and dilution similarly

to what is proposed in [7]. Our model is given by the Eqs. 4.

$$\frac{d\mathrm{KaiC}_{ijk}}{dt} = \left.\frac{d\mathrm{KaiC}_{ijk}}{dt}\right|^{in\ vitro} - V_d\mathrm{KaiC}_{ijk} - V\frac{\mathrm{KaiC}_{ijk}}{K+\mathrm{KaiC}_{ijk}} \quad \text{for } i,j,k \neq 0,0,0 \tag{2}$$

$$\frac{d\mathrm{KaiB.KaiC}_{ijk}}{dt} = \left.\frac{d\mathrm{KaiB.KaiC}_{ijk}}{dt}\right|^{in\ vitro} \quad \text{for } i,j,k \neq 0,0,0 \tag{3}$$

$$\frac{d\mathrm{KaiC}_{000}}{dt} = \left.\frac{d\mathrm{KaiC}_{000}}{dt}\right|^{in\ vitro} + K_s\mathrm{mRNA} - V_d\mathrm{KaiC}_{000} - V\frac{\mathrm{KaiC}_{000}}{K+\mathrm{KaiC}_{000}}$$

$$\frac{d\mathrm{mRNA}}{dt} = V_s\frac{K_i^4}{K_i^4+(\sum_{j\neq 0}\mathrm{KaiB.KaiC}_{ijk})^4} - V_m\frac{\mathrm{mRNA}}{K_m+\mathrm{mRNA}}$$

Firstly, we consider explicitly KaiC mRNA as a dynamical variable. Its production term is dependent on KaiC which acts as a negative feedback on its production. As in [7], we consider only active degradation and not dilution for mRNA as it is order of magnitude larger. Secondly, we add a production term for unphosphorylated KaiC from its mRNA. Finally, all forms of KaiC are assumed to have the same linear dilution rate and active degradation rate.

As in [7], we consider on top of the wild type (WT) cyanobacterial circadian clock described above, the case of a mutant cyanobacteria lacking the transcriptional feedback. This is simply done by replacing the production term of mRNA by a constant production rate V_{sptr}. This mutant is referred to as post-transcriptional (PTR) mutant while the WT clock has a transcriptional translational regulation (TTR).

We analyzed the sensitivity to parameter changes of the PTR mutant and showed that model does not requires fine tuning to generated oscillations, see Fig. 2. We observe that the main change between the WT cyanobacteria and the mutants lacking the TTR circuit is that the WT bacteria are more robust to changes in the translation rate. However, the TTR circuit is not crucial for the clock to be robust against changes in the dilution rate.

IV. DISCUSSION

We showed that our revised *in vivo* model of the cyanobacterial circadian clock is compatible with the robust oscillations of the cyanobacteria mutant lacking the TTR feedback. This result suggests that although the TTR feedback enhances the robustness of the clock, the effect is not as strong as initially suggested. Our conclusion is in agreement with the experiments performed with higher growth rates for (see Fig. S4 of [7]). Indeed, those experiments show that the mutants lacking the TTR regulation are able to generate oscillations in an extended range of growth rate. Although the growth rate of the bacteria is not explicitly modeled, it will impact the dilution rate. In the original model of the *in vivo* clock, the dilution rate needed to be finely tuned. The TTR regulation could actually play a more important role if the nonlinearity of the regulator terms was increased. Coordination of both mechanisms is key to enhance the robustness too. To sum up, we propose a revisited version of the *in vivo* cyanobacterial clock which is in agreement with current experiments. We expect that the synchronysation properties of the clock will also be enhanced by TTR regulation. In the future, we should to include the key proteins *RpaA* and *SasA* in the models, to be able to describe quantitatively how the clock's time is read as an output [9, 10].

Appendix A: Reaction rates depend on the state of the system

To obtain the dependence of the reaction rates on the various phosphoforms of KaiC, we need to describe the different allosteric states of KaiC. KaiC can be in a state comptent to bind KaiA and a state competent to bind KaiB, respectively denoted KaiC^A and KaiC^B (to simplify notations, we omit the i,j,k indices those allosteric state should carry). From the state comptent to bind KaiA, KaiC can be converted in the active form of KaiC, which we denote $\mathrm{KaiC}^*_{i,j,k}$ with indices specifying the phosphoform. The allosteric reactions are considered to be at equilibrium, and one can therefore obtain the ratio of KaiC in its different allosteric states. The fact that those ratios are depend on the specific (i,j,k)-phosphoform is key to the *in vitro* feedback mechanism. The (de)phosphorylation reaction rates are given by:

$$k_{XY}^{i,j,k} = F_A^{i,j,k}\,k_{XY}^A \ + (1-F_A^{i,j,k})\,k_{XY}^0\ , \tag{A1}$$

where $F_A^{i,j,k}$ denotes the fraction of KaiC in the state competent to bind KaiA. The first term is dominant as KaiC autokinase activities are enhanced by KaiA. The constants k_{XY}^A denotes the maximal phosphorylation rate from the state X to the state Y when KaiA is bound, with

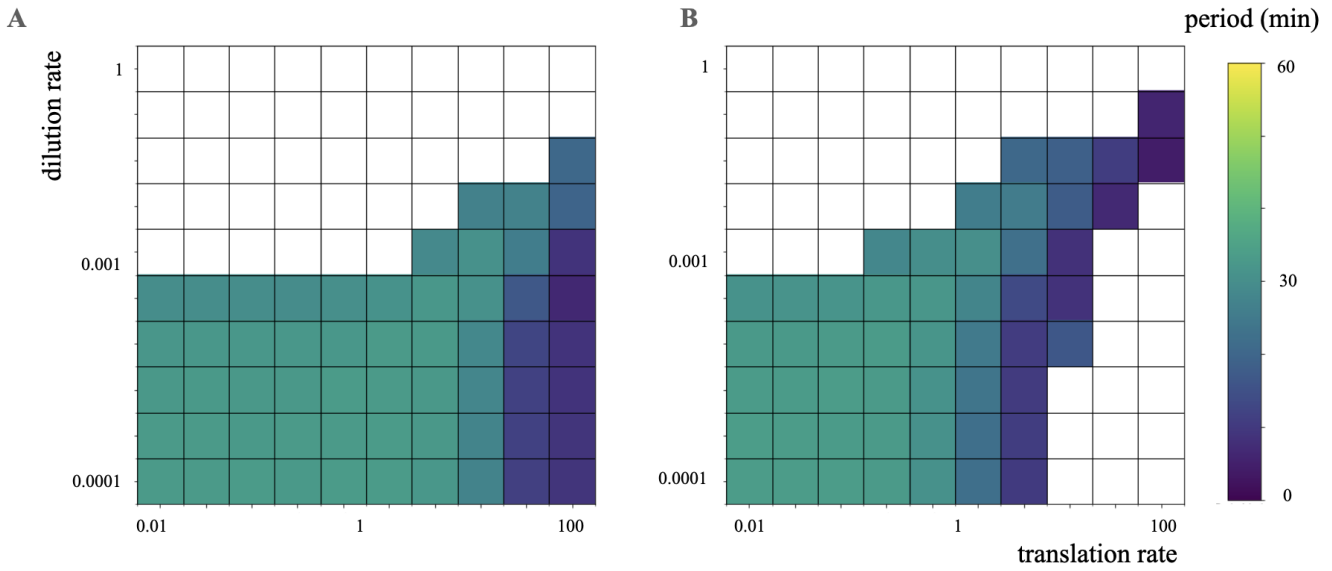

FIG. 2: Robustness analysis of the wild type model (panel A) and the model for the mutant lacking the transcriptional regulation (panel B) over parameter changes. We varied both the translation rate K_s and the dilution rate V_d over 4 orders of magnitudes.

X, Y representing the U, T, S or D state on the relevant subunit. Similarly, k^0_{XY} denotes the maximal phosphorylation rate when KaiA is not bound. The dependence of $F_A^{i,j,k}$ on the state of the system is given by

$$F_A^{i,j,k} \equiv \frac{\mathrm{KaiC}^{i,j,k}}{\mathrm{KaiC}^B + \mathrm{KaiC}^A + \mathrm{KaiC}^{*i,j,k}} \overset{\text{equilibrium}}{=} \frac{\mathrm{KaiA}}{\mathrm{KaiA} + K_m K_A^{i,j,k} + K_m}$$

where $K_m = \frac{k_2}{k_1}$ is the dissociation constant of the reaction $\mathrm{KaiC}^A \underset{k_1 \mathrm{KaiA}}{\overset{k_2}{\rightleftharpoons}} \mathrm{KaiC}^*_{i,j,k}$, and $K_A^{i,j,k} = e^{-\frac{\Delta G_{i,j,k}}{k_B T}}$ the dissociation constant of the allosteric transformation $\mathrm{KaiC}^B \rightleftharpoons \mathrm{KaiC}^A$, with $\Delta G_{i,j,k} = i\,\Delta G_{pT} + j\,\Delta G_{pS} + k\,\Delta G_{pSpT} + (n - (i+j+k))\Delta G_U$ being the free energy difference between the allosteric states.

The (un)binding reactions of KaiB are dependent on the fraction of KaiC in form competent to bind to KaiB which is given by

$$F_B^{i,j,k} \equiv \frac{\mathrm{KaiC}^B}{\mathrm{KaiC}^B + \mathrm{KaiC}^A + \mathrm{KaiC}^{*i,j,k}} = \frac{1}{1 + \frac{1}{K_A^{i,j,k}} + \frac{\mathrm{KaiA}}{K_m K_A^{i,j,k}}} \qquad \text{(A2)}$$

Finally, we should note that $\mathrm{KaiC}^{i,j,k}$ in Eqs. 1 represents the sum of all allosteric forms of KaiC in the (i, j, k) state.

TABLE I: Parameter values - taken from [5, 7, 8]

$k_{on,B}$	0.15 h^{-1}	$k_{off,B}$	$3.0\,10^{-2}$ h^{-1}
ΔG_{pT}	2.0 $\mathrm{k}_B T$	ΔG_{pS}	-3.5 $\mathrm{k}_B T$
ΔG_{pSpT}	-1.0 $\mathrm{k}_B T$	ΔG_U	1.0 $\mathrm{k}_B T$
k_m	0.43 μM	$kaiA0$	10 μM
k^0_{UT}	0.0 h^{-1}	k^0_{TD}	0.0 h^{-1}
k^0_{US}	0.0 h^{-1}	k^0_{SD}	0.0 h^{-1}
k^0_{DS}	0.31 h^{-1}	k^0_{DT}	0.0 h^{-1}
k^0_{TU}	0.21 h^{-1}	k^0_{SU}	0.11 h^{-1}
k^{act}_{UT}	0.48 h^{-1}	k^{act}_{TD}	0.21 h^{-1}
k^{act}_{US}	$5.32\,10^{-2}$ h^{-1}	k^{act}_{SD}	0.506 h^{-1}
k^{act}_{DS}	0.0 h^{-1}	k^{act}_{DT}	0.172 h^{-1}
k^{act}_{TU}	0.29 h^{-1}	k^{act}_{SU}	0.9 h^{-1}
V_{sptr}	$3.316\,10^{-2}$	V_s	2.0 $\mu M h^{-1}$
V_m	0.20 $\mu M h^{-1}$	K_m	0.20 μM
K	2.0 μM	V	$2.0\,10^{-3}$ $\mu M h^{-1}$
K_i	1.0 μM		
K_s	varied	V_d	varied

ACKNOWLEDGMENTS

SdB would like to warmly thank Susan Golden for an insightful discussion.

[1] A. Goldbeter and M. J. Berridge, *Biochemical Oscillations and Cellular Rhythms: The Molecular Bases of Periodic and Chaotic Behaviour*, 1st ed. (Cambridge Uni-

versity Press, 1996).
[2] A. Goldbeter, C. Gérard, D. Gonze, J.-C. Leloup, and G. Dupont, enSystems biology of cellular rhythms, FEBS Letters **586**, 2955 (2012).
[3] M. Nakajima, K. Imai, H. Ito, T. Nishiwaki, Y. Murayama, H. Iwasaki, T. Oyama, and T. Kondo, enReconstitution of Circadian Oscillation of Cyanobacterial KaiC Phosphorylation in Vitro, Science **308**, 414 (2005).
[4] J. Tomita, M. Nakajima, T. Kondo, and H. Iwasaki, enNo Transcription-Translation Feedback in Circadian Rhythm of KaiC Phosphorylation, Science **307**, 251 (2005).
[5] M. J. Rust, J. S. Markson, W. S. Lane, D. S. Fisher, and E. K. O'Shea, enOrdered Phosphorylation Governs Oscillation of a Three-Protein Circadian Clock, Science **318**, 809 (2007).
[6] H. Ito, H. Kageyama, M. Mutsuda, M. Nakajima, T. Oyama, and T. Kondo, enAutonomous synchronization of the circadian KaiC phosphorylation rhythm, Nature Structural & Molecular Biology **14**, 1084 (2007).
[7] S.-W. Teng, S. Mukherji, J. R. Moffitt, S. de Buyl, and E. K. O'Shea, enRobust Circadian Oscillations in Growing Cyanobacteria Require Transcriptional Feedback, Science **340**, 737 (2013).
[8] J. Lin, J. Chew, U. Chockanathan, and M. J. Rust, enMixtures of opposing phosphorylations within hexamers precisely time feedback in the cyanobacterial circadian clock, Proceedings of the National Academy of Sciences **111**, E3937 (2014).
[9] R. Tseng, N. F. Goularte, A. Chavan, J. Luu, S. E. Cohen, Y.-G. Chang, J. Heisler, S. Li, A. K. Michael, S. Tripathi, S. S. Golden, A. LiWang, and C. L. Partch, enStructural basis of the day-night transition in a bacterial circadian clock, Science **355**, 1174 (2017).
[10] A. G. Chavan, J. A. Swan, J. Heisler, C. Sancar, D. C. Ernst, M. Fang, J. G. Palacios, R. K. Spangler, C. R. Bagshaw, S. Tripathi, P. Crosby, S. S. Golden, C. L. Partch, and A. LiWang, enReconstitution of an intact clock reveals mechanisms of circadian timekeeping, Science **374**, eabd4453 (2021).